

AUTOPHAGY IN ZELLWEGER SYNDROME SPECTRUM DISORDER AND CANCER

APPROVED BY SUPERVISORY COMMITTEE

Beth Levine, M.D., Supervising Professor

Benjamin Tu, Ph.D., Committee Chair

Joseph A. Hill, M.D., Ph.D.

Ralph J. DeBerardinis, M.D., Ph.D.

ACKNOWLEDGMENTS

First and foremost, I thank my mentor, Dr. Beth Levine, for her continuous support throughout my training. Your passion for science and medicine, your relentless drive for excellence, and your collaborative attitude towards science inspire me every day. I have learned so much from you.

I would also like to thank my thesis committee chair Dr. Benjamin Tu and committee members Drs. Joseph Hill and Ralph DeBerardinis. Your critiques and suggestions made my work stronger.

To everyone in the Levine lab, it has been such a pleasure working with all of you. I have become close friends with some of you, and you are my family away from home. To Dr. Zhongju Zou and Ms. Lori Nguyen, thank you for all your help, especially on the mouse experiments. To the members of Team Mitophagy, including Drs. Rhea Sumpter, Yongjie Wei, and Salwa Sebti, thank you for sharing ideas, protocols, and reagents. To Drs. Hansi Jiang, Congcong He, and Yang (Guanshu) Liu, thank you for your help with the exercise-induced autophagy project. To all the other members of the Levine lab, including Ms. Tabitha Ting, Dr. Wei-Chung Daniel Chiang, Dr. Luis Franco, Dr. Yuting Zhao, Dr. Xiaonan Dong, Dr. Silvia Vega-Rubin de Celis, Mr. Shyam Sirasanagandla, Dr. Tobias Wijshake, Dr. Alvaro Fernandez Fernandez, Dr. Sanae Shoji-Kawata, Dr. Richard Wang, Dr. Yang Liu, and Dr. Zhenyi An, thank you for your help and support. To Ms. Haley Harrington-Smith, many thanks for your administrative assistance. To the other staff in the Center for Autophagy Research and the Department of Internal Medicine who keeping things running smoothly, I would like to thank Mr. Frederick Scott,

Mr. Stephen Ostermann, Ms. Paula Levier, Ms. Deborah Solomon, and Ms. Cindy Jozefiak.

For the peroxin project, I thank Dr. Denis Crane for providing critical reagents and his expertise on peroxin proteins. I also thank Dr. Suresh Subramani and his colleagues Drs. Taras Nazarko and Andreas Till for helpful discussions on peroxins and pexophagy. I thank Drs. Qing Zhong, Jing Zhang, and Yueguang Rong for help with the IP-MS experiments, Dr. Shi Chen for the IP-MS identification, and Dr. James Chen for critical reagents for the MAVS experiments.

For the exercise project, I would like to thank Dr. Lee Jones for helpful discussions on the exercise modalities, Dr. Clary Clish, Dr. Ralph DeBerardinis, Dr. Zeping Hu, Ms. Claire Klimko, and Dr. Ling Cai for help with the metabolomic screens, Dr. Kathryn Stone for help with the proteomic screen, and Drs. Guanghua (Andy) Xiao, Yang Xie, and Rui Zhong for help with the statistical analyses. Although I did not include my work on exercise-induced autophagy and adult neurogenesis in this dissertation, I would also like to thank the collaborators that helped me during this project. To Dr. Amelia Eisch, thank you for serving on my thesis committee initially and providing your valuable expertise on neurogenesis. To Dr. Shibani Mukherjee, Dr. Irene Masiulis Bowen, Dr. Tony Wyss-Coray, and Dr. Yingbo He, thank you for teaching me the techniques in evaluating neurogenesis.

Many thanks to the Integrative Biology Graduate Program. In particular, I thank our program chair Dr. Yi Liu, our administrative assistant Ms. Priyarama Sen, and my qualifying exam committee chair Dr. Kristine Kamm.

I am grateful for the tremendous support from the Medical Scientist Training Program (MSTP). Specifically, many thanks to the program leadership Dr. Andrew Zinn, Dr. James Amatruda, and Dr. Michael Brown and to the program administrators Ms. Robin Downing, Ms. Charletha Jordan, and Ms. Stephanie Robertson. I also want to thank the current and former MSTP colleagues who have advised me and encouraged me throughout this journey.

To my parents, thank you so much for your sacrifice to give me the best educational opportunities. To Michelle, Jennifer, Daniel, and my friends from the Penn Badminton Club and the Dallas Badminton Club, thank you for being supportive of my endeavors and for helping me keep things in perspective.

AUTOPHAGY IN ZELLWEGER SYNDROME SPECTRUM DISORDER AND CANCER

by

MING YEh (MINDY) LEE

DISSERTATION

Presented to the Faculty of the Graduate School of Biomedical Sciences

The University of Texas Southwestern Medical Center at Dallas

In Partial Fulfillment of the Requirements

For the Degree of

DOCTOR OF PHILOSOPHY

The University of Texas Southwestern Medical Center at Dallas

Dallas, Texas

May, 2018

Copyright

by

Ming Yeh Lee, 2016

All Rights Reserved

AUTOPHAGY IN ZELLWEGER SYNDROME SPECTRUM DISORDER AND CANCER

Publication No. _____

Ming Yeh Lee, Ph.D.

The University of Texas Southwestern Medical Center at Dallas, 2016

Supervising Professor: Beth Levine, M.D.

Autophagy is a lysosomal degradation pathway that breaks down unwanted proteins and organelles from the cytoplasm to regenerate cellular building blocks. This process is constitutively active at low basal levels, and can be upregulated by stress stimuli to promote cellular homeostasis. In this work, we investigated two aspects of autophagy regulation and relevance to human diseases. First, we examined how autophagy selectively removes viral components and damaged mitochondria from the

cytoplasm through PEX13, a peroxin protein mutated in Zellweger syndrome spectrum (ZSS). Second, we examined the role of autophagy as a potential mechanism contributing to exercise-mediated protection against cancer progression.

PEX13 is an integral membrane protein on the peroxisome that regulates peroxisomal matrix protein import during peroxisome biogenesis. Mutations in PEX13 and other peroxin proteins are associated with ZSS disorders, a subtype of peroxisome biogenesis disorder characterized by prominent neurodevelopmental, hepatic, and renal abnormalities leading to neonatal death. The lack of functional peroxisomes in ZSS patients is widely accepted as the underlying cause of disease; however, our understanding of disease pathogenesis is still incomplete. Here, we demonstrate that PEX13 is required for selective autophagy of Sindbis virus (virophagy) and of damaged mitochondria (mitophagy), and that disease-associated PEX13 mutants I326T and W313G are defective in mitophagy. The selective mitophagy function of PEX13 is shared with another peroxin family member PEX3, but not with two other peroxins, PEX14 and PEX19, which are required for general autophagy. Together, our results demonstrate that PEX13 is required for selective autophagy, and suggest that dysregulation of PEX13-mediated mitophagy may contribute to ZSS pathogenesis.

In the second part of this study, we evaluated physiological functions regulated by exercise-induced autophagy, including changes to the metabolome, proteome, and breast cancer progression. A previous study from our laboratory demonstrated that exercise is a potent inducer of autophagy and that autophagy contributes to exercise-mediated metabolic benefits. Therefore, we speculate that autophagy may contribute to

exercise-mediated protection against other diseases. Although many epidemiological and laboratory studies have provided strong evidence that physical exercise can decrease cancer development and mortality, the mechanisms are poorly understood. Using the E0771 injectable murine breast cancer, we show that exercise delays cancer progression in wild-type, but not in Bcl-2 AAA mice or Beclin 1 heterozygous knockout mice that are deficient in exercise-induced autophagy. We identified candidate factors and pathways regulated by exercise-induced autophagy, including plasma levels of pyrimidine, branched chain amino acids, LIF, and IL-15, as well as skeletal muscle expression of IDH2 and NDUFA13. Further studies are required to elucidate the metabolomic and proteomic alterations regulated by exercise-induced autophagy and the mechanism by which exercise-induced autophagy protects against tumor progression.

TABLE OF CONTENTS

Publications	xvi
List of Figures	xvii
List of Tables	xx
List of Abbreviations	xxi
Perspective	xxiv
Chapter I: Introduction and literature review on autophagy	1
I.1. The autophagy pathway	1
I.1.A. General autophagy.....	3
I.1.B. Selective autophagy.....	4
I.1.C. Molecular mechanisms of selective autophagy	5
I.1.D. Autophagy mutant mouse models.....	8
I.1.E. Assays for monitoring autophagy	10
I.2. Cellular functions of autophagy	11
I.2.A. Adaptation to metabolic stress	11
I.2.B. Removal of toxic intracellular components.....	12
I.2.C. Secretion	12
I.3. Autophagy in human health and disease.....	13
I.3.A. Autophagy in infectious diseases.....	14
I.3.B. Autophagy in development and differentiation	15
I.3.C. Autophagy defects in congenital neurodevelopmental disorders	16
I.3.D. Autophagy and cancer	18

I.3.E. Manipulating autophagy for clinical applications	22
Chapter II: PEX13 and PEX3 function in selective autophagy	24
II.1. Literature review	24
II.1.A. Genome-wide screen for selective autophagy factors.....	24
II.1.B. Peroxisome biogenesis factors	27
II.2. Introduction	30
II.3. Materials and methods.....	31
II.3.A. Cell culture	31
II.3.B. Generation of mouse embryonic fibroblasts	32
II.3.C. PCR genotyping	33
II.3.D. Generating and reviving frozen stocks of cultured cells	33
II.3.E. Chemicals and reagents	34
II.3.F. Antibodies	34
II.3.G. Constructs.....	35
II.3.H. Retroviruses and lentiviruses	35
II.3.I. Generating and titering Sindbis virus	36
II.3.J. Sindbis virophagy colocalization assay	37
II.3.K. Mitophagy assays	37
II.3.L. siRNA transfection	38
II.3.M. Western blot analyses.....	39
II.3.N. General autophagy analysis by western blot and GFP-LC3 puncta quantification	40

II.3.O.	Immunoprecipitation-mass spectroscopy	41
II.3.P.	Immunofluorescence microscopy	42
II.3.Q.	Image analysis	42
II.3.R.	Quantitative real time-PCR (qRT-PCR).....	43
II.3.S.	Mouse embryonic tissue sample preparation for electron microscopy ..	44
II.3.T.	Mouse embryonic fibroblast preparation for electron microscopy	44
II.3.U.	Electron microscopy imaging	45
II.3.V.	Statistical analyses.....	45
II.4.	Results.....	46
II.4.A.	PEX13 is required for Sindbis virophagy and not starvation-induced general autophagy	46
II.4.B.	PEX13 and PEX3 are required for mitophagy	49
II.4.C.	siRNA-resistant WT PEX13, but not disease-associated mutants PEX13 I326T and W313G rescue the mitophagy defect in PEX13 knockdown cells.....	56
II.4.D.	PEX13 colocalizes with peroxisomes, but not with mitochondria or early autophagosomes during CCCP-induced mitophagy	59
II.4.E.	PEX13 and PEX3 are required for selective mitophagy, whereas PEX14 and PEX19 are required for general autophagy	61
II.4.F.	PEX13 signaling through MAVS during selective autophagy	63
II.4.G.	Immunoprecipitation-mass spectroscopy identification of PEX13- interacting proteins during selective autophagy	66

II.4.H.	Generation and validation of HeLa cells with PEX3, PEX5, PEX13, PEX14, or PEX19 KO	73
II.4.I.	PEX13 KO and not PEX19 KO HeLa cells have defective mitophagy ..	79
II.4.J.	PEX19 KO and not PEX13 KO HeLa cells have defective general autophagy	80
II.4.K.	PEX13 localizes to the mitochondria and not the ER in PEX19 KO cells	81
II.5.	Discussion and future directions	85
Chapter III: Exercise-induced autophagy and cancer		93
III.1.	Literature review	93
III.1.A.	Exercise and autophagy protect against similar pathologies.....	93
III.1.B.	Exercise reduces cancer risk	93
III.1.C.	Proposed mechanisms mediating exercise protection against cancer ..	94
III.1.D.	Mouse models with altered Bcl-2/Beclin 1 interaction	97
III.2.	Introduction.....	101
III.3.	Materials and methods	102
III.3.A.	Cell culture	102
III.3.B.	Mouse colonies	102
III.3.C.	Genotyping PCR	103
III.3.D.	Aerobic training protocol #1	104
III.3.E.	Aerobic training protocol #2	104
III.3.F.	Voluntary wheel running physical activity	105

III.3.G.	Tumor measurements	105
III.3.H.	Tissue collection.....	106
III.3.I.	Processing for tissue sections.....	107
III.3.J.	Tissue homogenization	107
III.3.K.	Proteomic screen	108
III.3.L.	Metabolomic screen #1	110
III.3.M.	Metabolomic screen #2	110
III.3.N.	Quantitative real time-PCR with mouse tissues	111
III.4.	Results	112
III.4.A.	Evaluating the role of autophagy in chronic aerobic training protection against E0771 tumor progression.	112
III.4.B.	Evaluating the role of autophagy in voluntary physical activity protection against E0771 tumor progression	117
III.4.C.	Metabolomic screen for factors and pathways regulated by exercise- induced autophagy.....	122
III.4.D.	Proteomic screen for factors and pathways regulated by exercise- induced autophagy.....	126
III.4.E.	Targeted cytokine and chemokine panel analysis for factors regulated by exercise-induced autophagy	128
III.5.	Discussion and future directions.....	131
	References.....	134

PUBLICATIONS

Lee, M.Y., Zou, Z., Sumpter, R., Wei, Y., Crane, D.I., Levine, B. Peroxisomal protein PEX13 functions in selective virophagy and mitophagy. (Under Review).

Sumpter, R., Sirasanagandla S., Fernández A.F., Wei, Y., Dong, X., Franco, L., Zou Z., Marchal C., **Lee, M.Y.**, Clapp, D.W., Hanenberg, H., Levine, B. (2016) Fanconi anemia tumor suppressor genes function in selective autophagy, immunity and mitochondrial homeostasis. *Cell* 165, 867-881.

LIST OF FIGURES

Figure 1. Overview of the general autophagy pathway	2
Figure 2.1. Overview of the mammalian peroxisome biogenesis factors.....	28
Figure 2.2. PEX13 is required for Sindbis virophagy in HeLa cells	47
Figure 2.3. Pex13 is required for Sindbis virophagy in MEFs.....	48
Figure 2.4. PEX13 is not required for starvation-induced general autophagy	49
Figure 2.5. PEX13 is required for Parkin-mediated mitophagy in HeLa cells	51
Figure 2.6. PEX3 is required for Parkin-mediated mitophagy in HeLa cells.	53
Figure 2.7. Pex13 is required for mitophagy in MEFs.....	55
Figure 2.8. Pex13 KO embryos contain abnormal mitochondria	56
Figure 2.9. siRNA-Resistant WT PEX13, but not disease-associated mutants PEX13 I326T and W313G rescue the mitophagy defect in PEX13 knockdown cells.....	58
Figure 2.10. PEX13 colocalizes with peroxisomes, but not with mitochondria or early autophagosomes during CCCP-induced mitophagy	60
Figure 2.11. PEX13 and PEX3, but not PEX14 and PEX19, are required for selective mitophagy	62
Figure 2.12. PEX14 and PEX19, but not PEX13 and PEX3, are required for general autophagy	63
Figure 2.13. PEX13 signaling through MAVS during selective autophagy	65
Figure 2.14. IP-MS identification of PEX13-interacting proteins during mitophagy	72
Figure 2.15. Deep-sequencing genotyping to validate CRISPR knockouts.....	75

Figure 2.16. Phenotypic validation of CRISPR KO HeLa cells	78
Figure 2.17. PEX13 KO but not PEX19 KO HeLa cells are defective in mitophagy	80
Figure 2.18. PEX13 KO HeLa cells are competent for starvation-induced general autophagy	81
Figure 2.19. PEX13 does not localize to the ER in PEX19 KO cells	83
Figure 2.20. PEX13 localizes to the mitochondria in PEX19 KO cells.....	84
Figure 3.1. Summary of potential mechanisms underlying physical activity benefits to reduce cancer risk.....	95
Figure 3.2. Beclin 1 knockout mouse is deficient in autophagy	98
Figure 3.3. Bcl-2 AAA knock-in mouse is deficient in stress-induced autophagy	99
Figure 3.4. Beclin 1 F121A knock-in mouse has increased autophagy	100
Figure 3.5. Schematic for iTRAQ.	109
Figure 3.6. Chronic aerobic training delays breast cancer progression in WT and not Bcl-2AAA mice.....	115
Figure 3.7. Becn1F121A mice have excess exercise-induced autophagy	116
Figure 3.8. Voluntary wheel running pattern is similar between WT, Bcl-2AAA and Becn1+/- mice.....	119
Figure 3.9. Voluntary physical activity delays breast cancer progression in WT mice but not in Bcl-2AAA or Becn1+/- mice.....	121
Figure 3.10. Plasma metabolomic screen for factors and pathways regulated by exercise-induced autophagy	123

Figure 3.11. Plasma metabolomic screen for factors and pathways regulated by exercise-induced autophagy in mice with E0771 tumors	125
Figure 3.12. Skeletal muscle proteomic screen for factors and pathways regulated by exercise-induced autophagy	127
Figure 3.13. Targeted panel of candidate plasma proteins regulated by exercise- induced autophagy	130

LIST OF TABLES

Table 1. Diseases in mice with mutations in autophagy genes	9
Table 2.1. Mutagenesis primers for PEX13 constructs	35
Table 2.2. siRNA sequences.....	39
Table 2.3. qRT-PCR primer sequences for quantifying knockdown of PEX genes	43
Table 2.4. Candidate PEX13-interacting proteins from IP-MS screen.....	67
Table 2.5. CRISPR gRNA and cloning primer sequences.....	74
Table 3.1. Genotyping PCR primer sequences	103
Table 3.2. qRT-PCR primer sequences for evaluating expression of genes related to exercise training	112

LIST OF ABBREVIATIONS

AMPK	5' AMP-activated protein kinase
ASD	autism spectrum disorder
Atg	autophagy-related gene
ATP	adenosine triphosphate
Baf A1	bafilomycin A1
Bcl-2	B-cell lymphoma 2
CCCP	carbonyl cyanide m-chlorophenyl hydrazine
CRISPR	clustered regularly-interspaced short palindromic repeats
DMEM	Dulbecco's Modified Eagle Medium
DMSO	dimethylsulfoxide
DNA	deoxyribonucleic acid
EDTA	ethylenediaminetetraacetic acid
ELISA	enzyme-linked immunosorbent assay
FBS	fetal bovine serum
FDA	Food and Drug Administration
Fig.	figure
FLAG	the peptide N-DAKDDDDK-C, using the single letter amino acid code
g	gram
GFP	green fluorescent protein
IACUC	Institutional Animal Care & Use Committee
IL	interleukin
kDa	kilodalton

KI	knockin
KO	knockout
L	liter
LC3	microtubule-associated protein 1 light chain 3
LIR	LC3-interacting region
m	meter
M	molar
MEF	mouse embryonic fibroblast
mg	milligram
ml	milliliter
mm	millimeter
mM	millimolar
mmol	millimole
MOI	multiplicity of infection
MS	mass spectroscopy
MSTP	Medical Scientist Training Program
mTOR	mammalian target of rapamycin
OA	<u>o</u> ligomycin and <u>a</u> ntimycin A
PBS	phosphate buffered saline
PCR	polymerase chain reaction
PE	phosphatidylethanolamine
PI3K	phosphatidylinositol 3-kinase
PINK1	PTEN induced putative kinase 1

PTEN	phosphatase and tensin homolog
qRT-PCR	quantitative real-time polymerase chain reaction
RNA	ribonucleic acid
rpm	revolutions per minute
SIN	Sindbis virus
siRNA	small interfering ribonucleic acid
TEM	transmission electron microscopy
TSC	tuberous sclerosis complex
Tween 20	polyoxyethylenesorbitan monolaurate
UBD	ubiquitin-binding domain
ULK	Unc-51-like kinase
uM	micromolar
VPS	vacuolar protein sorting-associated protein
µg	microgram
µl	microliter
µm	micrometer

Perspective

Early during my training in the MSTP, I knew that I wanted to align my research focus with my clinical interests. However, I was, and still am, undecided on the clinical specialty I want to pursue in the future. Luckily for me, my training in Dr. Beth Levine's laboratory was an opportunity for me to become an expert in a basic science field which can be applied to any clinical specialty in the future. The primary research goal of the Levine laboratory is to study the molecular regulation and biological functions of the cellular process known as autophagy, with the hope that discoveries at the bench may lead to improved understanding of human disease pathogenesis and the development of clinical therapies. All the projects in the lab are related to autophagy in the context of different tissues and human diseases. Thus, I had the valuable opportunity to interact daily with colleagues who are experts in disciplines ranging from infectious diseases, metabolism, to cancer.

I explored two different projects during my dissertation research. The first project focused on understanding the molecular regulation of selective autophagy by the peroxin protein PEX13, for the clearance of viruses and damaged mitochondria from the cell. The second project characterizes the physiological changes regulated by exercise-induced autophagy, including changes to the metabolome, proteome, and breast cancer progression. These two projects are not directly related, but they appropriately reflect the two main research goals of our laboratory: to uncover the molecular mechanisms and the physiological functions of autophagy.

Chapter I: Introduction and literature review on autophagy

The word autophagy comprises two Greek roots: "auto" (self) and "phagy" (eating). It refers to any catabolic process that degrades cellular materials through the lysosome. Three main types of autophagy have been described, including macroautophagy, microautophagy, and chaperone-mediated autophagy. The most common form of autophagy in mammalian cells, macroautophagy (herein referred to as autophagy), is characterized by the formation of double-membraned structures which deliver cytoplasmic contents to the lysosome for degradation (Choi et al., 2013; Levine and Kroemer, 2008).

I.1. The autophagy pathway

Autophagy is constitutively active at low basal levels in virtually all eukaryotic cells to recycle proteins and organelles and to promote cellular homeostasis (Levine and Kroemer, 2008). Autophagy is also a highly dynamic process, regulated by various cellular stress signals such as nutrient deprivation, oxidative stress, temperature changes, physical exercise, and infections (He et al., 2012a; He et al., 2012b; Levine and Kroemer, 2008). The molecular machinery of autophagy is highly conserved from yeast to human. Yeast genetic screens led to the identification of more than 30 autophagy-related (ATG) genes, of which a subset is considered the core autophagy machinery. Numerous studies have characterized factors and pathways regulating autophagy in yeast and mammals, and are detailed in several recent reviews (Deretic et al., 2013; Feng et al., 2014; Green and Levine, 2014; He and Klionsky, 2009). The autophagy pathway proceeds in a series of steps: induction, vesicle nucleation,

membrane elongation and completion, docking and fusion with the lysosome, and finally vesicle degradation and recycling of the resulting macromolecules (Fig. 1). This section summarizes our current understanding of the autophagy pathway, including general autophagy and selective autophagy, and describes some standard assays for evaluating autophagy in tissue culture and animal models.

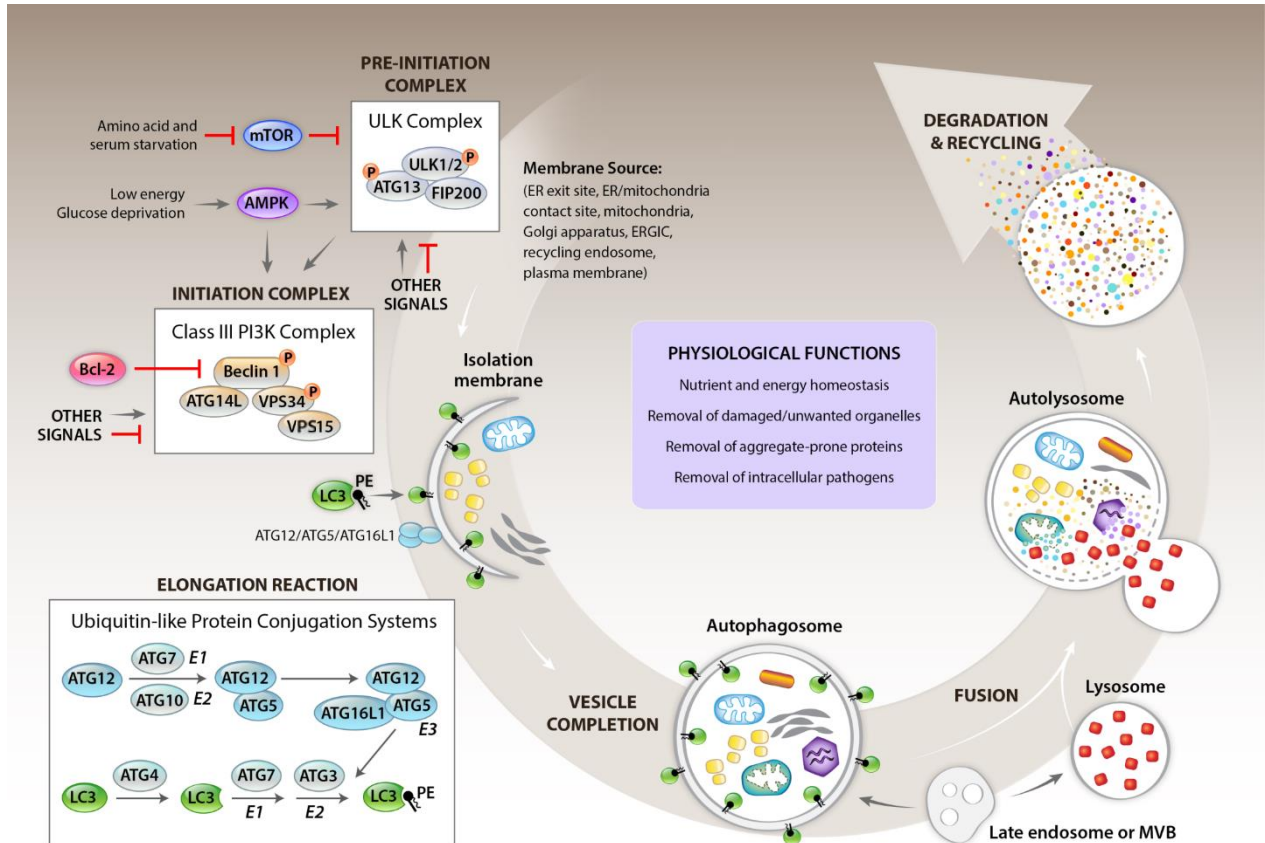


Figure 1. Overview of the general autophagy pathway.

Autophagy is activated by stress signals such as amino acid, serum, and glucose deprivation. These signals are sensed by mTOR and AMPK, then relayed to the pre-initiation ULK complex and the initiation Class III PI3K complex. Bcl-2 inhibition of Beclin 1 is important for regulating autophagy initiation. After autophagy initiation, two ubiquitin-like protein conjugation systems catalyze the generation of LC3-PE (also known as LC3-II), which stably associates with autophagic membrane and is degraded in the autolysosome. Completed autophagic vesicles are targeted to the lysosome for fusion to form the autolysosome. Lysosomal degradation regenerates cellular building blocks which are recycled to the cell. (Figure adapted from Green and Levine, 2014)

I.1.A. General autophagy

General autophagy (also known as canonical autophagy) is a nonselective process that randomly engulfs cytoplasmic contents for degradation in the lysosome. In mammalian cells, induction of general autophagy is mainly regulated by nutrient status (amino acids), growth factor signals (insulin and insulin-like growth factors), and energy levels (ATP) (He and Klionsky, 2009; Levine and Kroemer, 2008). Metabolic stress signals are integrated by mTOR and AMPK, relayed to the preinitiation complex containing ULK1/2, which then activates the initiation complex containing the Class III PI3 kinase VPS34, VPS15, ATG14L, and Beclin 1. Then, VPS34 generates phosphatidylinositol 3-phosphate (PI3P), leading to the recruitment of phagophore elongation factors to promote autophagy.

After initiation, the phagophore elongates using two ubiquitin-like protein conjugation systems involving the ubiquitin-like proteins Atg12 and LC3 (Ohsumi, 2001). These reactions conjugate LC3 to phosphatidylethanolamine (PE). The autophagy inactive precursor form of LC3-I is distributed throughout the cytosol, whereas the autophagy active form LC3-II (also known as LC3-PE) associates with autophagic membranes. LC3-II is actually the only known protein that stably associates with the autophagosome and is degraded by autophagy, thus making it a marker for monitoring autophagy.

When the double-membraned autophagosome is completely formed around the cargo, it is targeted to the lysosome for fusion to form the autolysosome. Many elements of the cellular machinery required for this process have been identified, including components of the microtubule transport machinery such as FYCO1, kinesin, and dynein, and the tethering and fusion machinery such as SNX18 (Khaminets et al.,

2016; Stolz et al., 2014). After fusion with the lysosome, the autophagosome inner membrane and the enclosed cytoplasmic substrates are degraded by lysosomal vacuolar hydrolases. In mammalian cells, autophagosomes may also fuse with endosomes to form amphisomes prior to fusion with lysosomes (Mizushima, 2007). Autophagosomes, amphisomes, and autolysosomes are not easily distinguishable by microscopy; thus, these structures are collectively termed “autophagic vacuoles”. Once the macromolecules have been degraded in the lysosome, the resulting cellular building blocks are recycled back to the cytosol for use.

I.1.B. Selective autophagy

While autophagy is generally considered a nonselective process, as early as the 1960s, Christian de Duve speculated that selective forms of autophagy may function in cells (De Duve and Wattiaux, 1966). Many subsequent yeast and mammalian studies have identified diverse substrates that can be targeted by selective autophagy, including mitochondria (mitophagy), protein aggregates (aggresophagy), peroxisomes (pexophagy), ribosomes (ribophagy), ER (reticulophagy), intracellular pathogens (xenophagy), viral components (virophagy) and lipid droplets (lipophagy) (Rogov et al., 2014; Stolz et al., 2014). In contrast to canonical autophagy (also known as general autophagy), selective autophagy functions during nutrient rich conditions to degrade specific harmful or superfluous structures while excluding other cytoplasmic contents. Thus, selective autophagy may have evolved as a more efficient way for the cell to clean house without expending excessive resources to regenerate essential cellular components. Similar to canonical autophagy, selective autophagy functions importantly in cellular homeostasis. Dysregulation of selective autophagy underlies numerous

human pathologies, including neurodegeneration, infectious diseases, metabolic diseases, cancer, and aging (Choi et al., 2013; Levine and Kroemer, 2008). The following section discusses the current molecular understanding of selective autophagy regulation and the proposed role for peroxisomal biogenesis factors PEX13 and PEX3 in selective autophagy.

I.1.C. Molecular mechanisms of selective autophagy

Selective autophagy requires the core autophagy machinery and additional factors to confer substrate specificity. Selective autophagy receptors dictate substrate specificity by physically binding to the cargo and to LC3/GABARAP family proteins on the autophagosomal membrane, thus promoting cargo engulfment by the autophagic membrane. p62, also known as sequestosome 1 (SQSTM1), is the first identified and one of the most well-characterized mammalian selective autophagy receptors. It was initially characterized in the context Huntingtin protein aggregophagy (Bjorkoy et al., 2005; Pankiv et al., 2007), and subsequently implicated in the degradation of intracellular bacteria (Yoshikawa et al., 2009) and peroxisomes (Deosaran et al., 2013). To date, more than two dozen mammalian selective autophagy receptors have been identified. Examination of these factors reveal some common themes in the molecular regulation of selective autophagy.

First, function of the selective autophagy receptor depends on its ability to associate with the phagophore. Structural analysis of p62 revealed an LC3-interacting region (LIR) domain, defined by the canonical motif W/F/Y-x-x-L/I/V (where x can be any amino acid) (Ichimura et al., 2008; Noda et al., 2008). The LIR motif has since been identified in

other autophagy receptors, including optineurin, NBR1, and NDP52, and is required for their functions in selective autophagy. Of note, the ability to bind to LC3 is not limited to autophagy receptors; core autophagy proteins such as ULK1 kinase also contains LIR motifs (Rogov et al., 2014).

The second hallmark of selective autophagy receptors is the ability to bind cargo selectively. For example, p62 contains a ubiquitin binding domain (UBD) for recognizing ubiquitinated substrates, including poly-ubiquitylated proteins during aggregophagy and mitophagy, and mono-ubiquitylated proteins during pexophagy (Rogov et al., 2014). Ubiquitination is a highly prevalent signal for marking selective autophagy substrates; however, some forms of selective autophagy are ubiquitin-independent (Khaminets et al., 2016). Optineurin, for example, mediates aggregophagy via both ubiquitin-dependent and -independent mechanisms (Korac et al., 2013). Mitophagy during reticulocyte maturation is also ubiquitin-independent. This form of mitophagy is mediated by the receptors NIX, BNIP3, and FUNDC1, which are all mitochondrial outer membrane proteins containing LIR that can directly associate with autophagic membranes (Hanna et al., 2012; Liu et al., 2012; Novak et al., 2010). In contrast, Parkin-mediated clearance of damaged mitochondria in most tissues requires ubiquitination of mitochondrial proteins. Pexophagy also occurs through both ubiquitin-dependent and ubiquitin-independent pathways (Deosaran et al., 2013; Farre et al., 2008; Motley et al., 2012). Therefore, the same substrate may have ubiquitin-dependent and ubiquitin-independent modes of clearance by autophagy. Currently characterized virophagy processes, including Sindbis viral capsid clearance mediated by SMURF1 (Orvedahl et al., 2011) and HIV-1 viral capsid clearance mediated by TRIM5 α (Mandell

et al., 2014), are ubiquitin-independent. Identification of various signals on cargos destined for selective autophagy is an active area of research.

Post-translational modifications allow another level of regulatory control during selective autophagy. As discussed above, ubiquitination commonly marks substrates for recognition by the autophagy receptors. Ubiquitination of autophagy receptors can also modulate their activity. For example, ubiquitination of optineurin by HACE1 enhances the interaction between optineurin and p62 and promotes the formation of autophagy receptor complexes (Liu et al., 2014). Aside from ubiquitination, other post-translational modifications on the selective autophagy receptors or cargos contribute to the regulation of selective autophagy. For example, phosphorylation of optineurin on its LIR increases its association with LC3, thereby promoting xenophagy of *Salmonella enterica* (Wild et al., 2011). In contrast, dephosphorylation of the LIR in FUNDC1 enhances its LC3 affinity and promotes mitophagy (Liu et al., 2012). Other forms of post-translational modifications such as acetylation contribute to general autophagy regulation (Huang et al., 2015); however, whether the same applies to selective autophagy is yet unknown.

In addition to regulation by autophagic receptors, selective autophagy also depends on factors known as autophagy adaptors. Distinct from autophagy receptors, autophagy adaptors can associate with LC3/GABARAP, but they are not degraded by autophagy. Autophagy adaptors promote various stages of autophagosome biogenesis, transport, and fusion with the lysosome (Khaminets et al., 2016; Stolz et al., 2014).

In summary, diverse selective autophagy substrates and some factors regulating their clearance have been identified. However, much of the molecular regulation for selective autophagy remains unclear. Systematic analysis through unbiased screening

approaches combined with mechanistic studies could identify novel regulators of the process.

I.1.D. Autophagy mutant mouse models

Many autophagy mutant mouse models are available for studying the role of autophagy in mammals. Most of the autophagy mutant models generated to date have systemic or tissue-specific deletions in the core autophagy machinery and lead to reduced autophagosome formation (Table 1). These mutants have defective basal autophagy as well as stress-induced autophagy and present with a wide array of disorders, including increased susceptibility to neurodegeneration, cancer, diabetes, and infectious diseases. Studies in these mice have revealed the important roles of autophagy in vivo in mammals, including development, cellular homeostasis, protein and organelle quality control, metabolism, and immunity (Levine et al., 2015).

Table 1. Diseases in mice with mutations in autophagy genes (Levine et al., 2015).

Gene	Mutation	Disease	Reference
Regulation of phagocytosis and autophagy			
<i>Irgm1</i>	Homozygous deletion	Paneth cell abnormalities and increased susceptibility to DSS-induced intestinal inflammation	S1
Autophagosome formation			
<i>Ambra1</i>	Heterozygous deletion	Increased neuropathic pain mediated by Schwann cell demyelination following peripheral nerve axonal degeneration and autism-like phenotype in females	S2, S3
<i>Atg4b</i>	Homozygous deletion	Inner ear pathology and balance disorders and decreased RGC survival after optic nerve axotomy	S4, S5
<i>Atg4c</i>	Homozygous deletion	Increased susceptibility to chemical carcinogen-induced fibrosarcomas	S6
<i>Atg5</i>	Macrophage-specific deletion	Increased inflammasome activation and atherogenesis and increased severity of pulmonary <i>M. tuberculosis</i> infection	S7–S10
	Hepatocyte-specific or mosaic system deletion	Increased liver inflammation, fibrosis, adenomas, and impaired liver regeneration after partial hepatectomy	S11–S13
	Intestinal epithelial cell-specific deletion	Paneth cell abnormalities and increased susceptibility to invasive <i>Salmonella</i> infection	S14, S15
	Neuron-specific deletion	Neurodegeneration and increased susceptibility to alphavirus encephalitis	S16, S17
	Dendritic cell-specific deletion	Impaired antigen cross-presentation and increased severity of HSV infection	S18
	Podocyte-specific deletion	Podocyte aging and increased susceptibility to glomerular diseases	S19
	Renal tubular cell-specific deletion	Impaired renal function	S20
	Lens-specific deletion	Age-related cataracts independent of organelle degradation	S21
	Thymic cell-specific deletion	Colitis and multi-organ inflammation	S22
	Myeloid cell-specific deletion	Increased susceptibility to intravenous <i>C. albicans</i> infection	S23
	B lymphocyte-specific deletion	Impaired long-lived humoral immunity	S24
	RGC-specific deletion	Decreased RGC survival after optic nerve axotomy	S5
	Inducible cardiac-specific deletion	Heart failure	S25
<i>Atg7</i>	Hepatocyte-specific deletion	Liver adenomas and impaired blood glucose regulation	S12, S26, S27
	Intestinal epithelial cell-specific deletion	Paneth cell abnormalities	S28
	Neuron-specific deletion	Neurodegeneration	S29
	Purkinje cell-specific deletion	Purkinje cell axonal degeneration	S30
	Macrophage/microglia-specific deletion	Increased susceptibility to cerebral and ocular toxoplasmosis	S31
	Hematopoietic cell-specific deletion	Anemia and lymphopenia and atypical myeloproliferation resembling human myelodysplastic syndrome	S32, S33
	Postnatal forebrain-specific conditional deletion	Age-dependent neurodegeneration	S34
	Pancreatic β -cell-specific deletion	Pancreatic β -cell destruction and diabetes	S35
	Skeletal muscle-specific deletion	Muscle atrophy	S36
	B lymphocyte-specific deletion	Impaired virus-specific B cell memory and increased susceptibility to lethal influenza virus challenge	S37
<i>Atg16l1</i>	Hypomorphic deletion	Paneth cell abnormalities and increased susceptibility to lethal chikungunya virus infection	S38, S39
	Null deletion	Enhanced IL-1 β production and susceptibility to DSS-induced colitis	S40
	T300A mutation	Defective bacterial clearance and increased inflammatory cytokine production	S41, S42
	Intestinal epithelial cell-specific deletion	Increased susceptibility to invasive <i>Salmonella</i> infection	S43
<i>Becn1</i>	Monoallelic deletion	Increased: incidence of spontaneous malignancies, susceptibility to Alzheimer's disease, severity of Desmin-related cardiomyopathy, hypoxia-induced angiogenesis, renal fibrosis following ureteral obstruction, basal renal collagen accumulation, bleeding time, susceptibility to cecal ligation and puncture-induced polymicrobial sepsis, dendritic cell-regulated Th2 cytokine production and lung pathology during respiratory syncytial virus infection, susceptibility to cerebral and ocular toxoplasmosis; reduced/impaird: platelet aggregation, exercise endurance, exercise-induced insulin sensitivity	S31, S44–S54
<i>Bif1</i>	Homozygous deletion	Increased incidence of spontaneous malignancies	S55
<i>FIP200</i>	Neuron-specific deletion	Cerebellar degeneration	S56
<i>LC3b</i>	Homozygous deletion	Increased renal fibrosis following ureteral obstruction, increased susceptibility to hypoxia-induced pulmonary hypertension	S49, S57
<i>Nrbf2</i>	Homozygous deletion	Focal liver necrosis	S58
<i>Vps15</i>	Skeletal muscle-specific deletion	Autophagic vacuolar myopathy	S59
<i>Vps34</i>	Sensory neuron-specific deletion	Neurodegeneration (through impaired endocytosis)	S60
	T lymphocyte-specific deletion	Defective T cell homeostasis and inflammatory wasting syndrome in aged mice	S61
	Liver-specific deletion	Hepatomegaly and hepatic steatosis	S62
	Cardiac-specific deletion	Cardiomegaly and decreased cardiac contractility	S62
	Podocyte-specific deletion	Proteinuria, glomerular scarring, and premature death (impaired autophagy and endocytosis)	S62
	Lens-specific deletion	Congenital cataracts and microphthalmia	S21
Autophagosome maturation and degradation			
<i>Epg5</i>	Homozygous deletion	Neurodegenerative features similar to amyotrophic lateral sclerosis	S63
<i>Lamp2</i>	Homozygous deletion	Vacuolar cardiomyopathy and skeletal myopathy	S64
<i>Sumf1</i>	Homozygous deletion	Lysosomal storage disorder and neurodegeneration	S65
<i>MPS-III A</i>	D31N missense mutation	Lysosomal storage disorder and neurodegeneration	S65
Selective autophagy			
<i>Park2/Parkin</i>	Homozygous deletion	Increased susceptibility to <i>M. tuberculosis</i> infection	S66
<i>Sqstm1/p62</i>	P394L mutation (equivalent to human P392L)	Paget's-like disease of bone	S67

DSS, dextran sodium sulphate; RGC, retinal ganglion cell.

I.1.E. Assays for monitoring autophagy

This section describes three standard assays for monitoring autophagy in mammalian systems. Detailed descriptions of other recommended assays to evaluate autophagy have been compiled by experts in the field (Klionsky et al., 2016). LC3 is the only known protein that stably associates with the autophagosome membrane, and it is degraded by autophagy. Thus, it is an important marker for autophagy. In a highly sensitive assay, fluorescence microscopy quantification of punctate LC3 with an N-terminal green fluorescent protein tag (GFP-LC3) measures autophagosome numbers (Klionsky et al., 2016; Mizushima et al., 2010). Cells or mice expressing the GFP-LC3 transgene (Kabeya et al., 2000; Mizushima et al., 2004; Orvedahl et al., 2010) are widely used to assess autophagy levels during stress (e.g. starvation). Since autophagy is a dynamic process, the number of autophagosomes in a cell is determined by both the rate of generation and the rate of degradation. When autophagic flux is blocked during late stages such as during fusion, the observed increase in GFP-LC3 puncta number is due to a decrease in clearance and not due to increased autophagy induction. To determine autophagic flux, GFP-LC3 puncta numbers should be assessed carefully in the presence and absence of lysosomal inhibitors. Lysosomal inhibitors commonly used in autophagy assays include inhibitors of lysosome acidification (e.g. Bafilomycin A1, chloroquine) and lysosomal protease inhibitors (e.g. combination of pepstatin A and E64d). Lysosomal inhibitors suppress the late stages of autophagy, which further increases GFP-LC3 puncta numbers when autophagic flux is intact. GFP-LC3 puncta quantification is typically the most sensitive method for detecting changes in autophagy.

Typically, the GFP-LC3 quantification assay is used in combination with biochemical methods for evaluation of autophagy. Conversion of endogenous LC3-I to LC3-II is monitored by western blot analysis, which shows a band shift from 19 kDa to 17 kDa. Furthermore, western blot detection of the degradation of p62, an autophagic adaptor protein and substrate, is another common assay for monitoring autophagy. Autophagic flux can also be evaluated by western blots using lysosomal inhibitors. Furthermore, the traditional gold standard for evaluating autophagy is transmission electron microscopy (TEM) image analysis. Whenever possible, the use of multiple complementary methods to assess autophagy provides the strongest evidence.

I.2. Cellular functions of autophagy

I.2.A. Adaptation to metabolic stress

During low cellular energy states, signals integrated by mTOR and AMPK upregulate autophagy as a pro-survival mechanism. Cells undergoing nutrient starvation can activate autophagy to degrade non-essential cellular proteins and organelles to generate amino acids, fatty acids, and carbohydrates to sustain macromolecular synthesis, anaplerosis, and energy production (Jiang et al., 2015). While normal cells are able to recover from short-term nutrient deprivation and continue growing and proliferating after the re-introduction of nutrients, autophagy-deficient cells are more susceptible to die during starvation (Galluzzi et al., 2014). During other forms of metabolic stress, including hypoxia and growth factor deprivation, autophagy is important for degrading non-essential components to regenerate basic building blocks

for de novo synthesis of proteins essential for stress adaptation (Levine and Kroemer, 2008).

I.2.B. Removal of toxic intracellular components

Autophagy and the proteasome system work in concert to degrade unwanted cellular components, but they have non-redundant roles. Importantly, autophagy is the only known cellular process for degrading structures too large for the proteasome system, such as intracellular pathogens, toxic protein aggregates, and damaged organelles (Choi et al., 2013; Levine and Kroemer, 2008). Autophagy selectively degrades intracellular pathogens (xenophagy), thus providing host defense against medically relevant pathogens including *Mycobacterium tuberculosis*, *Toxoplasma gondii*, and herpes simplex virus type I. Autophagy is important for the clearance of aggregate-prone mutant proteins (aggregophagy) associated with numerous neurodegenerative disorders, including Alzheimer's, Parkinson's, and Huntington's disease. Furthermore, autophagy removes damaged organelles from the cytoplasm, including mitochondria (mitophagy). Accumulation of damaged mitochondria is toxic to the cell because they produce reactive oxygen intermediates, which may promote DNA damage and genomic instability, leading to aging, cancer, and other pathologies. Thus, autophagy has an important house-cleaning function in the cell to remove toxic intracellular structures.

I.2.C. Secretion

Autophagy is traditionally viewed as a catabolic pathway; however, emerging evidence is connecting the autophagy pathway to secretion (Deretic et al., 2012; Kaur

and Debnath, 2015; Manjithaya and Subramani, 2011). In yeast, autophagy factors Atg1, Atg6, and Atg8 are required for the secretion of Acyl-CoA binding protein (Acb1), a protein known to be secreted by an unconventional mechanism because it lacks a signal peptide directing it through the classical endoplasmic reticulum-Golgi secretory pathway (Manjithaya et al., 2010). Autophagy stimulation by nutrient starvation or by rapamycin can induce Acb1 secretion in yeast and primary astrocytes from mice (Manjithaya and Subramani, 2011).

In mammals, autophagy has a role in secretion of immune mediators. Autophagy-mediated unconventional secretion regulates the secretion of the proinflammatory interleukin (IL)-1 family cytokines, IL-1 beta and IL-18 (Dupont et al., 2011). Although autophagy suppresses inflammation under basal conditions, autophagy may temporarily increase inflammation under stress conditions. Additionally, autophagy is required for the release of adenosine triphosphate (ATP) from dying cancer cells after chemotherapy (Michaud et al., 2011). In this context, extracellular ATP serves as a chemotactic ligand for immune cells, attracting T lymphocytes to the tumor to elicit immunogenic cell death. Furthermore, autophagy influences extracellular release of immune mediators including lysozymes granules, IL-6, IL-8, immunoglobulins from plasma cells (Deretic et al., 2013). Emerging evidence suggests a secretory role of autophagy, extending its cellular functions beyond autodigestion and cellular quality control. In mammals, autophagy-regulated secretion may impact inflammation and immunity.

I.3. Autophagy in human health and disease

Both the non-selective and selective types of autophagy, as well as basal and induced levels of autophagy, are important for regulation of human health and disease. Dysregulation of autophagy underlies numerous human pathologies including cancer, neurodegeneration, aging, infectious diseases, cardiovascular diseases, and pulmonary diseases, thus highlighting the important physiological roles of autophagy (Choi et al., 2013; Levine and Kroemer, 2008). The following section discusses the connection between autophagy and human disease pathogenesis and how autophagy may be manipulated for clinical therapy, focusing especially on infectious diseases, developmental disorders, and cancer.

I.3.A. Autophagy in infectious diseases

Autophagy is important for the regulation of innate and adaptive immunity, thus it has important implications in infectious diseases. Direct elimination of microorganism through autophagic degradation (xenophagy) is a major mechanism by which autophagy protects against infections. Xenophagy in vitro protects against several clinically important bacteria (e.g. group A streptococcus, *Mycobacterium tuberculosis*, *Shigella flexneri*, *Salmonella enterica*, *Listeria monocytogenes*, and *Francisella tularensis*), viruses (e.g. herpes simplex virus type 1, chikungunya virus), and parasite (e.g. *Toxoplasma gondii*) (Choi et al., 2013). In vivo, autophagy also protects against infections. For example, neuronal *Atg5*-deficiency increases cell death and mortality after Sindbis virus infection in mice (Orvedahl et al., 2010). Furthermore, treatment with Tat-beclin 1, an autophagy-inducing peptide, reduces mortality in mice infected with

chikungunya or West Nile virus, suggesting the therapeutic potential for autophagy inducers in treating some infectious diseases (Shoji-Kawata et al., 2013). The importance of xenophagy as an anti-microbial defense system is highlighted by the numerous microbial countermeasures and adaptations that microbes have evolved to evade autophagy (Deretic and Levine, 2009). In addition to degrading intracellular pathogens, autophagy also regulates inflammation, adaptive immunity, and secretion of immune mediators during infection (Deretic et al., 2013).

I.3.B. Autophagy in development and differentiation

In mammals, autophagy is important for embryonic development, survival during neonatal starvation, and cellular differentiation. Numerous whole body or tissue specific *Atg*-gene knockout mouse models suffer developmental defects and often die prematurely during embryogenesis or early postnatal period (Levine et al., 2015; Mizushima and Levine, 2010). Several underlying mechanisms have been proposed for the role of autophagy in development. First, autophagy is required for cellular remodeling by rapidly degrading unnecessary proteins and organelles. Second, autophagy is important for regeneration of amino acids for protein synthesis and glycogen for glucose and energy production. During the embryo-to-neonate transition period, autophagy is normally activated to provide an energy source when the placental nutrient supply is removed. *Atg* knockout neonates have reduced amino acids in plasma and tissues, which may contribute greatly to the premature death phenotype during the early neonatal period. Third, absence of basal autophagy in neurons of *Atg* knockout mice may contribute to suckling defects, which further exacerbates the malnutritional state. Fourth, a defect in the clearance of apoptotic corpses was observed in *Atg5*^{-/-}

embryos. The buildup of apoptotic cells could contribute to the developmental abnormalities in *Atg5*-deficient and potentially other autophagy deficient organism.

Although abundant evidence demonstrates that autophagy is required during development, it is yet unclear why different *Atg*-gene knockout mouse models present with variable severity. For example, mice deficient in some *Atg* -genes (*Beclin 1*, *FIP200*, and *Ambra1*) are embryonic lethal, mice deficient in other *Atg* -genes (*Atg3*, *Atg5*, *Atg7*, *Atg9*, and *Atg16L1*) are neonatal lethal, and mice deficient in yet other *Atg* -genes (*LC3B*) are phenotypically normal. Possible explanations may be that some *Atg* -genes may have additional functions outside of autophagy and some *Atg* -genes may have redundancy or compensatory mechanisms. Furthermore, defects in different stages of autophagy may account for the difference in phenotype severity, as mice deficient in early stages of autophagy initiation generally have more severe phenotype compared to mice deficient in later steps of autophagosome elongation (Mizushima and Levine, 2010).

I.3.C. Autophagy defects in congenital neurodevelopmental disorders

Autophagy is critical for the development and maintenance of many cell types, especially post-mitotic cells such as neurons, the role of autophagy in neural development is highlighted by the connection between autophagy defects and several neurodevelopmental disorders with multisystem involvement. Recently, autophagy genes and pathway have been implicated in the pathogenesis of several congenital neurodevelopmental disorders (Ebrahimi-Fakhari et al., 2016; Jiang and Mizushima, 2014), including Vici syndrome (Cullup et al., 2013), beta-propeller protein-associated

neurodegeneration (Saito et al., 2013), *SNX14*-associated autosomal-recessive cerebellar ataxia and intellectual disability syndrome (Akizu et al., 2015; Thomas et al., 2014), and hereditary spastic paraplegia (Oz-Levi et al., 2012; Vantaggiato et al., 2013).

This section will focus on Vici syndrome as an example of autophagy dysregulation in a monogenic congenital disorder with multisystem involvement. Vici syndrome is a multisystem disorder characterized by agenesis of the corpus callosum, bilateral cataracts, cardiomyopathy, immunodeficiency, and hypopigmentation (del Campo et al., 1999). Some patients also present with chronic anemia, liver dysfunction, and thymic aplasia (Ebrahimi-Fakhari et al., 2016). Whole exome sequencing of Vici syndrome patients identified *EPG5* as the causal mutation (Cullup et al., 2013). Fibroblasts derived from Vici syndrome patients with *EPG5* deficiency contain accumulation of LC3-positive autophagic vacuoles and autophagic adaptors NBR1 and p62 in the cytoplasm. Furthermore, *Epg5* knockdown leads to the accumulation of autophagosomes in *Caenorhabditis elegans* (Tian et al., 2010; Zhao et al., 2013), and Vici syndrome patient cells have reduced colocalization between autophagosomes and lysosomes (Cullup et al., 2013). Together, these evidences suggest that *EPG5* deficiency blocks the late stage of autophagy. Systemic impairment in autophagic flux may explain the multisystem involvement of Vici syndrome. However, the underlying mechanisms are currently unclear. Of note, *EPG5* is also involved in the endocytic pathway (Zhao et al., 2013), so further studies are required to elucidate the contribution of endocytic trafficking and autophagy to disease pathogenesis.

Additionally, the autophagy pathway is also implicated in mTOR-associated neurodevelopmental diseases such as autism spectrum disorders (ASD) (Ebrahimi-

Fakhari et al., 2016; Lee et al., 2013). Despite the complicated and heterogeneous pathophysiological mechanisms underlying ASD, a subset of ASD is caused by dysregulation in the PI3K, Akt, TSC, and mTOR signaling pathway, which also is important in regulating autophagy initiation. A recent study implicated autophagy in neuronal synaptic development, and linked autophagy deficiency with ASD behavioral phenotype in mice (Tang et al., 2014). In the *Tsc2*^{+/-} mouse model of ASD, mTOR over-activation leads to defects in dendritic spine pruning, which causes ASD-like social behaviors in mice. The defects in dendritic spine pruning and ASD-like behaviors were corrected after treatment with the mTOR inhibitor rapamycin in *Tsc2*^{+/-} mice, but not in *Tsc2*^{+/-}:*Atg7*^{CKO} neuronal autophagy-deficient mutants. Additionally, postmortem ASD patient brains contained elevated levels of p62 and reduced levels of LC3-II. Together, these data suggest that autophagy deficiency may contribute to the pathogenesis of a subset of ASD.

I.3.D. Autophagy and cancer

The exact role of autophagy in cancer is complicated and likely context- and tissue-dependent. While autophagy is generally considered as a suppressor of tumor initiation, its role in established tumors is more controversial. Several studies show that autophagy can promote tumor cell survival during metabolic stress while autophagy-deficiency in other contexts contributes to tumor progression (Choi et al., 2013; Jiang et al., 2015; Levine and Kroemer, 2008; White, 2015).

Mounting evidence support the tumor suppressive function of autophagy during the early stage of tumor initiation. The first genetic evidence for autophagy functioning as a

tumor suppressor was demonstrated using the *beclin 1* heterozygous knockout mouse, which have decreased autophagy and increased spontaneous tumorigenesis in vivo (Qu et al., 2003; Yue et al., 2003). Furthermore, monoallelic deletion of *beclin 1* is found in high percentage of human breast, ovarian, and brain tumors (Liang et al., 1999; Miracco et al., 2007; Tang et al., 2015). Together, this suggests that Beclin 1 mutation and autophagy deficiency are likely important in the pathogenesis of human cancers. Furthermore, targeted deletion of other core autophagy genes, *Atg5* and *Atg7*, also promotes tumorigenesis in liver in mice (Inami et al., 2011; Takamura et al., 2011).

Genetic studies reveal that many important signals regulating autophagy and tumorigenesis overlap, and that autophagy modulation is mechanistically important in the cancer regulatory function of some tumor suppressors and oncogenes (Levine and Kroemer, 2008). Tumor suppressor genes in the TOR signaling pathway, including AMPK, PTEN, TSC1, and TSC2, are also positive regulators of autophagy (Levine and Kroemer, 2008). The most commonly mutated tumor suppressor gene in human cancers, p53, is another positive regulator of autophagy (Crighton et al., 2006; Feng et al., 2005). Moreover, several proto-oncogenes have overlapping functions as autophagy inhibitors. For example, Bcl-2 and Bcl-X_L function as apoptosis suppressors at the mitochondria, and they are commonly overexpressed in cancers (Kroemer, 1997). Endoplasmic reticulum-localized Bcl-2 and Bcl-X_L can inhibit autophagy initiation by binding to Beclin 1 (Klionsky et al., 2012; Pattingre et al., 2005). Akt and EGFR can also exert their oncogenic potential through inhibition of Beclin 1 and autophagy (Wang et al., 2012; Wei et al., 2013). Thus, autophagy is generally accepted as a tumor suppressive pathway in pre-cancer cells.

Possible mechanisms by which autophagy inhibits tumor initiation include removal of damaged mitochondria. Abnormal mitochondria are a source of oxidative stress that could lead to activation of the DNA damage response and genomic instability, which is a well characterized tumorigenic process (Choi et al., 2013; Levine and Kroemer, 2008; White, 2015). In addition, although autophagy is generally a pro-survival pathway, certain stresses cause excess autophagy activation and autophagic cell death. Removal of cells undergoing extreme stress and damage may serve as an additional mechanism by which autophagy protects against development of tumors (Jiang et al., 2015).

Though autophagy is generally considered as an inhibitor of tumor initiation, autophagy may serve a paradoxical role in promoting continued progression in certain established cancers. As solid tumors grow rapidly, focal regions suffer metabolic stresses due to insufficient blood supply. Under such conditions, autophagy provides an energy source for continued survival and enables the cells to resume growth and proliferation after restoration of nutrients (Jiang et al., 2015; Mathew et al., 2007a). Similarly, during cancer chemotherapy or radiation therapy, autophagy may be activated to promote tumor survival by helping cancer cells cope with cytotoxic stress (Amaravadi et al., 2007; Maiuri et al., 2007). Additionally, a highly active autophagy pathway is essential for tumor cell mitochondrial homeostasis in certain tumors which are driven by *Ras* and *B-Raf* oncogenes. These tumors have an “autophagy addiction”, and die when autophagy is inhibited (Guo et al., 2011; Guo et al., 2013; Strohecker et al., 2013; Yang et al., 2011a).

Whether autophagy protects against the progression of established tumor is unclear, although several possible mechanisms have been proposed. First, as mentioned above,

excess autophagy activation can lead to autophagic cell death and may be a mechanism for eliminating cancer cells under stress. When autophagy is unable to help cancer cells overcome stress induced during chemotherapy or radiation treatments, autophagy may switch from a cytoprotective process to a cytotoxic process. (Choi et al., 2013; Jiang et al., 2015). Tumor cells that are deficient in both apoptotic and autophagy pathways may die from necrosis under metabolic stress, leading to local inflammation which may further stimulates tumor growth (Degenhardt et al., 2006). Second, autophagy deficiency may lead to genomic instability and further activation of oncogenes in metabolically stressed cells such as rapidly growing cancers (Mathew et al., 2007b). A third possibility is that autophagy directly downregulates growth by degrading specific cellular components essential for cell cycle regulation. Beclin 1 expression in tumor cells causes a decrease in expression of cyclin E and phosphorylated Rb, and is associated with decreased proliferation while not affecting cell death (Koneri et al., 2007; Liang et al., 1999). Furthermore, autophagic degradation of lamin B1 may be a mechanism by which autophagy promotes oncogene-induced senescence (Liu et al., 2013; Shimi et al., 2011; Young et al., 2009). By promoting senescence in cells expressing oncogenes, autophagy provides dual protective functions to inhibit the cell from malignant transformation (cell-intrinsic function) and to activate danger signals through factors secreted by the senescent cell that promote innate immunity responses against cancer cells. This benefits the whole organism and is a cell-extrinsic function of autophagy in cancer protection (Galluzzi et al., 2016). Finally, emerging evidence suggests that autophagy may be required for chemotherapy-induced anti-cancer immune responses via the release of adenosine triphosphate (ATP)

from dying tumor cells (Michaud et al., 2011). Ongoing research efforts are focused on clarifying the relationship between autophagy activation and cancer protection after tumor initiation and exploring the possibility of autophagy modulation in cancer therapy.

I.3.E. Manipulating autophagy for clinical applications

Manipulation of autophagy has important potential therapeutic potentials for numerous human diseases; autophagy induction may benefit the numerous diseases related to autophagy deficiency whereas autophagy suppression may be helpful in combination of cancer chemo- and radiation-therapy.

Rapamycin is one of the most commonly used drugs to stimulate autophagy (Meijer and Codogno 2006). It functions by inhibiting mTOR, a major negative regulator of autophagy. Other over-the-counter nutritional supplements including caffeine, vitamin D, spermidine, resveratrol, omega-3 polyunsaturated fatty acids, and trehalose induce autophagy and provide health benefits (Levine et al., 2015). However, these autophagy-inducing agents generally have pleiotropic downstream effects. Thus, development of more selective autophagy inducers may provide a broader therapeutic window and will be helpful for research efforts to clarify the role of autophagy in various disease pathogenesis. Besides inducing autophagy via bioactive molecules, caloric restriction and physical exercise are lifestyle modification methods that induce autophagy. Further clinical studies are required to define safe and efficacious levels of lifestyle modification for the prevention of disease in the general population and as an adjuvant treatment in specific disease populations.

Several pharmacological inhibitors for autophagy are available, including the FDA-approved antimalarial drugs chloroquine and its derivative hydroxychloroquine. These drugs inhibit lysosomal acidification thus block the late stage of autophagy, but they also have other effects on lysosome-dependent pathways (Yang et al., 2011b). Currently, multiple clinical trials are ongoing to evaluate the efficacy of inhibiting autophagy during cancer therapy (Choi et al., 2013; Kroemer, 2015). However, the safety of these and any future autophagy-inhibitory compounds should be carefully assessed, as chronic and systemic suppression of autophagy may induce many adverse effects (Karsli-Uzunbas et al., 2014).

Chapter II. PEX13 and PEX3 function in selective autophagy

II.1. Literature Review

II.1.A. Genome-wide screen for selective autophagy factors

While the understanding of the selective autophagy process has improved rapidly during recent years especially in yeast, many questions remain regarding its molecular regulation as well as its relevance to human health and disease. To address this gap in knowledge, the Levine laboratory conducted a genome-wide siRNA screen to systematically identify novel mammalian selective autophagy factors (Orvedahl et al., 2011). Since the phenomenon of autophagic degradation of viral components has been described, but the mechanism is largely unknown (Orvedahl et al., 2010; Sumpter and Levine, 2010), the primary screen was designed to identify genes regulating viroplasm formation.

Previously, autophagy-mediated protection against viruses was demonstrated using in vivo and in vitro models of Sindbis virus (SIN) infections. SIN is a neurotropic single-stranded RNA virus of the alphavirus family, which includes medically important pathogens such as Chikungunya virus. SIN was chosen for these studies because it can be used simultaneously as a neuronal pathogen and a vector for gene delivery in vivo (Orvedahl et al., 2010). Expression of Beclin 1 promoted autophagy and protected mice from fatal SIN encephalitis, reduced cell death in infected neurons, and restricted viral replication in infected brains (Liang et al., 1998). Furthermore, inactivation of another core autophagy gene, *Atg5*, in SIN-infected neurons delayed clearance of viral nucleocapsid and increased neuronal cell death (Orvedahl et al., 2010). Together, these studies demonstrated the protective function of autophagy against SIN infection. Thus,

the screen used SIN infection to identify factors that selectively regulate targeting of viruses to the autophagosome but are not required for general autophagy.

The mechanisms of xenophagy, mitophagy, and other forms of selective autophagy have a high level of overlap, possibly stemming from a common evolutionary history of these pathways. For example, p62 is implicated in both mitophagy and xenophagy (Stolz et al., 2014). Thus, to determine whether factors required for selective SIN virophagy intersects with factors required for selective mitophagy, positive candidates from the primary virophagy screen were tested in a secondary screen for Parkin-mediated mitophagy.

In contrast to virophagy, a relatively recently described phenomenon, mitophagy is one of the best-characterized forms of selective autophagy in higher eukaryotes. Two major forms of mitophagy have been described: Parkin-independent and Parkin-dependent. Parkin-independent mitophagy regulates clearance of mitochondria during erythrocyte differentiation, and is mediated by NIX, BNIP3, and FUNDC1 (Hanna et al., 2012; Liu et al., 2012; Novak et al., 2010). Parkin-mediated mitophagy is the major pathway for removing damaged mitochondria from cells. During this process, PTEN-induced kinase 1 (PINK1) functions as a sensor of membrane potential, a major distinguishing feature between healthy and damaged mitochondria. PINK1 is constitutively imported into functional mitochondria for degradation in a membrane potential-dependent manner. In depolarized mitochondria, PINK1 is stabilized on the outer mitochondrial membrane, leading to the recruitment of Parkin, a cytosolic E3 ubiquitin ligase. Parkin subsequently ubiquitylates multiple mitochondrial outer

membrane proteins, which are recognized and clustered through the polymerization of p62 (Narendra et al., 2010).

Our understanding of the mitophagy process has expanded rapidly during recent years, likely due to the connection between mitophagy defects and neurodegenerative disorders. Although the prevailing model suggests that clustering of ubiquitinated mitochondrial proteins recruit autophagy receptors to initiate mitophagy (Green and Levine, 2014), some evidence suggests Parkin and p62 may not be essential mitophagy under certain conditions (Lazarou et al., 2015; Narendra et al., 2010). Recent work by Dr. Richard Youle's group showed that PINK1 generates a phospho-ubiquitin signal on the mitochondria, independently of Parkin, and that this signal recruits the receptor optineurin and NDP52 to initiate mitophagy (Lazarou et al., 2015). Thus, the functional significance of p62, Parkin, and mitochondrial clustering in mitophagy is still controversial. The exact mechanism by which the phagophore forms around damaged mitochondria likely requires other yet-to-be-identified factors.

In summary, the genome-wide siRNA screen identified 141 candidate virophagy factors, of which 96 genes were also required for Parkin-mediated mitophagy. Follow up biochemical and imaging experiments confirmed that the candidate SMURF1 is indeed required for selective virophagy, mitophagy, and not starvation-induced general autophagy (Orvedahl et al., 2011). Thus the screen revealed molecular factors that may be involved in autophagic targeting of viral nucleocapsids as well as damaged mitochondria. Molecular characterization of these candidate selective autophagy factors may provide novel insights into the regulation and disease relevance of selective autophagy.

II.1.B. Peroxisome biogenesis factors

Peroxin family members *PEX13* and *PEX3*, were identified as candidate factors involved in selective virophagy and mitophagy in the previous genome-wide siRNA screen described above (Orvedahl et al., 2011). Fourteen human *PEX* genes have been characterized thus far, encoding peroxin proteins that function in various stages of peroxisome biogenesis, including membrane formation, import of peroxisomal matrix proteins, and peroxisome proliferation (Fig. 2.1) (Fujiki et al., 2014; Wanders, 2004). Similar to other *PEX* genes, *PEX13* (Gould et al., 1996; Liu et al., 1999) and *PEX3* (Ghaedi et al., 2000; Shimozawa et al., 2000) were originally identified and have been best-studied in the context of their roles in peroxisome biogenesis and Zellweger syndrome spectrum (ZSS) disorders, a subtype of peroxisome biogenesis disorders characterized by prominent neurodevelopmental, hepatic, and renal abnormalities leading to neonatal death. Severe hypotonia, facial dysmorphic signs, sensorineural deafness, and ocular abnormalities have also been described in ZSS patients (Klouwer et al., 2015; Wanders, 2004).

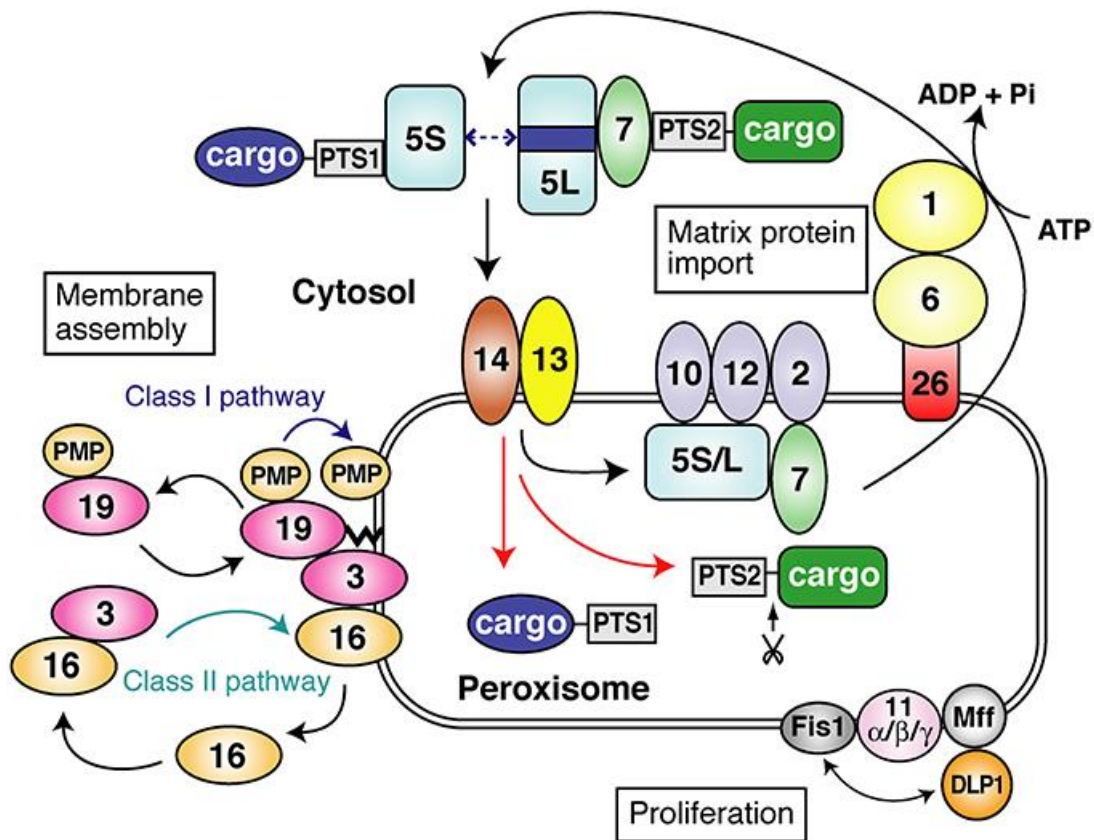


Figure 2.1. Overview of mammalian peroxisome biogenesis factors.

Peroxisins are classified into three categories: factors required for membrane assembly; factors required for matrix protein import; and factors required for peroxisome proliferation. The cytosolic or peroxisome-membrane localization of these factors are shown in the figure. Of note, PEX3 and PEX19 both function as membrane assembly factors, and PEX13 and PEX14 function in matrix protein import. Cells with defective PEX3 or PEX19 have no peroxisome structures at all, whereas cells with defective matrix protein import machinery contain empty “peroxisome ghosts”. (Figure adapted from Fujiki et al., 2014).

Biochemically, many ZSS patients present with elevated levels of substrates normally processed by peroxisomes (e.g. very long-chain fatty acids) and reduced levels of products normally synthesized by peroxisome metabolism (e.g. plasmalogen) (Wanders and Waterham, 2006). However, ZSS patients with normal peroxisome metabolite levels have been described, and the degree of peroxisomal metabolite abnormality does not always correlate with clinical severity (Rosewich et al., 2006; Wanders and Waterham, 2005; Zeharia et al., 2007). The discrepancy in the

biochemical and clinical phenotypes of ZSS patients suggests that at least a subset of PEX mutations may contribute to ZSS disease pathogenesis via additional molecular mechanisms independently of their role in peroxisome biogenesis.

Aside from defects in peroxisomes, dysfunctional mitochondria are also frequently associated with ZSS and mutations in *PEX* genes. Abnormal mitochondrial structures with curvilinear cristae have been observed by ultrastructural analysis of tissues from ZSS patients and mouse models (Baumgart et al., 2001; Maxwell et al., 2003), and these abnormal mitochondria have been suggested to contribute to ZSS disease pathogenesis (Baumgart et al., 2001; Salpietro et al., 2015). The current prevailing paradigm is that mitochondrial dysfunction in ZSS is secondary to the defect in peroxisomal anti-oxidant functions and the accumulation of lipid metabolites from the β -oxidation process (Baumgart et al., 2001). In the current project, I am interested in evaluating whether certain *PEX* mutations can lead to mitophagy defects, and thereby contribute to the accumulation of abnormal mitochondria in ZSS.

The possibility that peroxin proteins are involved in selective virophagy and mitophagy raised some intriguing questions about peroxisome biology and function of peroxisome-associated proteins. Peroxisomes were first discovered in the 1960s (De Duve and Baudhuin, 1966) and most work characterizing peroxisomes have focused on the metabolic functions such as fatty acid beta-oxidation, cholesterol biosynthesis, hydrogen peroxide generation, and scavenging of reactive oxygen species. However, the peroxisome is increasingly recognized as a more complex organelle during the past decade. For example, Mitochondrial Antiviral Signaling Protein (MAVS) localizes to the both the mitochondria and the peroxisome, and peroxisomal MAVS has antiviral signal

transduction roles complementary to mitochondrial MAVS (Dixit et al., 2010). Furthermore, peroxisomes are implicated as an important signaling site for reactive oxygen species (ROS)-induced autophagy through the TSC1/TSC2 signaling complex (Zhang et al., 2013). These studies provide the first examples of peroxisome-associated proteins functioning as signaling nodes.

Through the current study characterizing *PEX13* and *PEX3* as selective autophagy factors, we have the potential to elucidate the regulation of the selective autophagy pathway as well as uncover novel functions for the peroxisome or peroxisome-associated proteins. One possible mechanism for peroxins functioning in selective autophagy is through their function in peroxisome formation. Currently, aside from pexophagy and pexophagy regulation, peroxisomes and peroxisomal proteins have not yet been linked to other forms of selective autophagy. Alternatively, the selective autophagy function of *PEX13* and *PEX3* may be independent of their canonical function as peroxisome biogenesis factors. In either scenario, this work would provide novel insight into peroxisome biology.

II.2. Introduction

PEX13 is an integral membrane protein on the peroxisome that regulates peroxisomal matrix protein import during peroxisome biogenesis. Mutations in *PEX13* and other peroxin proteins are associated with Zellweger syndrome spectrum (ZSS) disorders, a subtype of peroxisome biogenesis disorder characterized by prominent neurological, hepatic, and renal abnormalities leading to neonatal death (Wanders, 2004). The lack of functional peroxisomes in ZSS patients is widely accepted as the

underlying cause of disease; however, our understanding of disease pathogenesis is still incomplete. Here, we demonstrate that PEX13 is required for selective autophagy of Sindbis virus (virophagy) and of damaged mitochondria (mitophagy), and that disease-associated PEX13 mutants I326T and W313G are defective in mitophagy. The selective mitophagy function of PEX13 is shared with another peroxin family member PEX3, but not with two other peroxins, PEX14 and PEX19, which are required for general autophagy. Together, our results demonstrate that PEX13 is required for selective autophagy, and suggest that dysregulation of PEX13-mediated mitophagy may contribute to ZSS pathogenesis.

II.3. Materials and Methods

II.3.A. Cell culture

HeLa cells (Li et al., 1997) and HEK293T cells were cultured in DMEM containing 10% fetal bovine serum (FBS), 2 mM L-glutamine, and 1x penicillin/streptomycin at 37°C and 5% CO₂. HeLa/GFP-LC3 cells (Orvedahl et al., 2010) were cultured in media containing 10 µg/mL G418. HeLa/Parkin cells were generated by stable transfection of a pIRES-hyg 3 vector (Clontech) expressing Parkin cDNA and cultured in media containing 100 µg/ml hygromycin B. HeLa/HA-Parkin cells were generated by retroviral transduction and cultured in media containing 0.25 µg/ml puromycin (see “Retroviruses and Lentiviruses” section below for details). HeLa/Parkin cells were stably transfected with pIRES-neo 3 vectors expressing WT PEX13-Flag, PEX13-Flag I326T, PEX13-Flag W313G, or no cDNA, selected with media containing 500 µg/ml G418 until single colonies formed, and then maintained on media containing 100 µg/ml G418.

MEFs were maintained in DMEM containing 15% FBS, 1x penicillin/streptomycin, 120 μ M β -mercaptoethanol, and 1x MEM non-essential amino acids. Culture media was changed every 3-4 days and cells were passaged 1:5 or 1:10 when they reached confluency. Primary MEFs were passaged prior to reaching 100% confluency, and passaged no more than four times.

To harvest or passage cells, cells were washed with PBS once, trypsinized for 2-5 minutes at 37°C, then resuspended in fresh media to inactivate the trypsin. Cell numbers were counted using an automated cell counter (BioRad). For starvation experiments, cells were cultured in Hank's balanced salt solution (HBSS) (Sigma, H9269) or Earle's balanced salt solution (EBSS) (Sigma, E7510) for the indicated time period.

II.3.B. Generation of mouse embryonic fibroblasts

Pex13^{+/+} and *Pex13*^{-/-} primary MEFs were derived from embryonic day 13.5 (E13.5) embryos by crossing *Pex13*^{+/-} mice (Maxwell et al., 2003; Su et al., 2003). Additionally, mice that transgenically express GFP-LC3 (Mizushima et al., 2004) were crossed with *Pex13*^{+/-} mice to obtain *Pex13*^{+/-}/GFP-LC3 mice, and this strain was bred to harvest *Pex13*^{+/+}/GFP-LC3 and *Pex13*^{-/-}/GFP-LC3 MEFs. All animal procedures were performed in accordance with institutional guidelines and with approval from the UT Southwestern Medical Center Institutional Animal Care and Use Committee.

Pregnant female mice were euthanized by isoflurane (Butler Schein) and submerged in 70% ethanol for five minutes. Embryos were extracted into ice-cold PBS and dissected to remove placental tissues, the head, and internal organs. The remaining

embryonic tissue was washed three times with ice cold PBS, transferred to 50 ml conical tubes containing 3 ml DMEM, homogenized by passing through 18 gauge needles five times, then treated with 10 μ l DNase (50 mg/ml, Sigma) and 500 μ l Trypsin EDTA (0.25%, Gibco) for 15 minutes in a 37°C shaker. Cells were dispersed in 5 ml MEF media by pipetting, allowed to settle for 10 minutes, and then transferred to 10 cm culture dishes coated with gelatin. Cells were cultured at 37°C and 5% CO₂.

II.3.C. PCR genotyping

To extract genomic DNA from mouse tails, ears, or toes, a small piece of tissue was cut from each mouse, and digested in tail PCR DNA digestion solution and proteinase K at 55 °C for 4 hours to overnight, and then heat-inactivated at 85 °C for 1 hour. The samples were centrifuged for 1 minute at maximum speed to pellet the tissue debris. Supernatant containing genomic DNA was used for PCR genotyping. The following reaction mixes were used for PCR amplification of DNA: 0.5 μ l genomic DNA, 0.25 μ l primer #1 at 100 μ M, 0.25 μ l primer #2 at 100 μ M, 10 μ l SapphireAmp Fast PCR Master Mix (Takara, RR350A), and 9 μ l dH₂O. PCR products were separated using 1.0% to 2.0% agarose gels in TAE buffer containing ethidium bromide and visualized using an imager (Alphalmager HP).

II.3.D. Generating and reviving frozen stocks of cultured cells

All cell lines were expanded at low passage and frozen as stocks. Seventy-five cm² flasks of confluent cells were harvested by trypsinization and resuspended in 1 ml freezing medium (50% DMEM, 40% FBS, 10% DMSO). Cells were frozen at -80°C

overnight in a freezing container (Thermo Scientific) and then transferred to liquid nitrogen for long-term storage. Frozen cell stocks were thawed quickly in a 37°C water bath, and resuspended in 10 ml culturing media in 75 cm² flasks.

II.3.E. Chemicals and reagents

Antimycin A (Santa Cruz), oligomycin (Santa Cruz), CCCP (Sigma), and bafilomycin A1 (Sigma) were resuspended in DMSO (Sigma). Antimycin A and oligomycin were stored in aliquots at -80°C. CCCP and bafilomycin A1 were stored in aliquots at -20°C.

II.3.F. Antibodies

Primary antibodies for immunofluorescent staining include the following: rabbit anti-TOMM20 (Santa Cruz sc-11415, 1:1000), mouse anti-Parkin (Cell Signaling 4211, 1:1000), mouse anti-DNA (Millipore CBL186, 1:1000), mouse anti-PEX13 (Santa Cruz sc-271477, 1:100), rabbit anti-PMP70 (Thermo Scientific PA1-650, 1:1000), mouse anti-Flag (Sigma 184-200UG, 1:1000), and rabbit anti-WIP1 (Abcam ab105459, 1:500). Secondary antibodies were conjugated to AlexaFluor488, AlexaFluor594, and/or AlexaFluor647 (Invitrogen, 1:750). Primary antibodies for western blot analyses include the following: rabbit anti-ATG7 (Sigma A2856, 1:1000), mouse anti-PEX13 (Santa Cruz sc-271477, 1:200), guinea pig anti-p62 (Progen GP62-C, 1:1000), rabbit anti-LC3 (Novus NB100-2220, 1:1000), and HRP-conjugated mouse anti-actin (Santa Cruz sc-47778-HRP, 1:2000).

II.3.G. Constructs

The pCMV6 vector expressing human PEX13-MYC-DDK was purchased from Origene. *PEX13* disease-associated mutants I326T and W313G, siRNA-resistant constructs, and constructs without MYC-DDK tags were generated using QuikChange II Site-Directed Mutagenesis kit (Agilent Technologies). *PEX13* constructs with resistance to si*PEX13* oligo #2 were generated using two successive steps. Primers are listed in Table 2.1.

Table 2.1. Mutagenesis primers for *PEX13* constructs

Primer	Sequence
W313G Forward	AACCCAAAGTGCCTGGTGGGCTTCTGGCTAG
W313G Reverse	CTAGCCAGAAGCCCACCACGCACTTTGGGTT
I326T Forward	GCCTTGATGGCCAAACAACAGGACTTACGCCTGCGAATTATGTC
I326T Reverse	GACATAATTCGCAGGCGTAAGTCCTGTTGTTTGGCCATCAAGGC
siRNA-resistance Step 1 Forward	CTTTTCAGCTGTCTATAACAGTTTCCGTGCCGTCCTGGATGTAGCA AATCACTTTTCCC
siRNA-resistance Step 1 Reverse	GGGAAAAGTGATTTGCTACATCCAGGACGGCACGGAAACTGTTAT AGACAGCTGAAAAG
siRNA-resistance Step 2 Forward	TTTCAGCTGTCTATAACAGCTTTCCGTGCCGTCCTGGATGT
siRNA-resistance Step 2 Reverse	ACATCCAGGACGGCACGAAAGCTGTTATAGACAGCTGAAA
Tag removal Forward	GAAAGATGGAGAAAAGCAAGATCTTTAGCGTACGCGGCCG
Tag removal Reverse	CGGCCGCGTACGCTAAAGATCTTGCTTTTCTCCATCTTTC

II.3.H. Retroviruses and lentiviruses

pMXs-IP-HA-Parkin (Yoshii et al., 2011) (Addgene #38248) was cotransfected with the helper plasmids pUMVC and pCMV-VSV-G (Stewart et al., 2003) (Addgene #8849 and #8454) into HEK293T cells. *PEX13* cDNAs containing WT, W313G mutation, and I326T mutation were cloned into pLenti-C-Myc-DDK-IRES-Neo vector (Origene), and then cotransfected into HEK293 cells with the helper plasmids pCMV Δ R8.91 (Zufferey et al., 1997) and pMDG (Naldini et al., 1996). Retro- or lentiviral supernatant was filtered through a 0.45 μ m membrane and then added to target cells in the presence of polybrene (8 μ g/ml). Cells were selected in media containing 0.5 μ g/ml puromycin or

500 µg/ml G418 and then maintained in media containing 0.25 µg/ml puromycin and/or 100 µg/ml G418.

II.3.I. Generating and titering Sindbis virus

Recombinant Sindbis virus strains SIN-mCherry.capsid (strain AO30) and SIN-mCherry.capsid/GFP-LC3 (strain AO28) were generated previously using the recombinant SIN vector dsTE12Q as a backbone (Liang et al., 1998; Orvedahl et al., 2010). Infectious virus was produced from SIN recombinant chimeric vectors as described (Hardwick and Levine, 2000). Ten µg plasmid DNA was linearized by XhoI digestion for 8 hours at 37°C, purified using QIAQuick PCR purification kit (Qiagen), and quantified using a spectrophotometer (NanoDrop2000). Linearized DNA templates were transcribed in vitro using mMessage mMachine SP6 kit (Invitrogen) and the resulting infectious viral RNA was immediately transfected into 95% confluent BHK21 cells using Lipofectamine 2000 (Thermo Fisher). Supernatant containing infectious SIN virus was collected 24 to 48 hours after transfection, centrifuged for 1 minute to remove cell debris, and stored in aliquots at -80°C to avoid freeze-thaw degradation.

Viral titers were determined using plaque assays on BHK21 cells and Vero cells. 5×10^5 BHK21 cells and Vero cells were seeded on 6-well plates and infected after overnight incubation when they reach 80-90% confluency. Viral stocks were diluted in DMEM with 1% FBS to generate 10-fold serial dilutions ranging from 10^{-4} to 10^{-7} . Medium was aspirated completely, and 0.2 ml virus dilution was added to each well in triplicates. Plates were rocked vigorously to ensure even infection covering the wells. Repeat rocking was performed every 10 minutes while plates incubated at 37°C for 1 hour. After infection, 2 ml overlay medium (1.5% methylcellulose, MEM without phenol

red, 1% FBS) was added to each well. The plates were incubated for 2 to 3 days at 37°C, until plaques were visible under the microscope. To stain for plaques, plates were shaken quickly to remove overlay media, fixed with 100% methanol >10 minutes, stained with 0.5% crystal violet for >10 minutes, and washed under running tap water until plaques were visible. After plates air-dried, plaques were counted in all wells that contained 5-150 plaques to determine the viral titer.

II.3.J. Sindbis virophagy colocalization assay

SIN-mCherry.capsid infections of HeLa/GFP-LC3 cells were performed at a multiplicity of infection (MOI) of 5 plaque-forming units (PFUs) per cell for 10 hours. SIN-mCherry.capsid/GFP-LC3 infections of primary MEFs were performed at an MOI of 2.5 PFUs per cell for 16 hours. Fluorescent microscopy images were analyzed by an observer blinded to experimental condition and the number of mCherry-capsid puncta, GFP-LC3 puncta, and colocalized mCherry-capsid/GFP-LC3 puncta were counted per cell.

II.3.K. Mitophagy assays

HeLa/Parkin cells were treated with 10 μ M CCCP for 16 hours, fixed and then subjected to immunofluorescence staining to detect TOMM20. The number of cells with <10 mitochondria/cell and with >10 mitochondria/cell were counted by an observer blinded to experimental condition. For rescue experiments, HeLa/Parkin cells were treated with siRNA for 24 hours, transfected with plasmids expressing siRNA-resistant WT or mutant PEX13 for an additional 24 hours, and then treated with CCCP for 16

hours. Additionally, HeLa/HA-Parkin cells were treated with 2.5 μ M oligomycin A and 250 nM antimycin A for 8 hours, fixed, subjected to immunofluorescence staining to detect dsDNA, and analyzed by CellMask immunofluorescence imaging using Z-stacks (see “Immunofluorescence Microscopy and Image Analysis” section below for details). Primary MEFs were treated with 30 μ M CCCP for 24 hours, fixed, and then subjected to immunofluorescence staining to detect TOMM20. The number of cells with mitochondrial compaction around the nucleus and the number of cells with diffuse fragmentation of damaged mitochondria was counted by an observer blinded to experimental condition.

II.3.L. siRNA transfection

siRNA sequences and the source of siRNAs are provided in Table 2.2. siRNA was transfected using Lipofectamine 2000 (Invitrogen) or RNAiMAX (Invitrogen) at a final concentration of 50 nM according to the manufacturer’s instructions 48 hours before experiments.

Table 2.2. siRNA sequences

Gene	siRNA #	Sequence	Source
NC	1	UAAGGCUAUGAAGAGAUAC	Dharmacon
NC	2	AUCCGCGCGAUAGUACGUA	Sigma
NC	3	UUACGCGUAGCGUAAUACG	
<i>ATG7</i>		GGGUUAAUUACUACAAUGGUG	Dharmacon
<i>PEX3</i>	1	GGAUAAUUUACCUGGAUA	
	2	CGAGACAUUACCACUUAUA	
	3	GUAAACGGACAGAUCCAUAU	
	4	CCAAGCACGACGACAAUAU	
<i>PEX5</i>	1	GCACACGGCCAGUGACUUU	
	2	CGUCAGCUACCUAUGAUAA	
	3	CUAUAGAGUUGCAGGCAGA	
	4	GCGGAGGUGUCUGGAGCUA	
<i>PEX13</i>	1	GAUGAUCUCCACCCAGUA	
	2	UUUCAGGGCUGUAUUGGAU	
	3	GUAUCUUUACAGACGGCUA	
	4	AGGACUUUAUACCUGCGAAU	
<i>PEX14</i>	1	GAACUCAAGUCCGAAUUA	
	2	CCUCAUAUCUCAGCCAUAAC	
	3	CCAGACAGUGACUCAGUUA	
	4	AGGCAUUGCAUUUGGCUUU	
<i>PEX19</i>	1	CUUCAGAACUCCAGCAUGU	
	2	GCUACAAGAUUUAGGCCAU	
	3	CAAUGAAGGAGUUGGCUGA	
	4	GCUCUUGAUGAUUUUCGAUA	
<i>MAVS</i>	1	CCACCUUGAUGCCUGUGAA	Integrated DNA Technologies
	2	CAGAGGAGAAUGAGUAUAA	
	3	AGUAGAGAGAGUAGAAUAACAAATC	
	4	GCAACCUAUUGAUCUCUAUCUCUGA	
	5	AGCCGAACAUACGUAAUAAACUGATC	
<i>GNAI3</i>	1	CCAAGGAGAUCUAUACUCA	Dharmacon
	2	GGGAAUAUCAGCUCAAUGA	
	3	GAAUAUCCCAGUCUAACUA	
	4	UGUUAUAGUUGGCGGCAGU	

II.3.M. Western blot analyses

Cultured cells were lysed in buffer containing 150 mM NaCl, 25 mM HEPES, 1 mM EDTA, 1% triton-X, protease inhibitor mixture (Roche Applied Sciences), and Halt phosphatase inhibitor cocktail (Thermo Scientific) for 1 hours at 4°C, centrifuged briefly to remove cell debris, boiled in Laemmli buffer containing 2.5% β -mercaptoethanol for 5 minutes to denature proteins. Proteins were separated by SDS-PAGE, and then transferred to PVDF membranes using transfer buffer containing 1x Tris/CAPS buffer

(BioRad 1610778) and 15% methanol in dH₂O. Membranes were blocked in 5% milk for 1 hours and then incubated in the indicated antibodies. Membranes were imaged using ECL Prime Western Blotting Detection Reagent (GE Healthcare) or Supersignal®West Pico Chemiluminescent Substrate kit (Pierce) on a digital imaging system (BioSpectrum, UVP).

II.3.N. General autophagy analysis by western blot and GFP-LC3 puncta

quantification

Autophagic flux was assessed by western blot detection of p62 and by quantitating GFP-LC3 puncta in the presence or absence of Baf A1. GFP-LC3 puncta in *Pex13^{+/+}*/GFP-LC3 MEFs, *Pex13^{-/-}*/GFP-LC3 MEFs, and in HeLa/GFP-LC3 cells were quantified by an observed blinded to experimental condition as previously described (Pattingre et al., 2005; Shoji-Kawata et al., 2013). Cells were cultured on glass chamber slides (Lab-Tek), treated for 3 hours with HBSS (Sigma, H9269) or normal culturing media, in the presence or absence of 10 nM Baf A1, a lysosomal inhibitor. Slides were washed once with PBS supplemented with calcium and magnesium, fixed with 2% paraformaldehyde (PFA) in PBS, and then mounted with VectaShield containing DAPI (Vector). Direct fluorescence images of GFP-LC3 were acquired with a Zeiss AxioImager Z2 microscope equipped with a Photometrics CoolSnap HQ2 camera and a Zeiss PLAN APOCHROMAT 63x/1.4 NA oil objective using the same acquisition time for all samples within each experiment. Triplicate samples of 50-100 cells were quantified per experiment.

II.3.O. Immunoprecipitation-mass spectroscopy

HeLa/Parkin cells stably expressing WT PEX13-Flag, PEX13-Flag W313G, and empty vector control were treated with either 10 μ M CCCP or DMSO vehicle control for 4 hours, and then collected for co-immunoprecipitation. Cells were scraped from ten 15 cm dishes for each experimental group, transferred to 50 ml conical tubes, centrifuged at 100 x g for 5 minutes, washed three times with ice cold PBS, then stored at -80 °C until lysis. Each sample was lysed with 10 ml lysis buffer (50 mM Tris HCl pH 7.4, 150 mM NaCl, 1% Triton X-100, Halt phosphatase inhibitor, and Roche EDTA-free proteinase inhibitor MINI cocktail) for 1 hour at 4 °C then centrifuged at max speed for 3 minutes to remove cell debris. Meanwhile, protein G beads and Flag-AC beads (Sigma) were washed with the lysis buffer three times. Next, lysates were precleared with 10 μ l protein G beads for 1 hours at 4°C then centrifuged at 3,000 rpm for 1 minute to remove the beads. Five percent of precleared lysates were collected to measure input protein level. Remaining precleared lysates were incubated with 10 μ l Flag-AC beads at overnight at 4 °C for immunoprecipitation. Samples were centrifuged at 3,000 rpm for 1 minutes to pellet the Flag beads. Flag beads were washed three times for 5 minutes with washing buffer (25 mM HEPES, 150 mM NaCl, 1% TritonX-100, 1 mM EDTA), eluted twice with 100 μ l 3x Flag peptide (100 μ g/ml, Sigma F4799) for > 1 hour at 4 °C. The Flag elution fraction and the input lysate were boiled with Laemelli buffer with 2.5% β -mercaptoethanol and separated by SDS-PAGE for either silver staining, colloidal blue staining, or western blot analysis. Unique protein bands were identified on the silver stained gel, and the corresponding bands were cut on the colloidal blue gel for mass spectroscopy analysis by our collaborators Dr. James Chen at the University of Texas

Southwestern Medical Center and Dr. Shi Chen at the National Institute for Biological Sciences, Beijing.

II.3.P. Immunofluorescence microscopy

HeLa cells and MEFs were cultured on glass chamber slides (Lab-Tek), fixed in 2% PFA in PBS containing calcium and magnesium, permeabilized in 0.5% triton X-100/PBS, and then blocked with blocking buffer (0.5% BSA and 0.2% cold fish gelatin in PBS). Slides were incubated with primary antibodies overnight at 4°C, secondary antibodies at room temperature for 1 hours, and then mounted with VectaShield containing DAPI (Vector). Negative control samples with only secondary antibody staining were used to determine background immunofluorescence levels. For experiments involving cellular segmentation, CellMask Deep Red (ThermoFisher C10046, 1:5000) was applied with secondary antibodies. Z-stack images were acquired with a Zeiss AxioImager Z2 microscope equipped with a Photometrics CoolSnap HQ2 camera and a Zeiss PLAN APOCHROMAT 20x/0.8 NA air objective using the same acquisition time for all samples within each experiment.

II.3.Q. Image analysis

Z-stack images were deconvolved using AutoDeBlur (Bitplane) and analyzed using the Cell module in Imaris version 8.0 (Bitplane). For images stained for dsDNA related to quantitative image analysis of mitochondria DNA clearance, nuclear DNA staining was masked using Imaris by generating a nuclear surface using the DAPI channel and then setting non-DAPI signal within the nuclear surface to zero.

II.3.R. Quantitative real time-PCR (qRT-PCR)

Total RNA was isolated from cells using the RNeasy Plus Mini Kit and eluted in water (Qiagen). RNA quality and quantity were evaluated using a spectrophotometer (NanoDrop2000). RNA samples with 260/280 absorption ratio between 1.9 and 2.1 and 260/230 absorption ratio between 2.0 and 2.4 were considered to be of sufficient quality. One μ g RNA was used to generate cDNA using iScript cDNA synthesis kit (BioRad). The cDNA product was diluted 1:20 using water prior to qRT-PCR analysis. qRT-PCR analysis was performed using the SYBR Green Master Mix (Qiagen) in a 96-well format. Each reaction contained 1x Quantifast SYBR Green PCR Master Mix, 5 μ l dilute cDNA product, and 1 μ M final concentration of the forward and reverse primers. The PCR included 5 minutes at 95°C for heat activation, then 45 cycles of 10 seconds at 95°C for denaturation and 30 seconds at 60°C for annealing/extension using a 7500 Fast Real-Time PCR System (Applied Biosystems). Relative quantification for mRNA levels was calculated using delta delta CT analysis, using ACTB or GAPDH as housekeeping gene control. Primers for the reactions are listed in Table 2.3.

Table 2.3. qRT-PCR primer sequences for quantifying knockdown of *PEX* genes

Gene	Forward	Reverse
<i>Actin</i>	CGTGAAAAGATGACCCAGATCA	CTGGATGGCTACGTACATGGCT
<i>GAPDH</i>	ACCACCATGGAGAAGGCTGG	CTCAGTGTAGCCCAGGATGC
<i>PEX3</i>	TCTGTATGGAATTTTCTGAAACGCC	ACCCGCAAAAGAACAACCAG
<i>PEX5</i>	AGCAGATTGAGCAGTCAAACCTT	TTGGGACCAGTCAGTCTCATT
<i>PEX13</i>	GGGCCCCACTTTCCAATCTG	TACACGGAGGCGGTTGTAGC
<i>PEX14</i>	GCCACGGCAGTGAAGTTTCTA	GCTGGAAGGCCATATCAATCTC
<i>PEX19</i>	GATCACAGAAAAGTATCCAGAATGGTT	CGAGCCTTTTGAGTGGTTTCAC

II.3.S. Mouse embryonic tissue sample preparation for electron microscopy

Tissues from *Pex13*^{+/+} and *Pex13*^{-/-} day 18.5 (E18.5) embryos were collected from pregnant *Pex13*^{+/-} female mice that were crossed with *Pex13*^{+/-} male mice. Embryos were extracted into PBS on ice and then dissected individually. The heart, brain, liver, and skeletal muscle from the thigh were dissected as quickly as possible and fixed with 2.5% glutaraldehyde in 0.1 M sodium cacodylate buffer (pH 7.4) overnight at 4°C. The heart, liver, and skeletal muscles were dissected into 1 mm³ pieces prior to fixation, and the whole brain was fixed to preserve architecture. Samples were rinsed in 0.1 M sodium cacodylate buffer, post-fixed with 1% osmium tetroxide and 0.8% potassium ferricyanide in 0.1 M sodium cacodylate buffer for 1.5 hours at room temperature, rinsed with water, and then en bloc stained with 4% uranyl acetate in 50% ethanol for 2 hours. Next, samples were dehydrated with increasing concentrations of ethanol, transitioned into resin with propylene oxide, infiltrated with Embed-812 resin and polymerized in a 60°C oven overnight. Blocks were sectioned with a diamond knife (Diatome) on a Leica Ultracut 6 ultramicrotome (Leica Microsystems) and collected onto copper grids, post stained with 2% aqueous uranyl acetate and lead citrate.

II.3.T. Mouse embryonic fibroblast preparation for electron microscopy

Pex13^{+/+} and *Pex13*^{-/-} primary MEF cells were cultured in 10 cm dishes, treated with 30 µM CCCP or DMSO vehicle control for 24 hours, rinsed with PBS, and then fixed with 2.5% glutaraldehyde in 0.1 M sodium phosphate buffer. After 10 minutes fixation, cells were released from the plastic dishes by gentle scraping, transferred into conical tube, kept in the same fixative for 1 hour at room temperature, and then pelleted. Cell

pellets were rinsed once with 0.1 M sodium phosphate buffer, twice with 0.1 M sodium cacodylate buffer, and then embedded in 3% agarose. Agarose blocks were sliced into 1 mm³, rinsed with 0.1 M sodium cacodylate buffer, and post-fixed in 1% osmium tetroxide and 0.8 % potassium ferricyanide in 0.1 M sodium cacodylate buffer for 1.5 hours at room temperature. Cells were rinsed with water and en bloc stained with 4% uranyl acetate in 50% ethanol for 2 hours. They were dehydrated with increasing concentrations of ethanol, transitioned into propylene oxide, infiltrated with Embed-812 resin and polymerized in a 60°C oven overnight. Blocks were sectioned with a diamond knife (Diatome) on a Leica Ultracut 6 ultramicrotome (Leica Microsystems) and collected onto copper grids, post stained with 2% aqueous uranyl acetate and lead citrate.

II.3.U. Electron microscopy imaging

Transmission electron microscopy images were acquired using a JEOL 1200EX microscope equipped with an SIS Morada CCD camera at 120 kV. Tissue samples were imaged from 7,500x to 25,000x and MEFs were imaged at 30,000x.

II.3.V. Statistical analyses

Student's t-test was used for pairwise comparisons of means of normally distributed data. ANOVA with adjustment for multiple comparisons was used for comparing multiple conditions to a single control. Mann-Whitney U-test was used for pairwise comparisons of non-normally distributed data. Kruskal–Wallis H-test was used for comparing multiple sets of non-normally distributed data.

II.4. Results

II.4.A. PEX13 is required for Sindbis virophagy and not starvation-induced general autophagy

To evaluate whether *PEX13* is a bona fide selective virophagy factor, we examined the colocalization of mCherry-labeled capsid protein from Sindbis virus (SIN) and the autophagosomal marker GFP-LC3 in cells with normal or reduced *PEX13* expression (Fig. 2.2). SIN is a single-stranded RNA virus in the alphavirus family, and numerous previous studies have shown that SIN viral nucleocapsids are degraded by selective autophagy (Orvedahl et al., 2010; Orvedahl et al., 2011). In HeLa cells stably expressing GFP-LC3 (HeLa/GFP-LC3 cells) and infected with SIN, four siRNA oligos that target *PEX13* (Fig. 2.2a) resulted in a decrease in colocalization between mCherry-capsid and GFP-LC3 puncta that was similar to that observed with an siRNA that targets *ATG7*, a core autophagy gene essential for autophagic vesicle elongation (Fig. 2.2b,c). The numbers of mCherry-capsid puncta and GFP-LC3 puncta were not decreased in *PEX13*-deficient cells (Fig. 2.2d,e), suggesting that the reduced number of colocalized puncta is likely due to a block in targeting the viral capsid to the autophagosome rather than deficiencies in either viral replication or autophagosome formation.

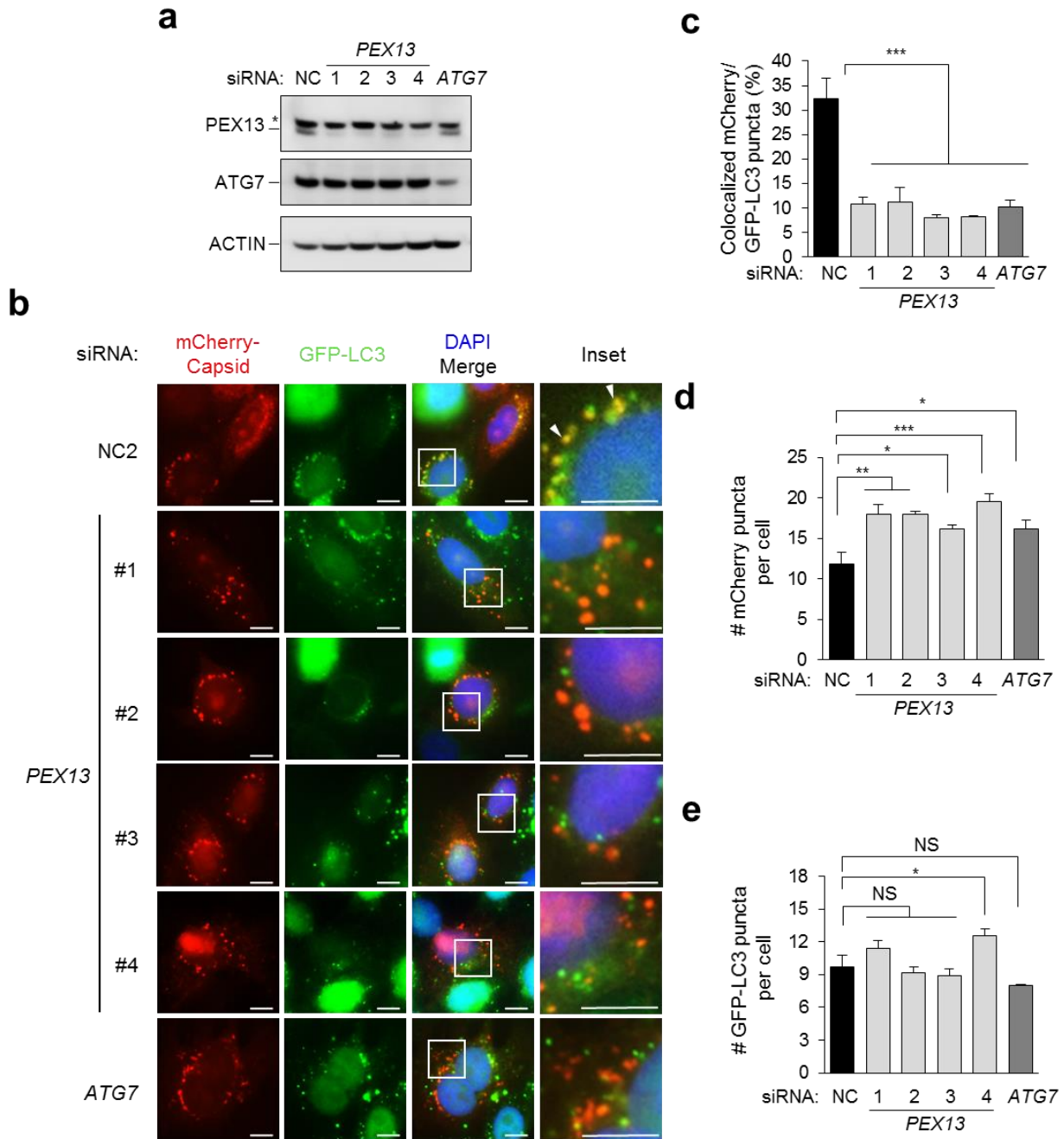


Figure 2.2. PEX13 is required for Sindbis virophagy in HeLa cells.

(a) Western blot detection of PEX13 and ATG7 in HeLa/GFP-LC3 cells transfected with the indicated siRNA. Asterisk denotes non-specific band. (b) Representative images of GFP-LC3 colocalization with mCherry-capsid at 10 h after Sindbis virus (strain AO30) infection of HeLa/GFP-LC3 cells treated with the indicated siRNA. Arrowheads denote representative colocalized GFP-LC3/mCherry-capsid puncta. Scale bars, 10 μ m. (c-e) Quantification of colocalized GFP-LC3 and mCherry-capsid puncta normalized to the number of mCherry-capsid puncta per cell (% colocalization) (c), mCherry-capsid puncta per cell (d) and GFP-LC3 puncta per cell (e) in the experiment shown in b. Bars are mean \pm SEM of triplicate samples (~100 cells analyzed per sample). Similar results were observed in more than three independent experiments. * p <0.05, ** p <0.01, *** p <0.001, NS= not significant; one-way ANOVA with adjustment for multiple comparisons.

Next, we utilized murine embryonic fibroblasts (MEFs) derived from wild-type *Pex13* (*Pex13*^{+/+}) and knockout *Pex13* (*Pex13*^{-/-}) embryos to further confirm whether *Pex13* is required for SIN virophagy (Fig. 2.3). After infection with SIN expressing mCherry-capsid and GFP-LC3, *Pex13*^{-/-} MEFs showed a defect in the colocalization of mCherry-capsid with GFP-LC3 (Fig. 2.3b), and no difference in the mCherry-capsid (Fig. 2.3c) or GFP-LC3 (Fig. 2.3d) puncta numbers.

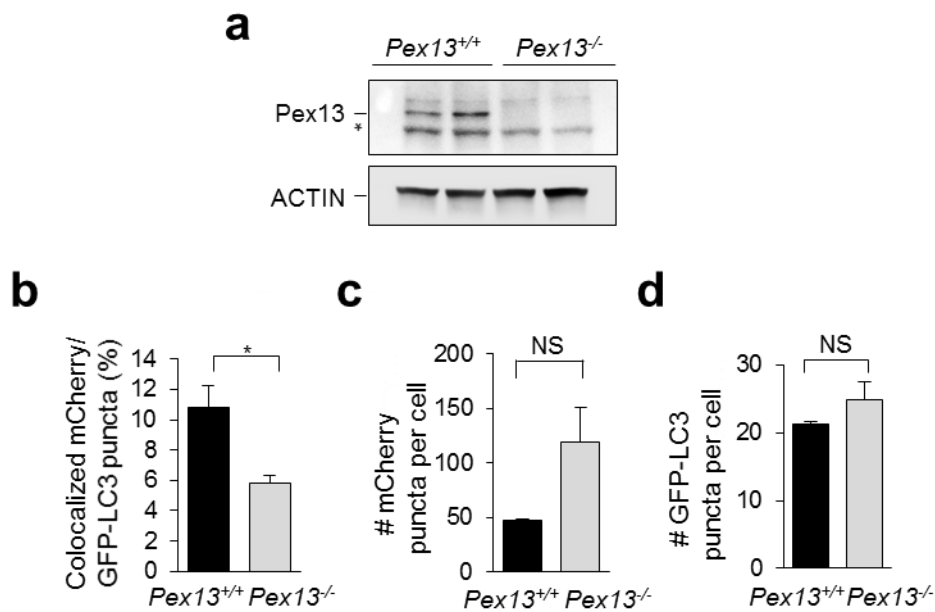


Figure 2.3. *Pex13* is required for Sindbis virophagy in MEFs.

(a) Western blot detection of *Pex13* in MEFs of indicated genotype. Asterisk denotes non-specific band. (b-d) Quantification of colocalized GFP-LC3 and mCherry-capsid puncta normalized to the number of mCherry-capsid puncta per cell (b), mCherry-capsid puncta per cell (c) and GFP-LC3 puncta per cell (d) at 8 h after Sindbis virus (AO28 strain) infection in MEFs of the indicated genotype. Bars are mean \pm SEM of triplicate samples (~100 cells analyzed per sample). Similar results were observed in more than three independent experiments. * $p < 0.05$, NS= not significant; t-test.

The defect in SIN virophagy in *Pex13*-deficient MEFs is not due to a defect in general autophagy, as assessed by three well-established assays to measure basal and starvation-induced autophagic flux. Data from western blot detection of p62 degradation, western blot detection of LC3-I to LC3-II conversion (Fig. 2.4a), and quantitation of

GFP-LC3 puncta (Fig. 2.4b) in the presence or absence of the lysosomal inhibitor, Baf A1, did not reveal any decreases in basal or starvation-induced autophagic flux in *Pex13*^{-/-} MEFs. Thus, taken together, our data indicate that PEX13 is required for selective virophagy but not for general autophagy in mammalian cells.

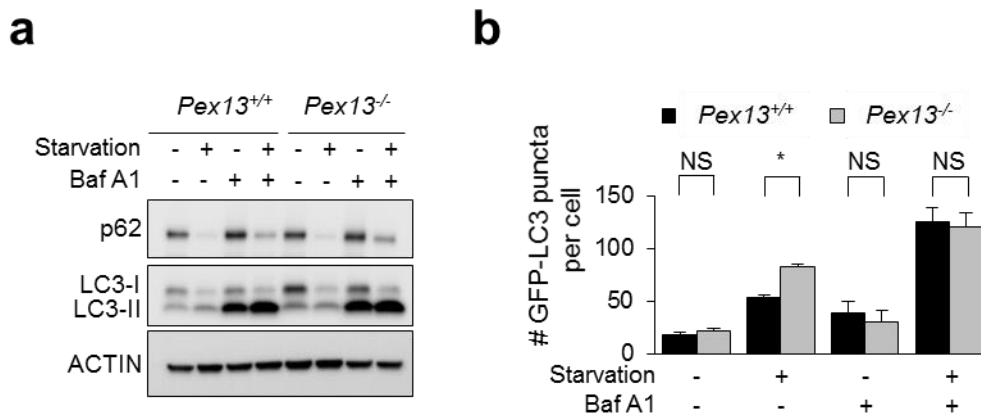


Figure 2.4. PEX13 is not required for starvation-induced general autophagy.

(a) Western blot detection of p62 and LC3 in MEFs of indicated genotype treated with 100 nM Baf A1 or DMSO vehicle and cultured in normal medium (starvation “-”) or EBSS (starvation “+”) for 3 h. Similar results were observed in three independent experiments. (b) Quantification of GFP-LC3 puncta in MEFs treated with 10 nM Baf A1 or DMSO vehicle and cultured in normal medium or HBSS (starvation “+”) for 3 h. Bars are mean ± SEM of triplicate samples (~100 cells analyzed per sample). *p<0.05, NS= not significant; t-test.

II.4.B. PEX13 and PEX3 are required for mitophagy

To evaluate whether PEX13 is a mitophagy factor, we first compared the effects of *PEX13* and *ATG7* siRNA knockdown on Parkin-mediated mitophagy after treatment with the mitochondrial uncoupling agent carbonyl cyanide m-chlorophenyl hydrazine (CCCP) using HeLa cells stably transfected with Parkin (HeLa/Parkin cells) (Fig. 2.5). *PEX13* or *ATG7* knockdown (Fig. 2.5a) did not affect basal mitochondrial morphology as assessed by immunofluorescence imaging of TOMM20, a mitochondrial outer membrane protein (Fig. 2.5b). After CCCP treatment, the majority of Parkin-expressing

cells treated with noncoding (NC) siRNA lacked TOMM20 signal, indicating clearance of damaged mitochondria (Fig. 2.5b,c). In contrast, the clearance of damaged mitochondria was impaired after treatment with four different siRNAs targeted against *PEX13*; the level of impairment was similar to that observed after treatment with siRNA targeted against *ATG7*. These results confirm the function of *PEX13* as a selective autophagy factor using similar criteria as the initial genome-wide screen (Orvedahl et al., 2011).

We confirmed the role of *PEX13* in mitophagy using a combination of more selective inhibitors of mitochondrial respiration, oligomycin and antimycin A (OA), as CCCP may have direct effects on inhibiting lysosomal function (Padman et al., 2013). We used the clearance of mitochondrial double-stranded DNA (dsDNA) as a marker for mitophagy in this assay, as the proteasomal system can contribute to the degradation of mitochondrial outer membrane proteins such as TOMM20 but not to dsDNA or mitochondrial inner membrane proteins (Yoshii et al., 2011). Our results indicate that four different siRNAs targeting *PEX13* block OA-induced dsDNA clearance as effectively as *ATG7* siRNA (Fig. 2.5d,e).

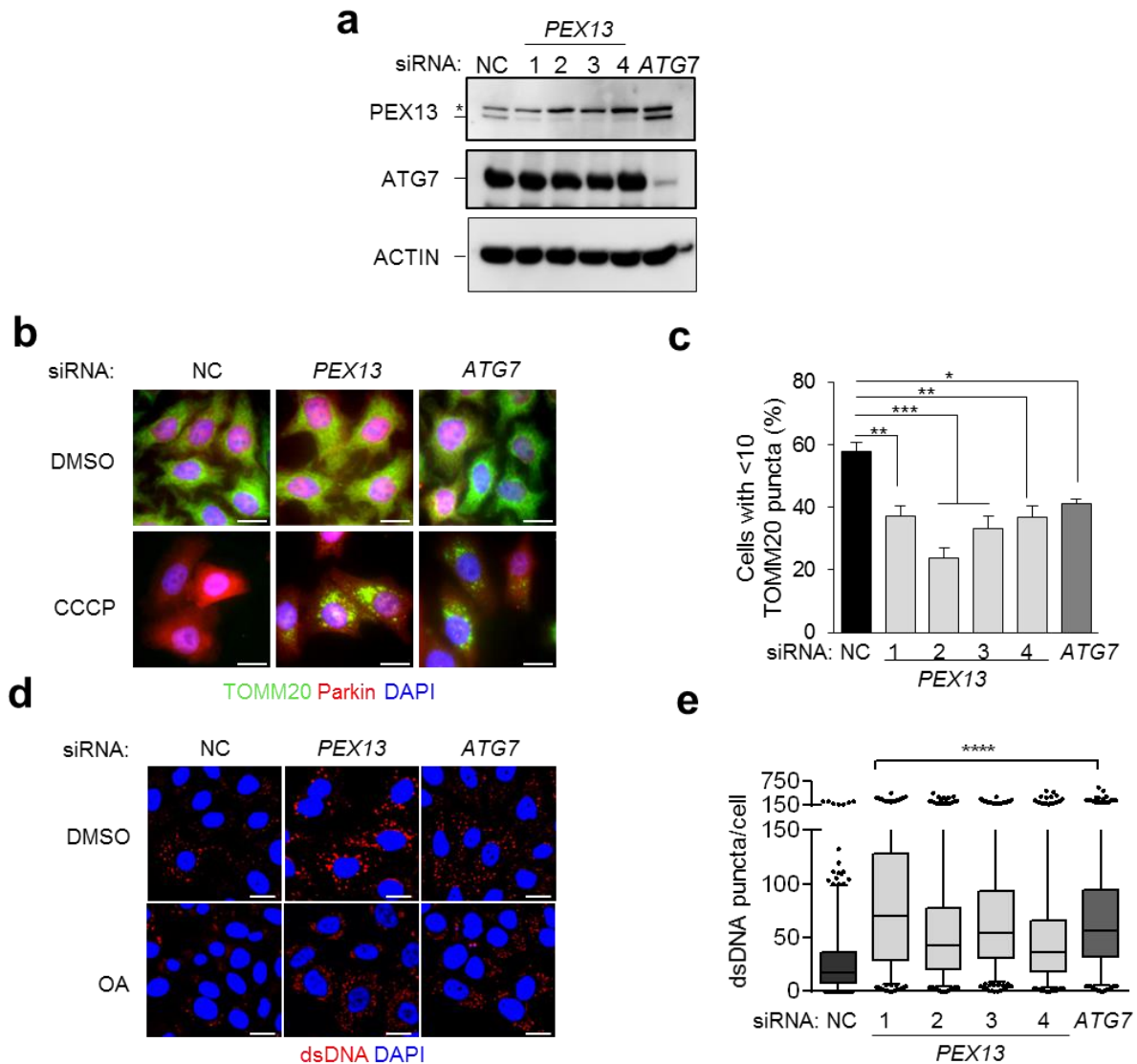


Figure 2.5. PEX13 is required for Parkin-mediated mitophagy in HeLa cells.

(a) Western blot detection of PEX13 and ATG7 in HeLa/GFP-LC3 cells transfected with the indicated siRNA. Asterisk denotes non-specific band. (b) Representative images of Parkin-mediated clearance of TOMM20 in HeLa/Parkin cells treated with indicated siRNA 16 h after treatment with 10 μ M CCCP or DMSO vehicle control. si*PEX13* oligo #2 is shown; similar results were observed with three other si*PEX13* oligos. Scale bars, 20 μ m. (c) Quantification of TOMM20 clearance in the experiment shown in b. Results represent mean \pm SEM of triplicate samples (\sim 100 cells analyzed per sample). Similar results were observed in more than three independent experiments. * p <0.05, ** p <0.01, *** p <0.001; one-way ANOVA with adjustment for multiple comparisons. (d) Representative images of Parkin-mediated clearance of mitochondrial double-stranded DNA (dsDNA) in HeLa/HA-Parkin cells treated with indicated siRNA at 8 h after treatment with 2.5 μ M oligomycin and 250 nM antimycin A (OA) or DMSO vehicle control. si*PEX13* oligo #1 is shown; similar results were observed with three other si*PEX13* oligos. Nuclear dsDNA staining was masked using DAPI channel. Scale bars, 20 μ m. (e) Quantification of dsDNA clearance in the experiment shown in d. Results represent box plots of > 150 cells analyzed per sample. Whiskers represent 5%-95% range, and each outlier is represented by a dot. Similar results were observed in three independent experiments. **** p <0.0001; Kruskal-Wallis H-test.

Using siRNA knockdown with four individual oligos targeting *PEX3*, we also evaluated whether *PEX3* is a mitophagy factor. *PEX3* knockdown (Fig. 2.6a) did not affect basal mitochondrial morphology as assessed by immunofluorescence imaging of TOMM20 (Fig. 2.6b). After CCCP treatment, TOMM20 clearance is defective in three out of four si*PEX3*-treated samples with greater than 80% mRNA knockdown (Fig. 2.6c). Cells treated with si*PEX3* oligo #4 showed 75% mRNA knockdown and a trend for reduced TOMM20 clearance (Fig. 2.6a-c). Additionally, OA-induced dsDNA clearance was defective in cells treated with four out of four si*PEX3* oligos (Fig. 2.6d,e). The discrepancy between the results for si*PEX3* oligo #4 from the two mitophagy assays may result from the increased sensitivity of quantifying dsDNA puncta number as a readout for mitophagy compared with a binary readout we used for TOMM20 clearance. Based on these data, we conclude that a deficiency in *PEX3* or *PEX13* are required for mitophagy, whereas *PEX14* and *PEX19* are dispensable.

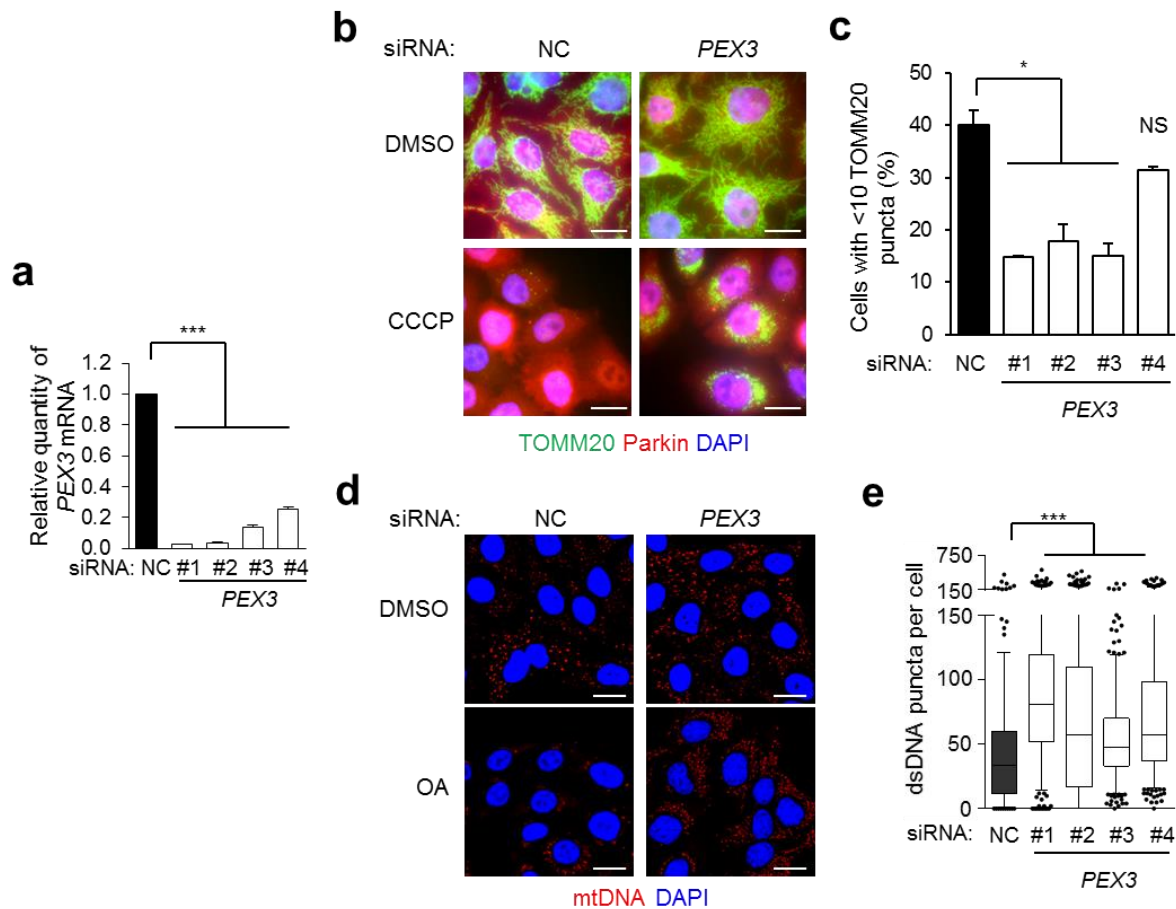


Figure 2.6. PEX3 is required for Parkin-mediated mitophagy in HeLa cells.

(a) Quantitative real-time PCR of *PEX3* detection in HeLa/Parkin cells transfected with indicated siRNA. *** $p < 0.001$; one-way ANOVA with adjustment for multiple comparisons. (b) Representative images of Parkin-mediated clearance of TOMM20 in HeLa/Parkin cells transfected with indicated siRNA and after treated for 16 h with DMSO vehicle control or 10 μ M CCCP. Scale bars, 20 μ m. (c) Quantification of TOMM20 clearance in the experiment shown in b. Results represent mean \pm SEM of triplicate samples (~100 cells analyzed per sample). Similar results were observed in more than three independent experiments. * $p < 0.05$, *** $p < 0.001$, NS, not significant; one-way ANOVA with adjustment for multiple comparisons. (d) Representative images of Parkin-mediated clearance of mitochondrial dsDNA after 8 h of treatment with 2.5 μ M oligomycin and 250 nM antimycin A (OA) or DMSO vehicle control in HeLa/HA-Parkin cells treated with indicated siRNA. si*PEX3* oligo #1 is shown, similar results were observed with three other si*PEX3* oligos. Nuclear dsDNA staining was masked using DAPI channel. Scale bars, 20 μ m. (e) Quantification of dsDNA clearance in the experiment shown in d. Results represent box plots of >150 cells analyzed per sample. Whiskers represent 5%-95% range, and each outlier is represented by a dot. Similar results were observed in three independent experiments. *** $p < 0.001$; Kruskal-Wallis H-test.

Next, we evaluated mitochondrial morphology in *Pex13*^{+/+} and *Pex13*^{-/-} primary MEFs.

Endogenous Parkin expression is negligible in MEFs (Yoshii et al., 2011), and Parkin

overexpression in primary MEFs does not promote the complete clearance of TOMM20 during CCCP or OA-induced mitophagy as it does in HeLa cells. However, damaged mitochondria in primary MEFs do undergo Parkin-independent partial clearance and compaction around the perinuclear region (Orvedahl et al., 2011). Under basal conditions, we observed similar reticular mitochondria morphology in *Pex13*^{+/+} and *Pex13*^{-/-} MEFs, as assessed by TOMM20 immunostaining (Fig. 2.7a). After CCCP treatment, TOMM20 staining showed that damaged mitochondria were compacted around the perinuclear region and partially degraded in *Pex13*^{+/+} MEFs, whereas damaged mitochondrial fragments accumulated diffusely throughout the cytoplasm in *Pex13*^{-/-} MEFs (Fig. 2.7a,b). Using electron microscopy, however, we observed abnormal mitochondria with disorganized cristae in *Pex13*^{-/-} MEFs even during basal conditions (Fig. 2.7c). After CCCP-treatment, many autolysosomes containing mitochondria and only a few cytoplasmic damaged mitochondria were found in CCCP-treated wild-type MEFs, suggesting that damaged mitochondria were degraded via autophagy. In contrast, damaged mitochondria accumulated in CCCP-treated *Pex13*^{-/-} MEFs. Thus, Pex13 facilitates removal of damaged mitochondria, even in primary fibroblasts that lack Parkin expression.

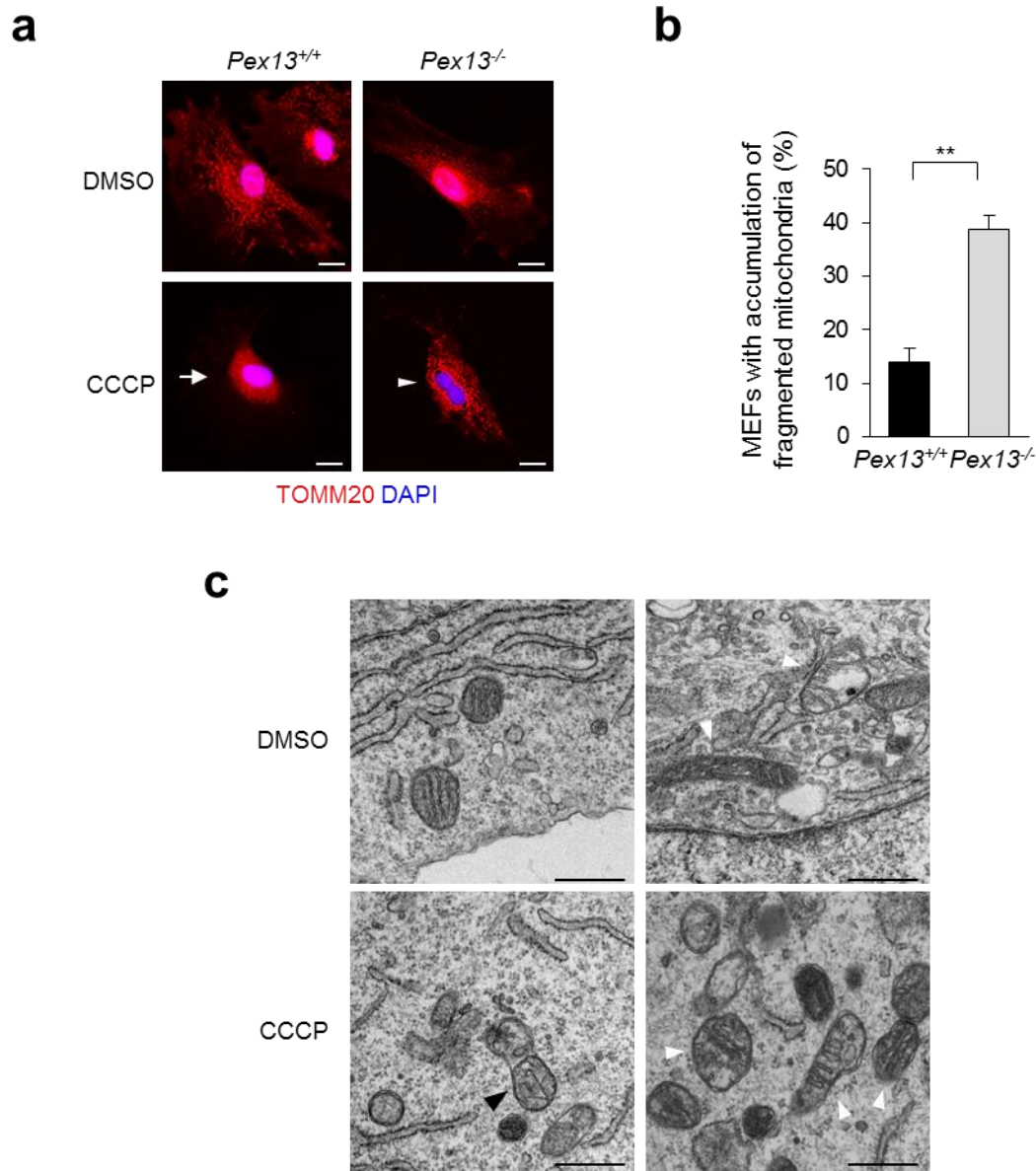


Figure 2.7. Pex13 is required for mitophagy in MEFs.

(a) Representative images of TOMM20 fragmentation (arrowhead) or compaction around perinuclear region (arrow) in MEFs of the indicated genotype 24 h after treatment with 30 μ M CCCP or DMSO vehicle control. Scale bars, 20 μ m. (b) Quantification of percentage of cells in experiment shown in e with accumulation of fragmented mitochondria (labeled by TOMM20 immunostaining) after CCCP treatment. Results represent mean \pm SEM of triplicate samples (~100 cells analyzed per sample). Similar results were observed in three independent experiments. ** $p < 0.01$; t-test. (c) Transmission electron microscopic analysis of MEFs in control conditions or following CCCP-induced mitochondrial damage. Shown are representative images of mitochondrial morphology in MEFs of the indicated genotype 24 h after treatment with 30 μ M CCCP or DMSO vehicle control. Black arrowhead denotes autolysosome containing damaged mitochondria; white arrowheads denote mitochondria with abnormal cristae morphology. Scale bars, 500 nm.

To evaluate whether Pex13 functions in mitophagy in vivo, we performed ultrastructural analysis of tissues from *Pex13*^{+/+} and *Pex13*^{-/-} mouse embryos (as *Pex13*^{-/-} mice die neonatally). We found widespread abnormal mitochondrial cristae structures in *Pex13*^{-/-} livers, hearts, and skeletal muscles (Fig. 2.8), consistent with a previous report (Maxwell et al., 2003). Since autophagy is the only pathway for degrading large cellular components such as organelles and protein aggregates, these observations are consistent with an important homeostatic role of Pex13-mediated mitophagy in regulating mitochondria quality in vivo.

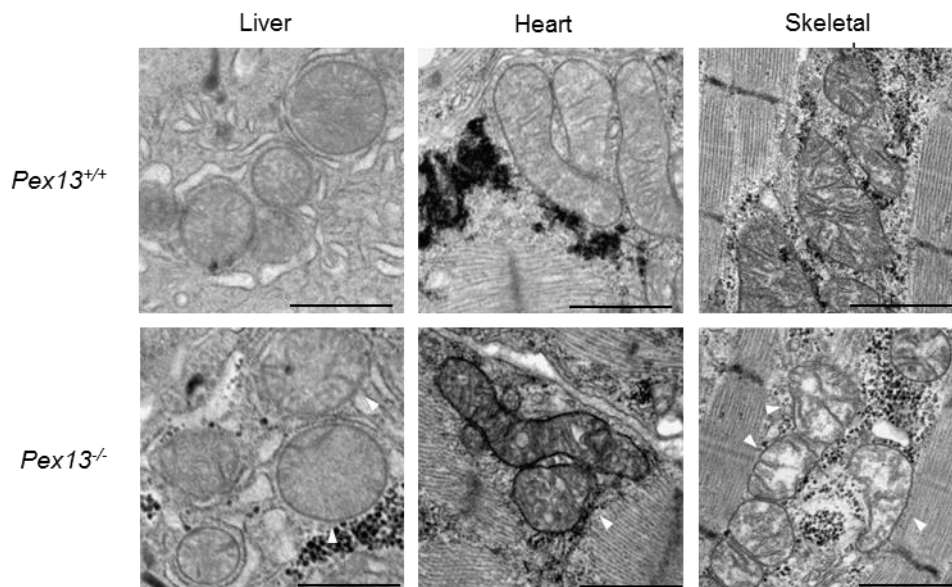


Figure 2.8. Pex13 KO embryos contain abnormal mitochondria.

Transmission electron microscopic analysis of E18.5 mouse embryonic liver, heart, and skeletal muscle. Shown are representative images from one mouse. Similar results were observed in three mice per genotype. Arrowheads indicate damaged mitochondria. Scale bars, 1 μ m.

II.4.C. siRNA-resistant WT PEX13, but not disease associated mutants PEX13

I326T and W313G rescue the mitophagy defect in PEX13 knockdown cells

Our findings raised the possibility that patients with ZSS due to *PEX13* mutations may have defects in selective autophagy. To test this hypothesis, we compared the

effects of siRNA-resistant wild-type (WT) and disease-associated mutation-encoding *PEX13* expression plasmids on the rescue of selective autophagy after *PEX13* siRNA knockdown in HeLa/Parkin cells (Fig. 2.9). We focused on mitophagy rather than virophagy because HeLa cells and MEF cells are resistant to SIN infection after plasmid transfection. *PEX13* I326T (Shimozawa et al., 1999) and *PEX13* W313G (Krause et al., 2013) mutants are less stable than WT *PEX13* protein, but with higher concentration of plasmid transfection we observed similar levels of protein expression of WT and mutated *PEX13* in HeLa/Parkin cells (Fig. 2.9a). By immunofluorescence imaging, endogenous *PEX13* was undetectable, but overexpressed WT and mutated *PEX13* could both be detected and are all colocalized with PMP70 (Fig. 2.9b). siRNA-resistant WT *PEX13*, but neither disease-associated mutant, *PEX13* I326T or *PEX13* W313G, partially rescued the mitophagy defect in CCCP-treated HeLa/Parkin cells with *PEX13* knockdown. Surprisingly, cells expressing the *PEX13* I326T or *PEX13* W313G mutants showed a greater mitophagy defect compared with cells with empty vector control (Fig. 2.8c,d) and mitochondria in mutant transfected cells appeared fragmented and aggregated even during basal conditions (Fig. 2.9e). These data suggest that *PEX13* proteins containing disease-associated mutations are not only defective in mitophagy, they may also have a gain-of-function effect on interfering with basal mitochondria quality control.

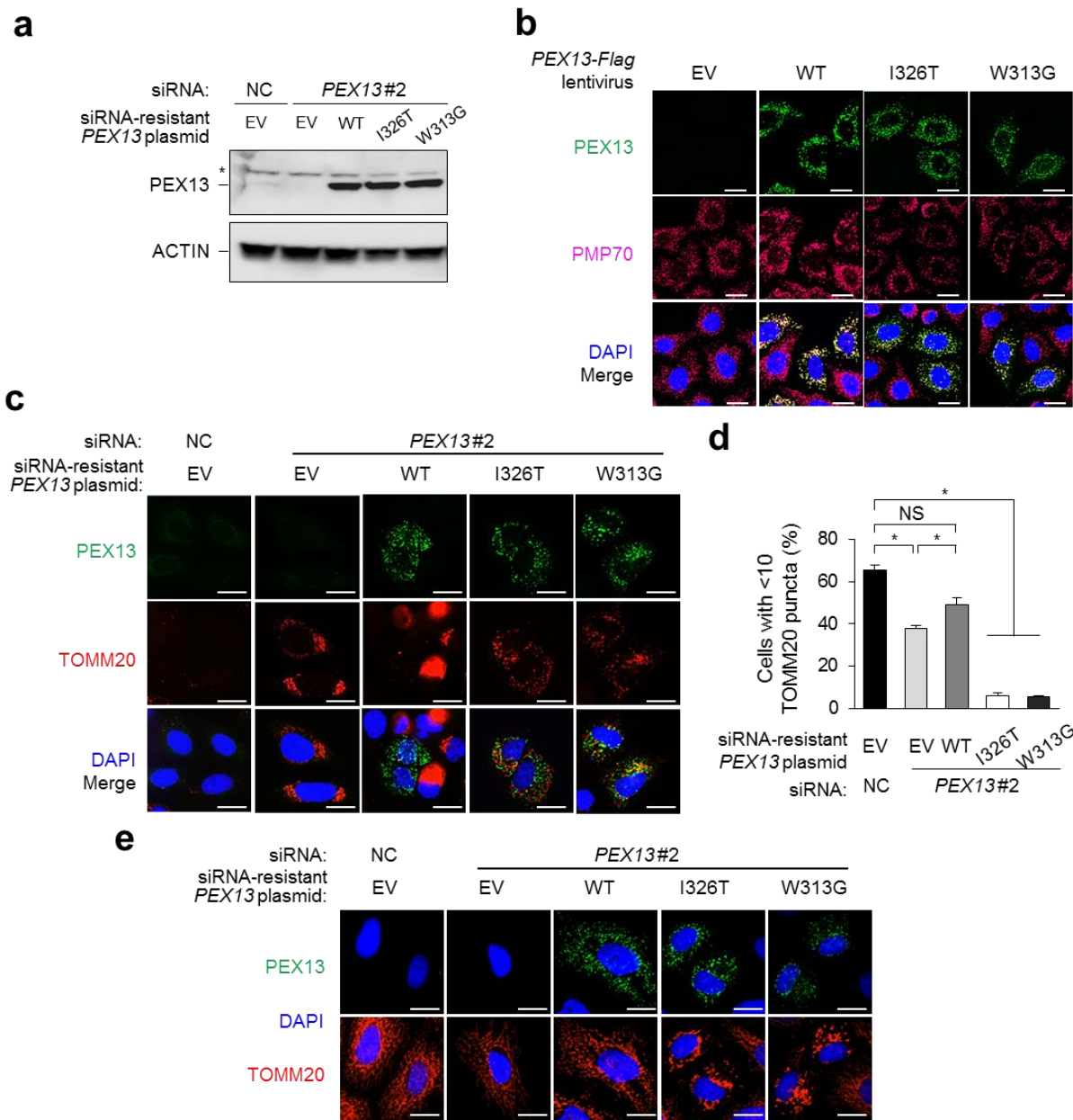


Figure 2.9. siRNA-Resistant WT PEX13, but not disease-associated mutants PEX13 I326T and W313G rescue the mitophagy defect in PEX13 knockdown cells.

(a) Western blot detection of PEX13 in HeLa/Parkin cells transfected with indicated siRNA and siRNA-resistant *PEX13* plasmid. To achieve similar PEX13 protein expression levels, 0.75 μ g *PEX13 I326T* and *PEX13 W313G* plasmids were transfected compared to 0.25 μ g WT *PEX13*. Total plasmid level was adjusted using empty vector. Asterix denotes non-specific band. (b) Representative images of PEX13 and PMP70 colocalization in HeLa/Parkin cells transduced with the indicated lentivirus. (c) Representative images of Parkin-mediated clearance of TOMM20 in HeLa/Parkin cells treated with the indicated siRNA and plasmids and then treated with CCCP (10 μ M, 16 h). (d) Quantification of TOMM20 clearance from experiment shown in c. * $p < 0.05$, NS= not significant; one-way ANOVA with adjustment for multiple comparisons. (e) Representative images of TOMM20 staining in HeLa/Parkin cells treated with the indicated siRNA and plasmids during basal state. Scale bars, 20 μ m. EV= empty vector.

II.4.D. PEX13 colocalizes with peroxisomes, but not with mitochondria or early autophagosomes during CCCP-induced mitophagy

PEX13 is known to localize to the peroxisome as an integral membrane protein, and it travels through the ER en route to peroxisomes during peroxisome biosynthesis (Agrawal et al., 2016). However, whether PEX13 localizes to other membrane compartments such as the mitochondria or autophagosomes is yet unknown. We sought to characterize the subcellular localization of PEX13 during basal and mitophagy conditions. Immunofluorescent imaging analysis showed that PEX13 formed punctate staining that strongly colocalized with PMP70 during both basal and mitophagy conditions (Fig. 2.10a). No appreciable PEX13 colocalization with TOMM20 (Fig. 2.10b) or with WIPI2, a marker of early autophagosomes (Polson et al., 2010) (Fig. 2.10c) were detected. Similarly, the majority of PEX13 colocalized with PMP70 and not with TOMM20 in MEFs during basal and mitophagy conditions. Since PEX13 remained localized to the peroxisomal membrane and not with either the selective autophagic cargo (the mitochondria) or the early autophagic membrane during mitophagy, it likely does not function as a direct adaptor during selective autophagy.

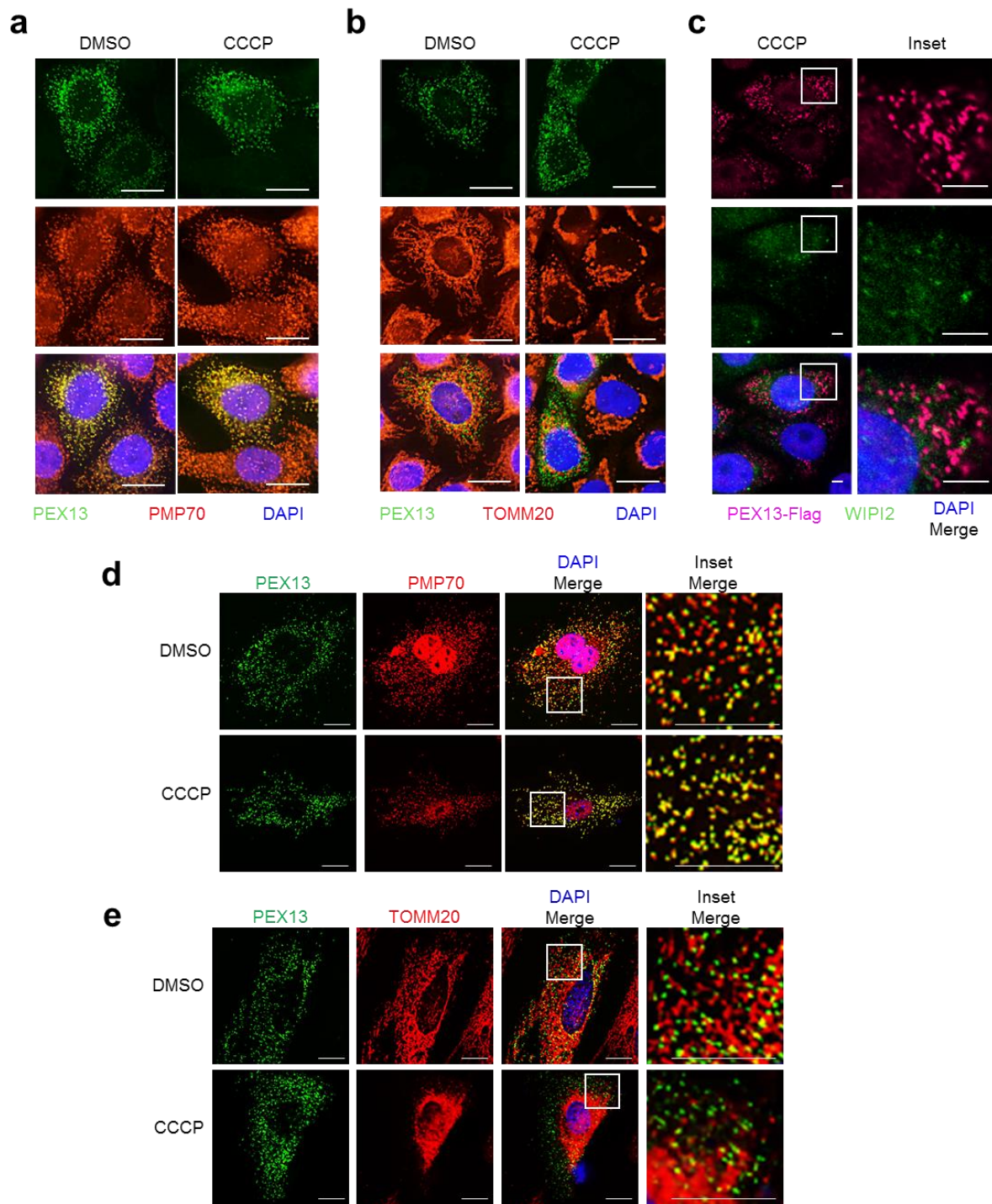


Figure 2.10. PEX13 colocalizes with peroxisomes, but not with mitochondria or early autophagosomes during CCCP-induced mitophagy.

(a-c) Representative images of PEX13 and PMP70 (a), PEX13 and TOMM20 (b), or PEX13-Flag and WIPI2 (c) colocalization in HeLa/Parkin cells transfected with PEX13 after 4 h treatment with 10 μ M CCCP or DMSO. Scale bars, 20 μ m (a-b) and 5 μ m (c). (d-e) Representative images of PEX13 and PMP70 (d) and PEX13 and TOMM20 (e) colocalization in primary MEFs transfected with PEX13 after 4 h treatment with 30 μ M CCCP or DMSO.

II.4.E. PEX13 and PEX3 are required for selective mitophagy, whereas PEX14 and PEX19 are required for general autophagy

Our findings raised the question of whether all proteins involved in peroxisome biogenesis function in mitophagy or whether PEX13 (and potentially certain other PEX proteins) have a function independent of peroxisome biogenesis in mitophagy. During peroxisome biogenesis, PEX13 interacts with PEX14 and PEX5 for peroxisomal matrix protein import, whereas PEX3 and PEX19 function upstream in the formation of peroxisomal membrane (Fujiki et al., 2014). Since the peroxisome biogenesis function of PEX13 depends on other peroxin family members, we evaluated whether other peroxins are required for mitophagy and general autophagy. Of note, *PEX5* and *PEX19* are involved in ROS-induced general autophagy (Zhang et al., 2013), and we previously identified *PEX3* as a candidate selective autophagy factor (Orvedahl et al., 2011). Using pools of four siRNAs targeting each gene, we knocked down *PEX3*, *PEX5*, *PEX13*, *PEX14*, or *PEX19* in HeLa cells (Fig. 2.11a). The siRNA pool did not knockdown *PEX5* efficiently; thus it was excluded from our study. *siPEX3* and *siPEX13* treatment inhibited CCCP-induced TOMM20 clearance (Fig. 2.11b) and OA-induced dsDNA clearance in HeLa cells expressing Parkin (Fig. 2.11c). Cells treated with *siPEX14*, *siPEX19*, or control siRNA achieved similar levels of CCCP-induced TOMM20 clearance (Fig. 2.11b) and OA-induced dsDNA clearance (Fig. 2.11c). These results were somewhat surprising, since *PEX19* is required for general autophagy, and a block in general autophagy (as in the case of *ATG7* knockdown) typically also manifests in a mitophagy defect.

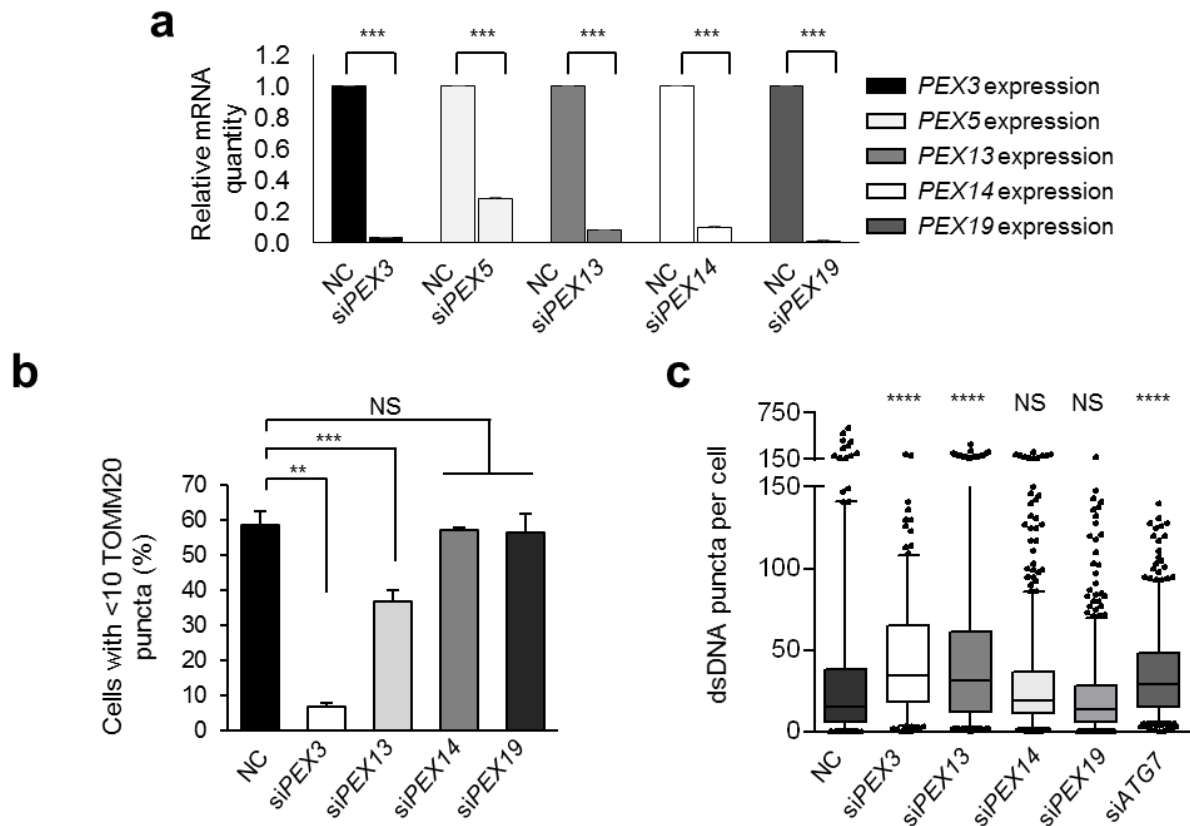


Figure 2.11. *PEX13* and *PEX3* are required for selective mitophagy while *PEX14* and *PEX19* are not. (a) Quantitative real-time PCR detection of mRNA levels for *PEX3*, *PEX13*, *PEX14*, and *PEX19* in HeLa cells transfected with the indicated siRNA. *** $p < 0.001$; t-test. (b) Quantification of Parkin-mediated TOMM20 clearance in HeLa/Parkin cells transfected with the indicated siRNA 16 h after treatment with 10 μ M CCCP. Results represent mean \pm SEM of triplicate samples (~100 cells analyzed per sample). Similar results were observed in three independent experiments. ** $p < 0.01$, *** $p < 0.001$, NS= not significant; one-way ANOVA with adjustment for multiple comparisons. (c) Quantification of mitochondrial dsDNA clearance in HeLa/HA-Parkin cells transfected with the indicated siRNA 8 h after treatment with 2.5 μ M oligomycin and 250 nM antimycin A (OA). Results represent box plots of >150 cells analyzed per sample. Whiskers represent 5%-95% range, and each outlier is represented by a dot. Similar results were observed in three independent experiments. **** $p < 0.0001$, NS= not significant; Kruskal-Wallis H-test.

Next, we evaluated whether these peroxins are involved in basal and starvation-induced general autophagy. We found that GFP-LC3 puncta numbers in HeLa/GFP-LC3 cells treated with siPEX3 or siPEX13 were not decreased as compared with control siRNA in basal and starvation conditions either in the presence or absence of Baf A1 treatment. In fact, *PEX13* siRNA increased autophagic flux in both conditions. Thus,

neither PEX3 nor PEX13 are required for general autophagy. In contrast, *PEX14* and *PEX19* siRNA reduced GFP-LC3 puncta number during basal and starvation conditions to a similar extent as *ATG7* siRNA, indicating reduced autophagic flux (Fig. 2.12). These results corroborate a previous report indicating that PEX19 is required for general (ROS-induced) autophagy (Zhang et al., 2013), and further identify starvation as an additional stimulus for PEX19-dependent autophagy pathway. In summary, we found that a subset of peroxins, PEX13 and PEX3, are required for selective autophagy, whereas another subset of peroxins, PEX14 and PEX19, are required for general autophagy.

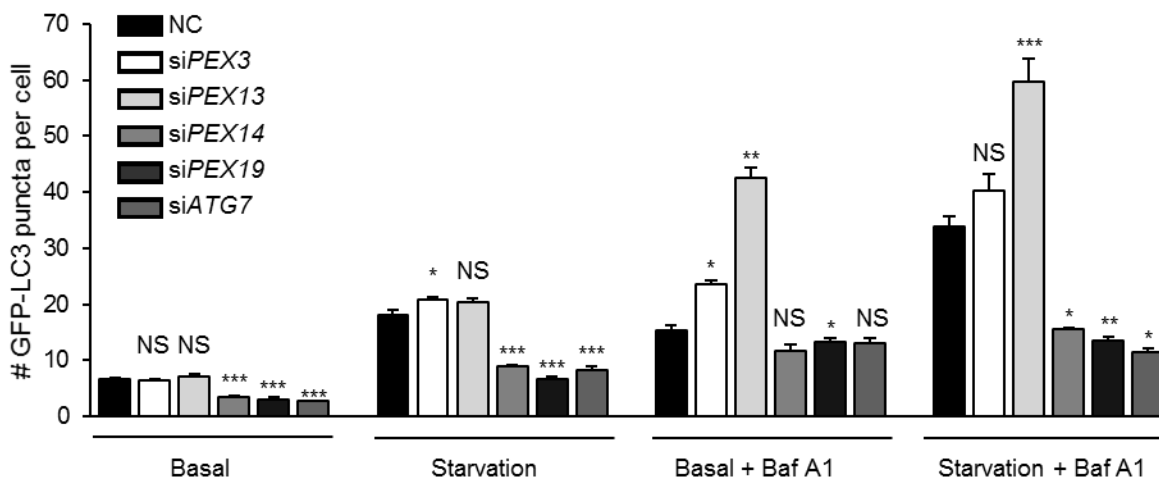


Figure 2.12. *PEX14* and *PEX19* are required for general Autophagy while *PEX13* and *PEX3* are not. Quantification of GFP-LC3 puncta in HeLa/GFP-LC3 cells treated with 10 nM Baf A1 or DMSO vehicle and cultured in normal medium or 3 h HBSS starvation media. Results represent mean \pm SEM in triplicate samples (~100 cells analyzed per sample). Similar results were observed in three independent experiments. * $p < 0.05$, ** $p < 0.01$, *** $p < 0.001$, NS= not significant; one-way ANOVA with adjustment for multiple comparisons.

II.4.F. PEX13 signaling through MAVS during selective autophagy

Mitochondrial Antiviral Signaling Protein (MAVS) is an antiviral signaling protein that mainly localizes to the mitochondria, but also localizes to the peroxisome. Given the dual function of MAVS on the mitochondria and peroxisome as an antiviral signaling

factor, we hypothesized that MAVS may serve as a signaling factor downstream of PEX13-mediated selective virophagy and mitophagy. To investigate this hypothesis, we first examined SIN virophagy in *MAVS*^{-/-} (MAVS KO) MEFs and MAVS KO MEFs reconstituted with WT MAVS-Flag (WT MEFs) (Fig. 2.13a). We found that SIN capsid colocalization with GFP-LC3 was reduced in MAVS KO MEFs (Fig. 2.13b), while the numbers of mCherry-capsid puncta (Fig. 2.13c) and GFP-LC3 (Fig. 2.13d) did not differ in these cells. These data suggest that MAVS is required for targeting SIN virus to the autophagosome.

Next, we evaluated Parkin-mediated mitophagy in immortalized MAVS WT or KO MEFs transiently transfected with mCherry-Parkin. Surprisingly, MAVS KO MEFs show an enhanced mitophagy response compared with WT MEFs (Fig. 2.13e). To evaluate the mitophagy phenotype further, we tested Parkin-mediated mitophagy in HeLa/Parkin cells using siRNA knockdown with five individual oligos. We found that all five oligos reduced MAVS expression (Fig 2.13f), but lead to variable mitophagy responses; three out of five siRNAs blocked mitophagy, while two oligos did not alter mitophagy compared with control cells (Fig. 2.13g). Next, we evaluated whether MAVS and PEX13 colocalize in the same subcellular compartment during selective autophagy. During basal state, the majority of YFP-MAVS colocalizes with the mitochondria and not with the peroxisome or PEX13 (Fig. 2.13h). During mitophagy, however, a subset of cells expressing YFP-MAVS show PEX13 and PMP70 recruitment to the perinuclear region. In these cells, PEX13 colocalization with TOMM20 signal increased. Together, these data suggest a role for MAVS in PEX13-mediated selective autophagy; however, further experiments are required to examine this hypothesis.

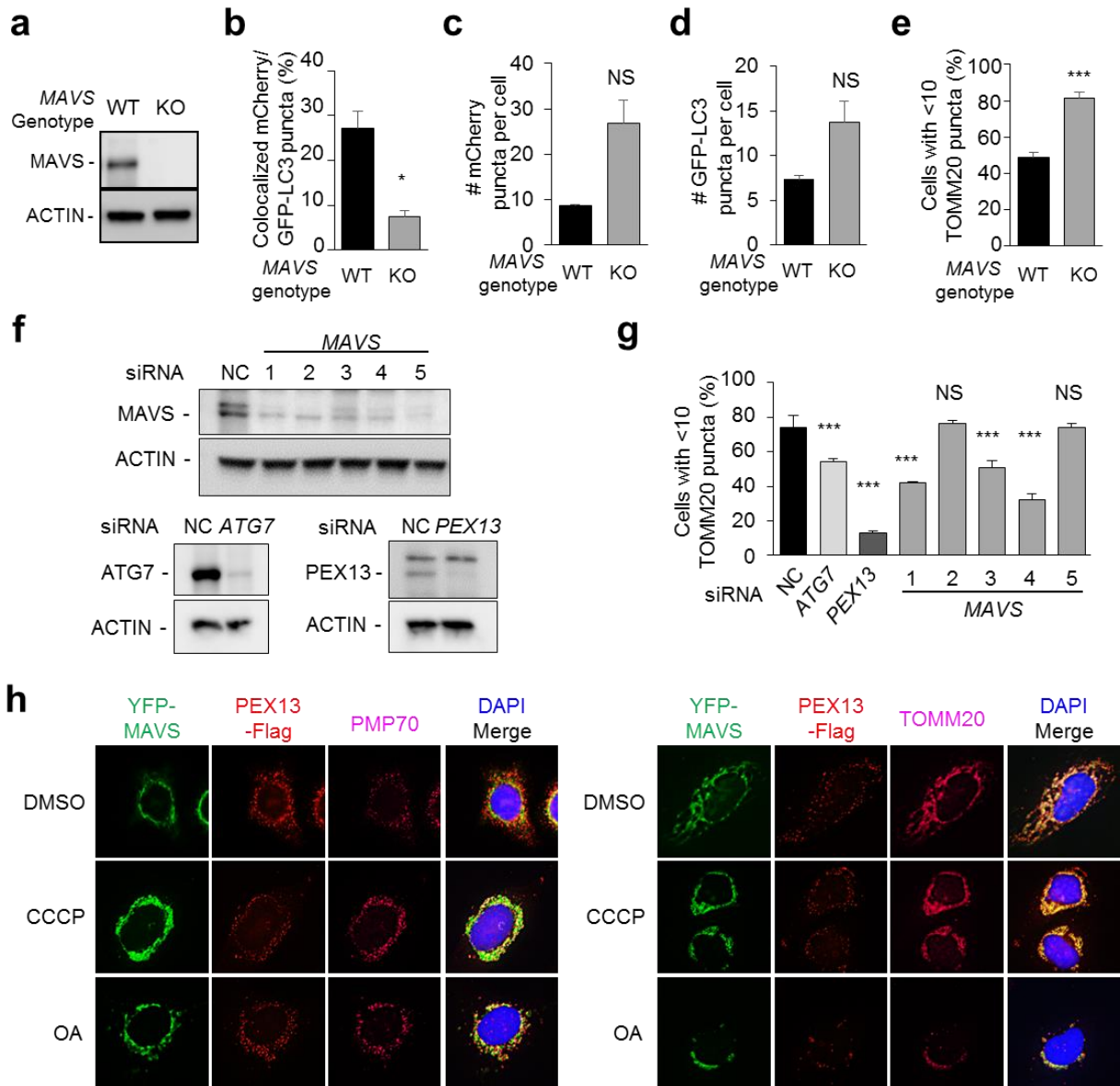


Figure 2.13. PEX13 signaling through MAVS during selective autophagy.

(a) Western blot detection of MAVS in immortalized MEFs of the indicated genotype. (b-d) Quantification of colocalized GFP-LC3 and mCherry-capsid puncta normalized to the number of mCherry-capsid puncta per cell (% colocalization) (b), mCherry-capsid puncta per cell (c), and GFP-LC3 puncta per cell (d) at 8 h after Sindbis virus (AO28) infection in MEFs. (e) Quantification of Parkin-mediated TOMM20 clearance at 16 h after treatment with 10 μ M CCCP in immortalized MEFs transfected with mCherry-Parkin. Results represent mean \pm SEM of triplicate samples (~100 cells analyzed per sample). * p <0.05, NS= not significant; t-test. (f-g) Western blot detection of MAVS, ATG7, and PEX13 (f) and quantification of TOMM20 clearance at 16 h after treatment with 10 μ M CCCP (g) in HeLa/Parkin cells transfected with the indicated siRNA. siPEX13 oligo #2 was used in this experiment. Results represent mean \pm SEM of triplicate samples (~100 cells analyzed per sample). *** p <0.001, NS= not significant; one-way ANOVA with adjustment for multiple comparisons. (h) Representative colocalization images at 6 h after treatment with 10 μ M CCCP, 2.5 μ M oligomycin and 250 nM antimycin A (OA), or DMSO vehicle control in HeLa/Parkin cells transfected with YFP-MAVS and PEX13-Flag.

II.4.G. Immunoprecipitation-mass spectroscopy (IP-MS) identification of PEX13-interacting proteins during selective autophagy

Next, to explore the hypothesis that PEX13 mediates selective autophagy as a signaling node using an unbiased screening approach, I conducted IP-MS identification of proteins that interact with wild-type (WT) or the PEX13 W313G mutant during basal and mitophagy conditions. In HeLa/Parkin cells stably expressing empty vector, WT, or W313G mutant PEX13-Flag, the expression of the W313G mutant is much lower than the WT protein after selection (Fig 2.14a). Silver staining showed a band at ~25 kDa that interacted strongly with WT PEX13 during mitophagy compared with other samples (Fig. 2.14b), suggesting that this protein could potentially mediate the function of PEX13 during mitophagy. Additionally, silver staining showed a band at ~60 kDa that interacted with the W313G mutant during mitophagy, suggesting that this protein could potentially mediate a dominant negative effect on mitophagy. Mass spectrometry identification of the protein bands did not yield any high confidence candidate interactors, possibly due to keratin contamination (data not shown).

In a repeat of the IP-MS experiment, silver staining showed a different pattern, with a unique band at ~40 kDa interacting with WT PEX13 during mitophagy (Fig 2.14c). Mass spectrometry did not identify significant amount of keratin contamination, suggestive of good sample quality (Table 2.4). Two proteins, guanine nucleotide binding protein, alpha inhibiting activity peptide 3 (GNAI3) and tropomodulin 3 (TMOD3) were present in the WT PEX13 + CCCP fraction, and absent from all other fractions; thus they were identified as candidate interactors with WT PEX13 during mitophagy. TMOD3 is a pointed-end actin-capping protein that facilitates actin filament assembly and

stabilization (Lim et al., 2015; Weber et al., 2007). GNAI3 is a heterotrimeric G-protein previously implicated in the regulation of general autophagy; GTP-bound GNAI3 inhibits autophagy, whereas GDP-bound GNAI3 stimulates autophagy (Pattingre et al., 2004).

Table 2.4. Candidate PEX13-interacting proteins from IP-MS screen

WT DMSO					
Accession number	Protein description	Mascot score	Molecular weight	Matched queries	Matched peptides
IPI00024348	PEX13	7590	44102	190	30
IPI00303476	ATP5B	2757	56525	66	21
IPI00021439	ACTB	1835	41710	63	21
IPI00440493	ATP5A1	1572	59714	49	25
IPI00021428	ACTA1	1092	42024	47	16
IPI00789324	JUP	869	66309	32	15
IPI00008669	- Keratin-81-like protein	643	53375	24	10
IPI00396485	EEF1A1	418	50109	15	8
IPI00554711	JUP	388	81693	9	5
IPI00219221	LGALS7B	373	15066	11	6
IPI00937615	EEF1G	330	50087	8	4
IPI00411639	LAMRL5	292	32975	6	3
IPI00099996	RG9MTD1	286	47317	14	9
IPI00218343	TUBA1C	279	49863	6	3
IPI00152871	LRRC15	275	64325	8	6
IPI00748502	CRTAP	259	46532	11	6
IPI00166738	ZADH2	226	40115	4	2
IPI00007797	FABP5	223	15155	9	5
IPI00003944	DBT	218	53453	3	2
IPI00013890	SFN	176	27757	6	3
IPI00910419	DDOST cDNA FLJ52929	164	46449	3	2
IPI00297084	DDOST	163	50769	4	3
IPI00025753	DSG1	143	113676	3	2
IPI00009104	RUVBL2	135	51125	2	1
IPI00000959	VIP	132	19157	2	1
IPI00003865	HSPA8	128	70854	2	1
IPI00334190	STOML2	118	38510	2	1
IPI00382516	PRMT1	107	40522	2	1
IPI00025512	HSPB1	104	22768	2	1
IPI00645452	TUBB	102	47736	4	2

WT CCCP					
Accession number	Protein description	Mascot score	Molecular weight	Matched queries	Matched peptides
IPI00021439	ACTB	7745	41710	214	27
IPI00024348	PEX13	7432	44102	195	31
IPI00021428	ACTA1	4005	42024	146	19
IPI00303476	ATP5B	3101	56525	73	22
IPI00479743	POTEE	1903	121286	63	11
IPI00003269	ACTBL2	1896	41976	75	12
IPI00440493	ATP5A1	1121	59714	32	17
IPI00017726	HSD17B10	587	26906	13	5
IPI00937615	EEF1G	457	50087	11	6
IPI00411639	LAMRL5	431	32975	7	4
IPI00095891	GNAS	422	110956	15	8
IPI00396485	EEF1A1	393	50109	19	9
IPI00382516	PRMT1	363	40522	10	6
IPI00099996	RG9MTD1	308	47317	16	11
IPI00005087	TMOD3	297	39570	6	4
IPI00328319	RBBP4	282	47626	9	5
IPI00217223	PAICS	278	49648	5	3
IPI00026612	PPM1B	272	52609	9	5
IPI00009104	RUUBL2 RuvB-like 2	269	51125	8	5
IPI00297084	DDOST	267	50769	9	4
IPI00166738	ZADH2	248	40115	5	3
IPI00000959	VIP	235	19157	4	1
IPI00297982	EIF2S3	217	51077	4	2
IPI00798401	- cDNA FLJ50992, highly similar to Coronin-1C	206	49347	10	6
IPI00003865	HSPA8	198	70854	5	3
IPI00220578	GNAI3	191	40506	6	4
IPI00028888	HNRNPD	178	38410	5	4
IPI00003348	GNB2	175	37307	6	3
IPI00220740	NPM1	173	29446	4	2
IPI00179330	RPS27A	165	17953	3	2
IPI00748502	CRTAP	156	46532	8	4
IPI00028091	ACTR3	136	47341	2	1
IPI00022624	GPRC5A	129	40225	2	1
IPI00166768	TUBA1C	121	36719	4	3
IPI00893518	FLOT1	111	9553	2	1
IPI00007765	HSPA9	104	73635	3	2
IPI00328987	BYSL	104	49570	2	1

W313G DMSO					
Accession number	Protein description	Mascot score	Molecular weight	Matched queries	Matched peptides
IPI00024348	PEX13	4593	44102	121	25
IPI00303476	ATP5B	4307	56525	96	26
IPI00021439	ACTB Actin	2453	41710	74	21
IPI00440493	ATP5A1	1940	59714	58	26
IPI00017726	HSD17B10	1461	26906	29	11
IPI00021428	ACTA1	1278	42024	53	16
IPI00009104	RUVBL2	996	51125	28	13
IPI00297084	DDOST	681	50769	24	11
IPI00937615	EEF1G	670	50087	21	11
IPI00003944	DBT	637	53453	17	9
IPI00396485	EEF1A1	495	50109	20	10
IPI00418471	VIM	455	53619	15	9
IPI00180675	TUBA1A	438	50104	14	7
IPI00299571	PDIA6	419	53867	7	4
IPI00022694	PSMD4	405	40711	12	6
IPI00328319	RBBP4	403	47626	17	8
IPI00003865	HSPA8	400	70854	11	6
IPI00411639	LAMRL5	394	32975	6	3
IPI00099996	RG9MTD1	360	47317	18	12
IPI00645452	TUBB	353	47736	12	7
IPI00000959	VIP	297	19157	6	1
IPI00382516	PRMT1	268	40522	7	4
IPI00028888	HNRNPD	259	38410	10	7
IPI00395865	RBBP7	257	47790	14	7
IPI00297982	EIF2S3	253	51077	8	4
IPI00022793	HADHB	217	51262	5	3
IPI00004506	KCTD5	213	26076	5	3
IPI00022624	GPRC5A	196	40225	4	2
IPI00026612	PPM1B	181	52609	7	4
IPI00043598	IKBIP	172	43057	6	4
IPI00166738	ZADH2	170	40115	2	1
IPI00022434	ALB	163	71658	3	1
IPI00009328	EIF4A3	149	46841	2	1
IPI00024317	GCDH I	142	48096	4	2
IPI00013881	HNRNPH1	130	49198	3	2
IPI00003362	HSPA5	124	72288	4	3
IPI00012972	NME4	108	20646	2	1
IPI00027107	TUFM	108	49843	2	1

W313G CCCP					
Accession number	Protein description	Mascot score	Molecular weight	Matched queries	Matched peptides
IPI00303476	ATP5B	3230	56525	72	24
IPI00021439	ACTB	2585	41710	80	22
IPI00024348	PEX13	1908	44102	49	17
IPI00021428	ACTA1	1351	42024	57	17
IPI00017726	HSD17B10	1155	26906	24	9
IPI00440493	ATP5A1	797	59714	21	11
IPI00297084	DDOST	790	50769	22	12
IPI00099996	RG9MTD1	616	47317	24	15
IPI00396485	EEF1A1	562	50109	19	9
IPI00937615	EEF1G	514	50087	15	8
IPI00382516	PRMT1	503	40522	15	7
IPI00328319	RBBP4	489	47626	15	8
IPI00028888	HNRNPD	388	38410	14	9
IPI00411639	LAMRL5	386	32975	6	3
IPI00026612	PPM1B	290	52609	7	4
IPI00179330	RPS27A	222	17953	5	3
IPI00005198	ILF2 I	186	43035	4	2
IPI00010157	MAT2A	183	43633	2	1
IPI00022624	GPRC5A	179	40225	4	2
IPI00029468	ACTR1A	169	42587	3	2
IPI00166738	ZADH2	167	40115	4	2
IPI00003865	HSPA8	166	70854	3	2
IPI00218343	TUBA1C	157	49863	4	3
IPI00027107	TUFM	154	49843	3	2
IPI00043598	IKBIP	154	43057	7	5
IPI00299571	PDIA6	143	53867	2	1
IPI00000959	VIP	137	19157	2	1
IPI00022974	PIP	121	16562	2	1
IPI00297982	EIF2S3	109	51077	2	1

Confirmation with PEX13-Flag co-IP showed nonspecific TMOD3 interaction with all samples (Fig 2.14d); thus it was excluded from further analysis. GNAI3 appeared to interact with PEX13 during mitophagy. This interaction was observed for WT PEX13 as well as with PEX13 mutants W313G and I326T that are dysfunctional for mitophagy (Fig.

2.14e). These data suggest that if GNAI3 mediates a mitophagy signal from PEX13, its function may be regulated by other post-translational modifications (e.g. ubiquitination, phosphorylation) or conformational changes not detected by a co-IP western blot experiment. To assess whether GNAI3 functions in selective autophagy, I evaluated whether GNAI3 siRNA knockdown can inhibit mitophagy in HeLa/Parkin cells. Pooled siRNA that knocked down GNAI3 protein (Fig. 2.14f) did not inhibit OA-induced dsDNA clearance (Fig. 2.14g). Thus, GNAI3 is likely not required for the mitophagy function of PEX13.

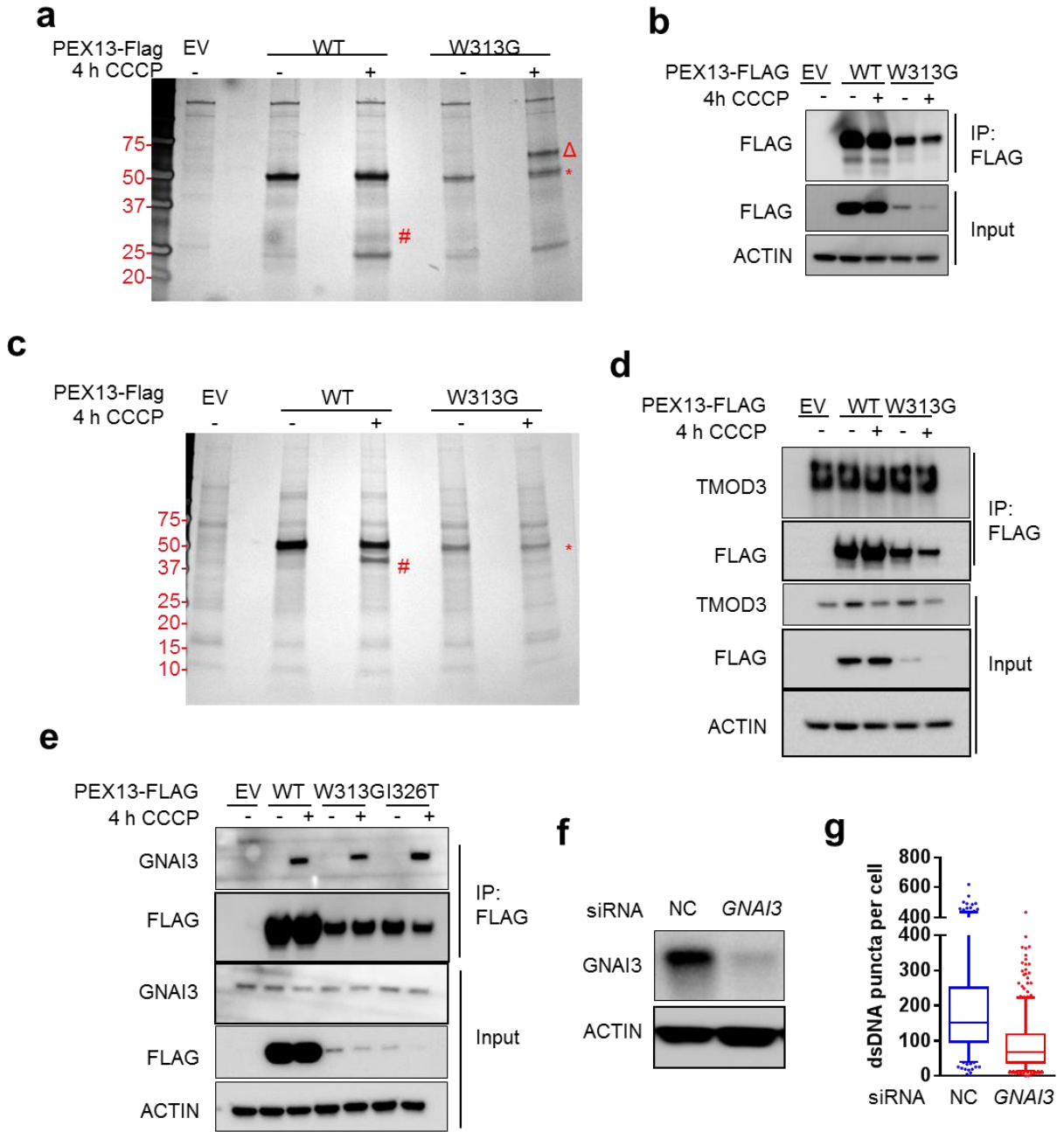


Figure 2.14. IP-MS identification of PEX13-interacting proteins during mitophagy

(a, c) Silver stained SDS-PAGE gel of the Flag-elute fraction from co-immunoprecipitation with PEX13-Flag in HeLa/Parkin cells stably transfected with the indicated plasmid at 4 h after treatment with 10 μ M CCCP or DMSO vehicle control. * indicate PEX13 protein, # indicate candidate signaling proteins interacting with WT PEX13 during mitophagy, and Δ indicates candidate signaling protein interacting with W313G mutant during mitophagy. (b) Western blot detection of PEX13-Flag from experiment shown in a. (d-e) Co-immunoprecipitation of TMOD3 (d) and GNAI3 (e) with PEX13-Flag in HeLa/Parkin cells stably transfected with the indicated plasmid at 4 h after treatment with 10 μ M CCCP or DMSO vehicle control. (f) Western blot detection of GNAI3 in HeLa/Parkin cells treated with the indicated siRNA. (g) Quantification of mitochondrial dsDNA in HeLa/Parkin cells treated with the indicated siRNA 8 h after treatment with 2.5 μ M oligomycin and 250 nM antimycin A (OA) or DMSO vehicle control.

II.4.H. Generation and validation of HeLa cells with PEX3, PEX5, PEX13, PEX14, or PEX19 KO.

While siRNA technology provides a quick and easy way to silence target genes, it is limited by the transient and incomplete nature of gene knockdown, as well as potential off-target effects. To address this, we wanted to confirm selective autophagy and general autophagy phenotypes in HeLa cells with *PEX3*, *PEX5*, *PEX13*, *PEX14*, or *PEX19* knockout using clustered regularly-interspaced short palindromic repeats (CRISPR)/Cas9 system. We collaborated with the Washington University Genome Engineering and iPSC Center (GEiC) to generate CRISPR guide RNA (gRNA) and cloning primer designs (Table 2.5), analyze for off-target effects for the gRNAs, and generate clonal knockout cell lines. Clonal mutants were genotyped by deep sequencing to confirm the presence of a frameshifting insertion or deletion (indel) mutation or a premature stop codon in the 5' exons leading to a loss-of-function mutation (Fig. 2.15).

Table 2.5. CRISPR gRNA and cloning primer sequences

Gene	Design #	Sequence	
PEX3	#1	gRNA	ATGATATTGTCGTCGTGCTTNGG
		forward oligo	ACACCGATGATATTGTCGTCGTGCTTG
		reverse oligo	AAAACAAGCACGACGACAATATCATCG
	#2	gRNA	AATGATATTGTCGTCGTGCTNNGG
		forward oligo	ACACCGAATGATATTGTCGTCGTGCTG
		reverse oligo	AAAACAGCACGACGACAATATCATTCTG
PEX5	#1	gRNA	GAATTCATCTCTGAAGTTACNNGG
		forward oligo	ACACCGAATTCATCTCTGAAGTTACG
		reverse oligo	AAAACGTAACCTCAGAGATGAATTCTG
	#2	gRNA	GCCCAGGAGTTTCTTGCAGCNGG
		forward oligo	ACACCGCCCAGGAGTTTCTTGCAGCG
		reverse oligo	AAAACGCTGCAAGAACTCCTGGGCG
PEX13	#1	gRNA	GAAGATCATCTACACGGAGGNGG
		forward oligo	ACACCGAAGATCATCTACACGGAGGG
		reverse oligo	AAAACCCTCCGTGTAGATGATCTTCTG
	#2	gRNA	GTGGAAGATCATCTACACGGNNGG
		forward oligo	ACACCGTGAAGATCATCTACACGGGG
		reverse oligo	AAAACCCGTGTAGATGATCTTCCACG
PEX14	#1	gRNA	ATGGCGAGATTACGGCGCCNNGG
		forward oligo	ACACCGATGGCGAGATTACGGCGCCCG
		reverse oligo	AAAACGGGCGCCGTAATCTCGCCATCG
	#2	gRNA	GGGCGCCGTAATCTCGCCATNNGG
		forward oligo	ACACCGGGCGCCGTAATCTCGCCATG
		reverse oligo	AAAACATGGCGAGATTACGGCGCCCG
PEX19	#1	gRNA	TGTCTCCTGGCGATCTCTTCNNGG
		forward oligo	ACACCGTGTCTCCTGGCGATCTCTTCTG
		reverse oligo	AAAACGAAGAGATCGCCAGGAGACACG
	#2	gRNA	GGGCCCCAGAAGAGATCGCCNNGG
		forward oligo	ACACCGGGCCCCAGAAGAGATCGCCG
		reverse oligo	AAAACGGCGATCTCTTCTGGGGCCCG

To validate the CRISPR KO HeLa cells, I performed western blot analysis for loss of protein expression and immunofluorescent imaging analysis for peroxisome staining. Western blot results confirmed the protein knockdown for two clones of *PEX13* KO HeLa cells (Fig. 16a) and *PEX19* KO HeLa cells (Fig. 16b). However, we do not have working antibodies to detect endogenous PEX3, PEX5, and PEX14 protein levels. Thus, most of the validation experiments focus on PEX13 and PEX19.

Next, I evaluated peroxisome membrane biogenesis and mitochondria morphology in these CRISPR cell lines by PMP70 immunostaining. Consistent with previously reported phenotypes for lost-of-function mutants, our *PEX3* KO and *PEX19* KO HeLa cell lines are devoid of punctate PMP70 staining, indicating a functional defect in the generation of peroxisome membranes (Fig 16c). Of note, siRNA knockdown of *PEX19* did not deplete PMP70 punctate staining during the time period assessed (48 hours after transfection, data not shown), likely because peroxisome turnover by pexophagy is a relatively slow process in mammalian cells (Ezaki et al., 2009). This highlights one advantage of using constitutively knockout system versus transient RNAi. HeLa cells with *PEX5* KO, *PEX13* KO, or *PEX14* KO contained PMP70 puncta, which may represent empty peroxisome ghosts present in cells lacking peroxisome matrix protein machinery (Fujiki et al., 2014; Ma et al., 2011). *PEX13* KO HeLa cells contained fewer and larger PMP70 puncta compared with parental WT HeLa cells. Previously, fibroblasts derived from a ZSS patient with homozygous nonsense mutation W234ter (which resulted in the loss of the SH3 domain and the putative transmembrane domain) also showed larger and fewer PMP70 punctate staining (Shimozawa et al., 1999). We

did not observe changes to the basal mitochondrial morphology suggestive of abnormal mitochondria quality control in any of the *PEX* KO HeLa cells, as measured by TOMM20 staining (Fig. 2.16c). This is similar to what we observed in HeLa/Parkin cells after treatment with siRNA targeting *PEX* genes (data not shown). Together, these results suggest that the *PEX13* and *PEX19* KO HeLa cells have on-target disruptions of the genes and recapitulate anticipated peroxisome phenotypes.

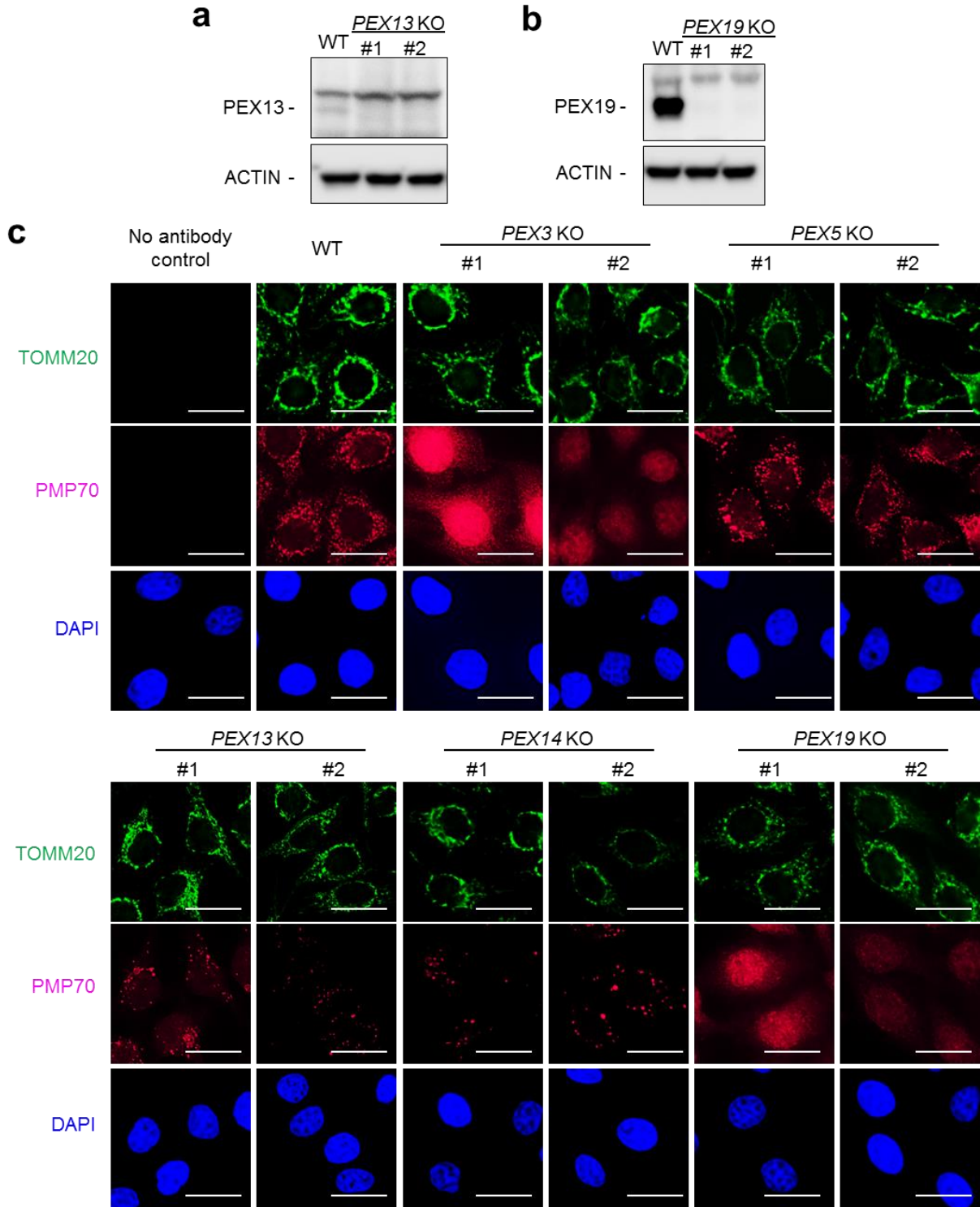


Figure 2.16. Phenotypic validation of CRISPR KO HeLa cells

(a,b) Western blot detection of PEX13 (a) or PEX19 (b) in HeLa cells of the indicated genotype. (c) Representative images of TOMM20 (mitochondria marker) and PMP70 (peroxisome membrane marker) in HeLa cells of the indicated genotype.

II.4.I. PEX13 KO but not PEX19 KO HeLa cells have defective mitophagy

To confirm the role of PEX13 and PEX19 in mitophagy, we evaluated CCCP- or OA-induced Parkin-mediated mitophagy in the *PEX13* KO and *PEX19* HeLa cells. CCCP-induced TOMM20 clearance was blocked in both clones of *PEX13* KO HeLa cells transfected with mCherry-Parkin, compared to parental WT HeLa cells (Fig. 2.17a,b). In contrast, two clones of *PEX19* KO HeLa cells showed no defects in Parkin-mediated TOMM20 clearance. *PEX19* KO clone 2 actually had increased level of TOMM20 clearance compared with parental control cells.

Furthermore, we assessed OA-induced mitochondrial dsDNA clearance by immunofluorescence and OA-induced clearance of mitochondrial outer membrane protein (TOMM20), inner membrane protein (COXIV), and matrix protein (HSP60) using western blot analysis in cells stably expressing Parkin. Our results show that *PEX13* KO clone 2 had defective clearance of HSP60, COXIV, and TOMM20 after treatment with OA for 4 to 12 hours, as compared with WT cells. However, *PEX13* KO clone 1 did not show a defect in mitophagy by western blot analysis. Consistent with our previous siRNA mitophagy experiments, two clones of *PEX19* KO cells exhibited comparable levels of mitophagy compared with WT cells (Fig. 2.17c). The inconsistent mitophagy phenotype found in the two clones of *PEX13* KO HeLa cells may be due to off-target effects of CRISPR/Cas9. To address this, future experiments will assess mitophagy in *PEX13* KO clone 2 cells infected with *PEX13*-expressing lentivirus. We will also further rescue *PEX13* KO clone 2 cells with *PEX13* mutants I326T and W313G to evaluate the involvement of these disease-associated mutations in mitophagy. Furthermore, future experiments assessing OA-induced dsDNA clearance in *PEX13* KO HeLa cells may

provide more evidence in support of our hypothesis that PEX13 is required for mitophagy.

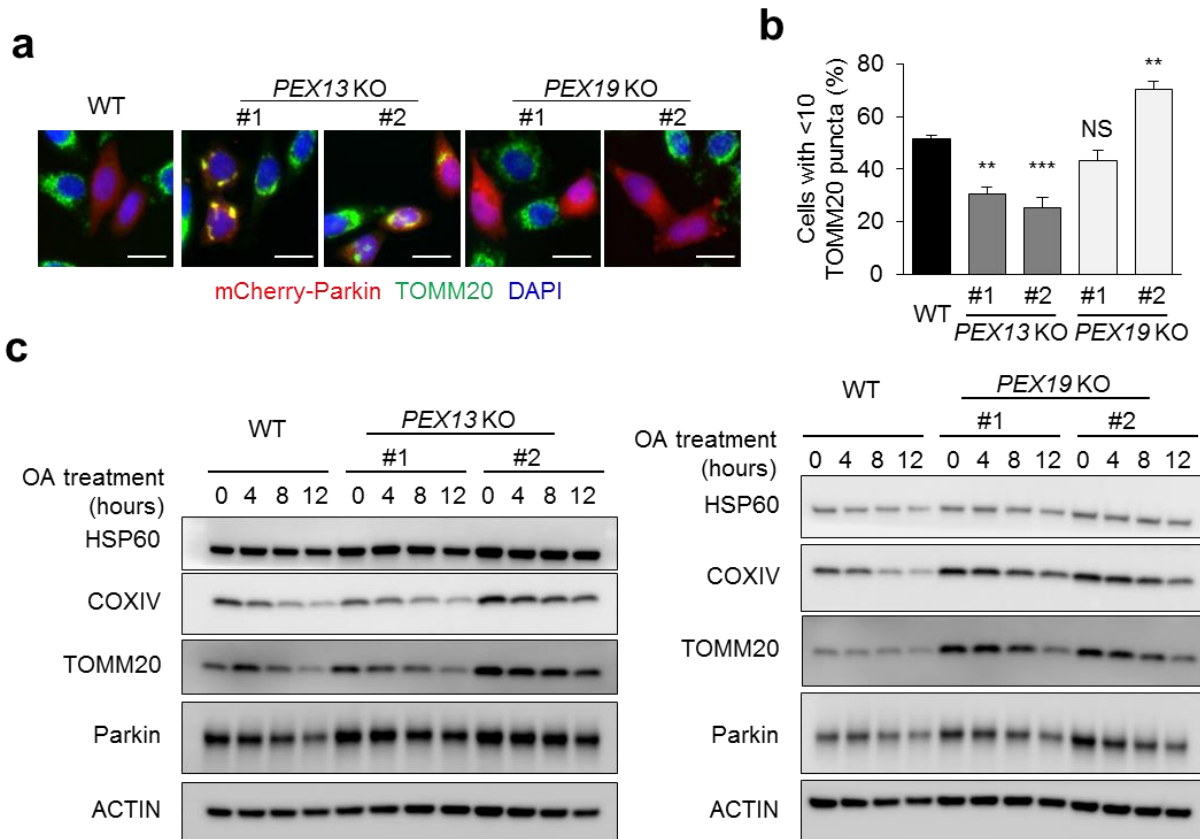


Figure 2.17. PEX13 KO but not PEX19 KO HeLa cells are defective in mitophagy.

(a) Representative images of Parkin-mediated clearance of mitochondrial outer membrane protein TOMM20 at 16 h after treatment with 10 μ M CCCP in HeLa/Parkin cells of the indicated genotype transfected with mCherry-Parkin. Scale bars, 20 μ m. (b) Quantification of experiment shown in a. Results represent mean \pm SEM of triplicate samples (>100 cells analyzed per sample). ** $p < 0.01$, *** $p < 0.001$, NS= not significant; one-way ANOVA with adjustment for multiple comparisons. (d) Western blot detection of HSP60 (mitochondrial matrix protein), COXIV (mitochondrial inner membrane protein), TOMM20 (mitochondrial outer membrane protein), and Parkin in HeLa/Parkin cells treated with OA for the indicated time.

II.4.J. PEX13 KO HeLa cells are competent for general autophagy

By western blot detection of p62 degradation and LC3-I to LC3-II conversion in the presence or absence of Baf A1, two clones of *PEX13* KO HeLa cells did not show a reduction in basal or starvation-induced autophagic flux (Fig. 2.18), consistent with data from the siRNA knockdown experiments in HeLa cells and in *PEX13* KO MEFs. These

results suggest that the mitophagy defect observed in PEX13 KO HeLa cells is not due to a defect in the general autophagy pathway. Future experiments assessing starvation-induced general autophagy in *PEX13* KO and *PEX19* KO HeLa cells by GFP-LC3 puncta assay could provide more evidence supporting our hypothesis that PEX13 is competent for general autophagy while PEX19 is not.

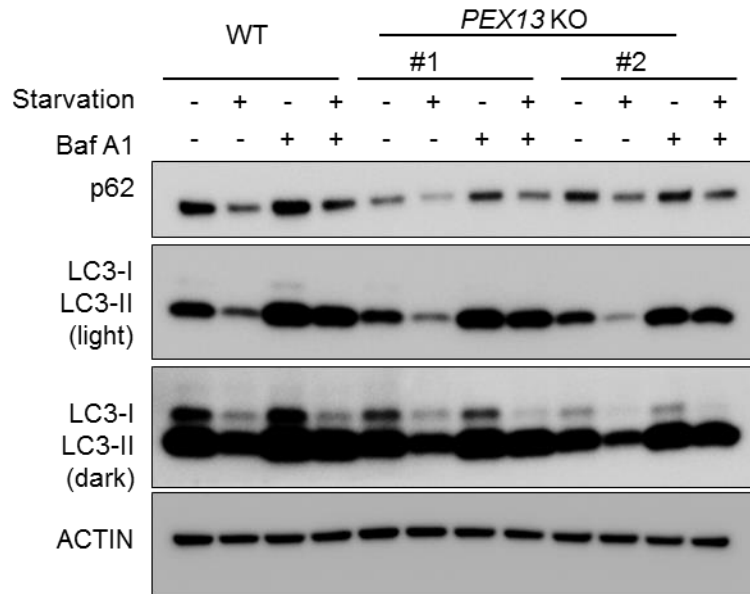


Figure 2.18. PEX13 KO HeLa cells are competent for starvation-induced general autophagy. Western blot detection of p62 and LC3 in HeLa cells of the indicated genotype treated with 100 nM Baf A1 or DMSO vehicle and cultured in normal medium (starvation “-”) or HBSS (starvation “+”) for 3 h.

II.4.K. PEX13 localizes to the mitochondria and not the ER in PEX19 KO cells.

Since we observed PEX13 localization to the peroxisome and to the mitochondria or early autophagosome during mitophagy, we presume that PEX13 functions on the peroxisome membrane during mitophagy. Yet, our finding that peroxisome-deficient *PEX19* KO HeLa cells were competent for mitophagy raised the possibility that a fraction of PEX13 localizes to non-peroxisome compartments that are important for mitophagy regulation. In yeast, PEX13 and other peroxins in the docking complex (PEX14 and PEX17) localize to the ER in PEX19-deficient cells (Agrawal et al., 2016).

However, we found that the majority of PEX13-Flag does not colocalize with the ER marker PDI during basal and mitophagy conditions (Fig. 2.19). In PEX19-deficient cells, PEX13-Flag staining shows a reticular pattern during basal state and compacts to the perinuclear region during CCCP-induced mitophagy. This staining pattern resembles mitochondria staining patterns we observed previously. Thus we examined PEX13 colocalization with TOMM20, the mitochondrial outer membrane protein and observed that in *PEX19* KO HeLa cells, the majority of PEX13 colocalizes with TOMM20 during basal and mitophagy conditions (Fig. 2.20).

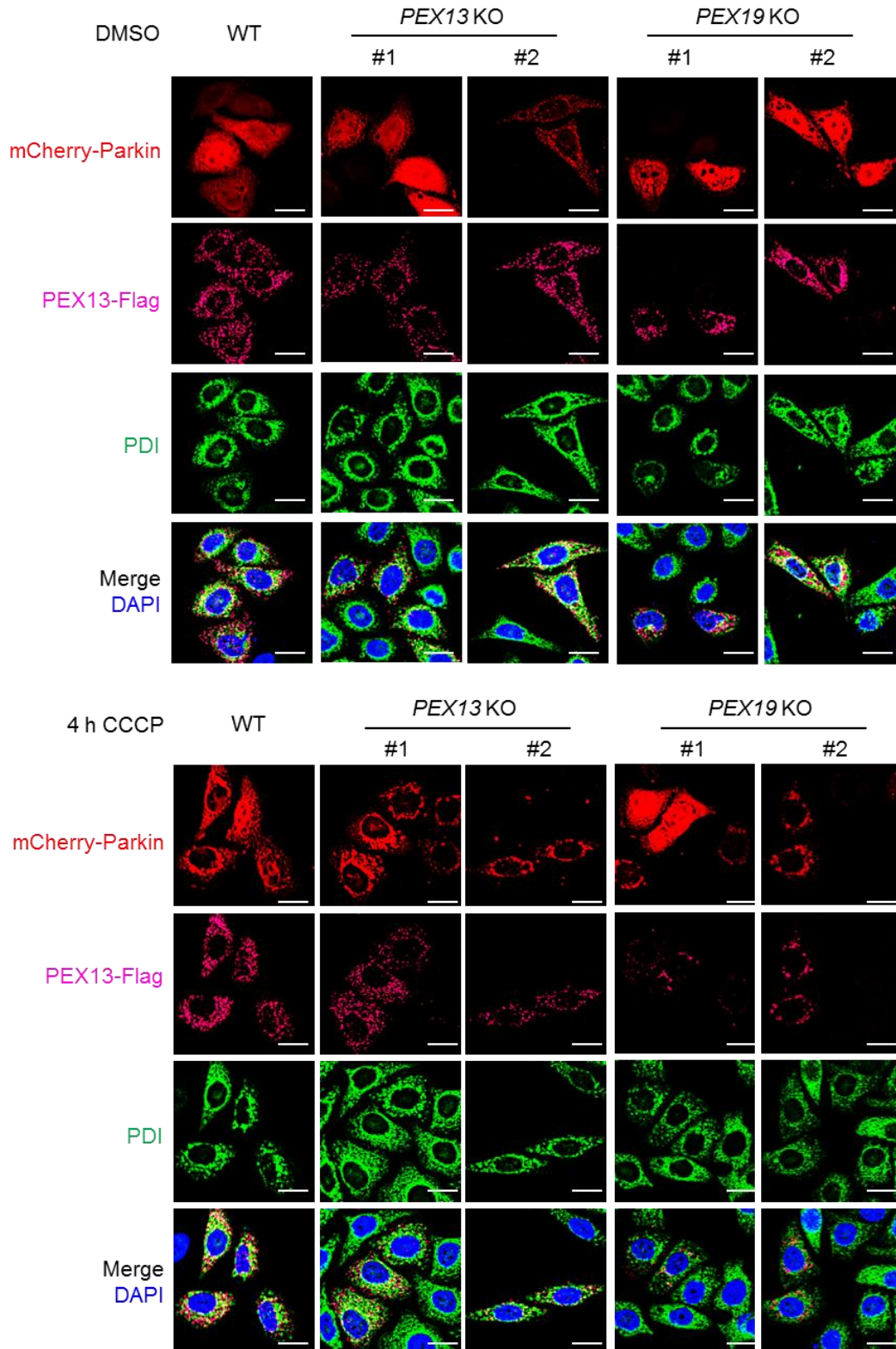


Figure 2.19. PEX13 does not localize to the ER in PEX19 KO cells.

Representative images of PEX13-Flag and PDI (ER marker) colocalization in HeLa cells of the indicated genotype transfected with mCherry-Parkin after 4 h treatment with 10 μ M CCCP or DMSO vehicle control.

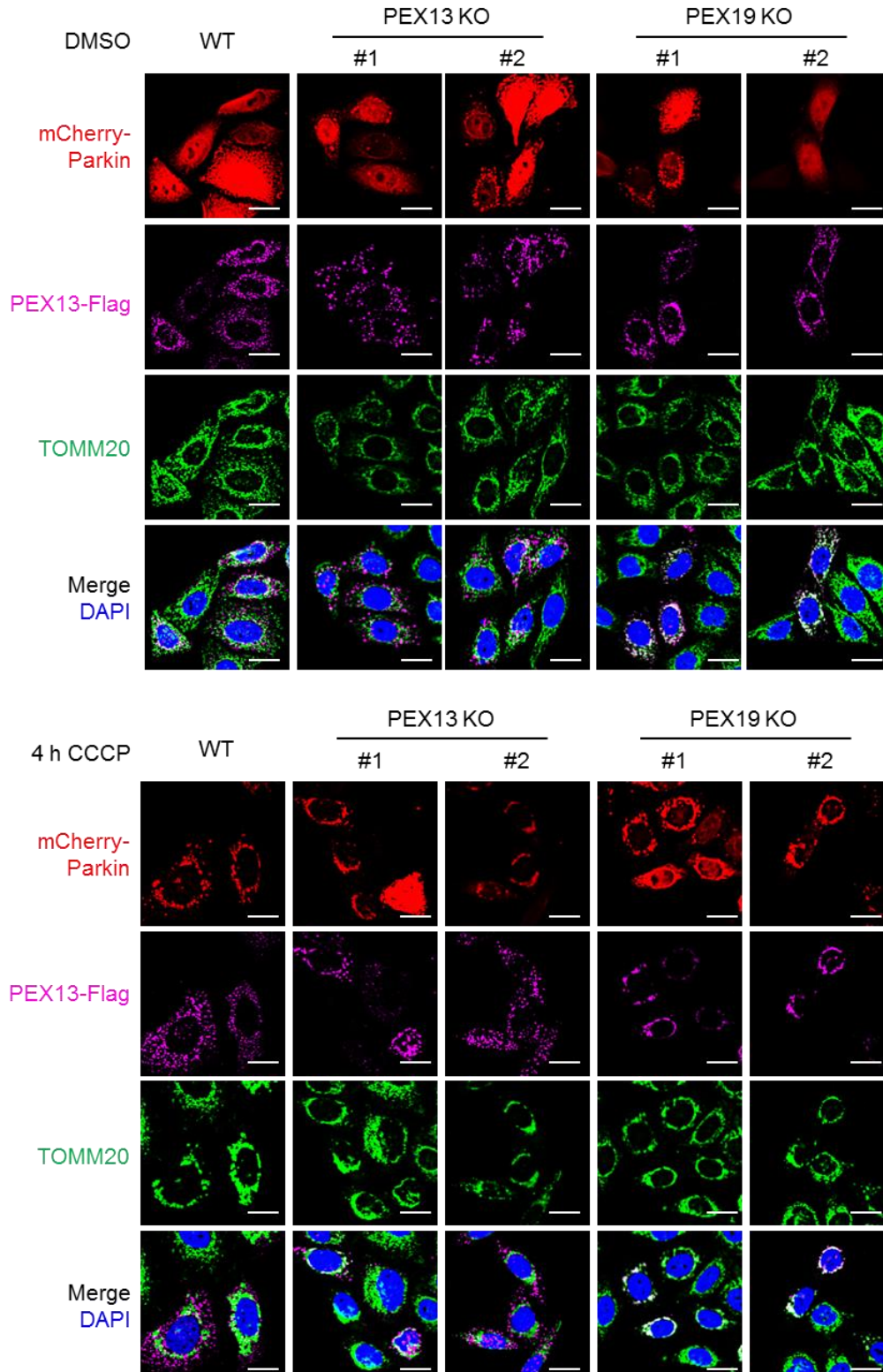


Figure 2.20. PEX13 localizes to the mitochondria in PEX19 KO cells.

Representative images of PEX13-Flag and TOMM20 (mitochondrial marker) colocalization in HeLa cells of the indicated genotype transfected with mCherry-Parkin after 4 h treatment with 10 μ M CCCP or DMSO vehicle control.

II.5. Discussion and future directions

In this study, we provide multiple lines of evidence demonstrating the essential role of *PEX13* and *PEX3* in selective, and not general, autophagy in mammalian cells. We showed that *PEX13* is required for selective autophagy of two very different targets, a viral nucleocapsid protein and mitochondria, and that *PEX3* is required for selective autophagy of mitochondria. Additionally, previous studies demonstrated that *PEX3* is required not only for peroxisome biogenesis, but also for peroxisomal degradation via pexophagy in yeast (Burnett et al., 2015) and in mammalian cells (Yamashita et al., 2014). Given that many factors involved in selective autophagy, including autophagy receptors (e.g. p62, NBR1, optineurin) and targeting signals (e.g. ubiquitin) mediate clearance of diverse substrates (Stolz et al., 2014), we speculate that the functions of *PEX3* and *PEX13* may also be extend to other forms of selective autophagy.

Autophagy receptors facilitate the selective engulfment of cargo by the autophagosome by directly binding to the cargo and the autophagosomal membrane (Stolz et al., 2014). We observed that the majority of *PEX13* remained associated with the peroxisome during both basal and mitophagy-inducing conditions in wild-type HeLa cells and MEFs. In contrast, the staining pattern of *PEX13* is very different from that of WIPI2 (the early autophagosome) or TOMM20 (the mitochondria). Since only a few regions of colocalization were observed between *PEX13* and these markers, *PEX13* likely does not function as a selective autophagy receptor.

In addition to receptors, other layers of selective autophagy regulation include post-translational modifications and autophagy adaptors. Given the precedent of peroxisome-associated proteins functioning as signaling platforms (Dixit et al., 2010;

Zhang et al., 2013), we speculate that PEX13 may regulate selective autophagy as a membrane-associated signaling node. PEX13 signals may lead to downstream post-translational modifications such as ubiquitination (Kirkin et al., 2009) or phosphorylation (Matsumoto et al., 2011; Wild et al., 2011), and thus activation of other yet-to-be identified selective autophagy regulators. Unbiased proteomics approaches will be helpful to interrogate this pathway.

One potential signaling factor downstream of PEX13 is MAVS, which is localized to both the mitochondria and peroxisome, and is a known antiviral signaling protein. The results of this study suggest that MAVS may be involved in selective autophagy, although this hypothesis needs to be evaluated further. Our results show that MAVS is required for virophagy in MEFs, but its role in mitophagy is less clear. MAVS-deficiency led to mitophagy defects in HeLa cells treated with 3 individual siRNA oligos, led to no change in mitophagy in HeLa cells treated with 2 individual siRNA oligos, and led to increased mitophagy in immortalized MEFs. One caveat for the experiment is the use of siRNAs, which may have off-target effects. Currently, it is yet unclear whether oligos that led to a mitophagy defect were false positives, or whether the oligos that led to no mitophagy defect were false negatives. This question can be addressed by assessing whether siRNA-resistant *MAVS* can rescue mitophagy defects after knockdown with si*MAVS* oligos #1, #3, and #4 (which showed a mitophagy defect). Another caveat for assessing mitophagy using immortalized MEFs is that these cells often acquire pro-survival mutations during the immortalization process. Thus, it may be best to evaluate Parkin-mediated mitophagy in a better characterized system, using HeLa cells with targeted knockout of *MAVS* using CRISPR/Cas9 technology and stably transfected with

Parkin. Even in CRISPR KO cells, off-target effects are a concern; thus reconstitution experiments are critical.

Although the molecular mechanism underlying PEX13 regulation of selective autophagy remains to be determined, our study provides important insights into ZSS pathogenesis. Cells expressing disease-associated PEX13 I326T and W313G mutant proteins showed a greater mitophagy defect compared with cells with PEX13 knockdown alone. Furthermore, overexpression of PEX13 with these mutations, but not wild-type PEX13, disrupted the normal reticular staining pattern of mitochondria during basal growth conditions. These results suggest that the disease-associated mutations interfere with mitophagy and mitochondrial quality control. It would be interesting to examine mitophagy or general autophagy in fibroblasts or tissues from ZSS patients, especially patients with mutations in PEX13 or PEX19. Further studies are required to examine the role of autophagy defects in the pathogenesis of developmental disorders associated with mutations in *PEX* genes.

Abnormal mitochondria are frequently observed in patients with *PEX* mutations and have been suggested to contribute to ZSS disease pathogenesis (Baumgart et al., 2001; Salpietro et al., 2015). The current prevailing paradigm is that mitochondrial dysfunction in ZSS is secondary to the defect in peroxisomal antioxidant functions and accumulation of lipid metabolites from the β -oxidation process (Baumgart et al., 2001). Based on our discovery that a subset of *PEX* genes are required for selective autophagy (*PEX3* and *PEX13*) while another subset are required for general autophagy (*PEX14* and *PEX19*), we propose that dysregulation of mitochondrial quality control in cells with defective mitophagy or general autophagy contributes to ZSS pathogenesis. Defects in

mitophagy-specific genes or core autophagy genes both lead to abnormal mitochondrial function, which contributes to the pathogenesis of aging, neurodegeneration, and cancer (Ding and Yin, 2012). Our model is not mutually exclusive with the previous paradigm of ZSS pathogenesis; the two functions of *PEX13* could be additive in promoting mitochondrial health. From a teleological perspective, it is reasonable to postulate the dual function of certain proteins such as PEX13 in the biogenesis of peroxisomes – organelles that detoxify reactive oxygen intermediates – and in mitophagy, a process that involves the removal of damaged mitochondria that generate reactive oxygen intermediates.

One outstanding question raised by this study is the functional significance of mitochondria-localized PEX13. Based on the colocalization analysis, we were unable to definitively rule out a small, yet functional pool of PEX13 localized at the mitochondria. Interestingly, during certain conditions including MAVS overexpression and PEX19 knockout, the majority of PEX13 localizes to mitochondria. Furthermore, *PEX19* KO HeLa cells are competent in mitophagy, suggesting mitochondria-localized PEX13 may be sufficient for mitophagy. This finding is consistent with our hypothesis that selective autophagy depends on only a subset of peroxins (PEX13 and PEX3); it does not on other peroxisome biogenesis factors (PEX14 and PEX19), nor on a functional peroxisome. Our findings raise the possibility that a fraction of PEX13 may normally localize to, and have a functional role at, the mitochondria and that this is a process regulated by yet unknown signals. We may address the question of whether PEX13 targeting to mitochondria is biologically meaningful through several steps, including: 1) determine whether PEX13 localizes to the mitochondria during physiological conditions,

2) identify signals regulating PEX13 localization to the peroxisome versus the mitochondria, and 3) determine whether the peroxisome-associated and/or mitochondria-associated PEX13 contribute to selective autophagy. These studies may provide further understanding of peroxisome-mitochondria connections and the functional significance of this inter-organellar crosstalk.

First, we can evaluate whether PEX13 localizes to the mitochondria during physiological conditions (without MAVS overexpression or PEX19 KO) to address limitations from our previous qualitative colocalization analysis using light microscopy. The two major limitations of that system are the resolution of the microscopy and the lack of quantification. Imaging using super-resolution microscopy provides much improved spatial separation compared with conventional light microscopy, reducing the spatial resolution from ~200 nm to ~20 nm (Fernandez-Suarez and Ting, 2008). Thus, super-resolution technologies such as photoactivated localization microscopy (PALM) and stochastic optical reconstruction microscopy (STORM) may be a better method to evaluate whether PEX13 is indeed closely associated with mitochondria. Colocalization experiments are useful first steps to determine whether two proteins of interests reside in proximity in situ. However, qualitative observation of colocalization may not be sufficiently informative when the degree of change is minor between test conditions. Both PEX13 and TOMM20 signals account for a large area in the cytoplasm. Thus, random chance alone may result in overlap of the signals. In the future, quantification of colocalization using Pearson's correlation coefficient and/or Mander's overlap coefficient may provide useful information (Costes et al., 2004; Zinchuk et al., 2007). Pearson's coefficient describes the correlation of shape distribution between two signals while

ignoring the intensities of the signals. The output ranges between -1.0 and 1.0, with 0 indicating no significant correlation and 1.0 indicating complete correlation. Negative Pearson's coefficients indicate negative correlation; however, Mander's overlap coefficient is generally recommended for these samples. Mander's coefficient indicates an overlap of the pixels, thus represents the true degree of colocalization. The combination of super-resolution microscopy and quantitative analysis of colocalization would improve the sensitivity for this assay.

In addition to microscopy techniques, subcellular fractionation to separate the mitochondria and peroxisome allows us to examine whether endogenous PEX13 is present in the mitochondrial fraction. Alternatively, immunoprecipitation of whole mitochondria using mitochondria outer membrane markers such as TOMM20 after mechanical lysis of the cell, and then western blotting for the presence of PEX13 associated with the mitochondria could also be informative. In combination, these microscopic and biochemical approaches may clarify whether a fraction of mitochondria-associated PEX13 is indeed present in physiological conditions. These techniques can also be applied to determine whether PEX13 localization to the mitochondria increases during mitophagy (cells treated with or without OA). Furthermore, these techniques can be applied to evaluate whether mitophagy-deficient *PEX13* mutants I326T and W313G localize to the mitochondria.

Second, it is important to identify how PEX13 localization to the peroxisome or the mitochondria is regulated. Currently, no mitochondrial targeting signal has been identified in PEX13 yet, and the molecular mechanism underlying PEX13 targeting to the peroxisomal membrane is somewhat unclear. One model for direct post-

translational targeting of PEX13 and other PMPs to the peroxisome proposes that PEX19 functions as a soluble chaperone that stabilizes newly synthesized PMPs in the cytosol, targets them to the peroxisome, and inserts them into the membrane through the membrane receptor PEX3 (Kim and Hettema, 2015). For PEX13, the predicted peroxisomal membrane targeting signal includes two non-overlapping binding sites to PEX19 (the cytosolic chaperon), a cluster of positively charged amino acid residues, and two putative transmembrane domains for membrane insertion (Jones et al., 2001; Van Ael and Fransen, 2006). It is possible that other cytoplasmic chaperones (perhaps ones containing mitochondria targeting signals) may bind newly synthesized PEX13 and facilitate its mitochondrial localization. IP-MS for PEX13-interacting proteins in *PEX19* KO cells may be useful for identification of such chaperones. Alternatively, we may mutate the predicted PEX19-binding domains in PEX13, and use IP-MS to identify chaperones that bind to this PEX19-binding-deficient PEX13 mutant.

Other pathways for PEX13 transport to the mitochondria are possible. For example, PEX13 may intrinsically contain a mitochondria targeting signal, similar to fission factors Fis1, DLP1, and Mff that localize to both peroxisomes and mitochondria and contain targeting signals to both organelles (Bonekamp and Schrader, 2012; Delille and Schrader, 2008; Gandre-Babbe and van der Bliet, 2008; Kobayashi et al., 2007; Koch et al., 2005). Alternatively, PEX13 could achieve both a peroxisome and mitochondrial localization via direct transfer through mitochondria-peroxisome contact sites, or through a vesicular trafficking from one organelle to another. Close connection between the mitochondria and peroxisomes have been described, suggesting intimate pathways for crosstalk (Schrader et al., 2015; Schumann and Subramani, 2008). Recent studies

are beginning to clarify the molecular regulation of this crosstalk. Studies from Heidi McBride and colleagues described a vesicular transport system between the mitochondria and the peroxisome in mammals (Braschi et al., 2010; Neuspiel et al., 2008). A recent report demonstrated a direct mitochondria-peroxisome contact site at the ERMES complex in yeast (Mattiuzzi Usaj et al., 2015). The importance of organelle interplay and interactions in disease is increasingly recognized. Studying how PEX13 localization is regulated may provide broader insight into the biology of their regulation.

Third, another outstanding question is whether the mitochondria-associated PEX13 is sufficient and necessary for mitophagy. To address this, we need to generate mutant PEX13 that target to mitochondria (and not peroxisomes) during physiological conditions without *PEX19* KO or MAVS overexpression. By evaluating whether this mitochondrial-targeted PEX13 mutant can rescue mitophagy defects in PEX13-deficient cells, we may be able to assign a functional role for mitochondrial-localized PEX13.

Chapter III: Exercise-induced autophagy and cancer

III.1. Literature review

III.1.A. Exercise and autophagy protect against similar pathologies

Autophagy functions in basal conditions as a cellular recycling system and can be up-regulated in response to energetic stress. When energetic demand exceeds nutrient input, autophagy is activated to degrade cytosolic components for regenerating building blocks for ATP energy production. Exercise is a potent stimulus for autophagy in many tissues including skeletal muscle, cardiac muscle, liver, pancreas, adipose tissue, and brain (He et al., 2012a; He et al., 2012b). Exercise-induced autophagy promotes glucose homeostasis during acute exercise; it also mediates exercise protection against high-fat-diet induced glucose intolerance (He et al., 2012a). Therefore, autophagy mediates both short-term and long-term adaptation to exercise. Since autophagy and exercise both have been independently associated with protection against a wide range of pathologies, including cardiovascular diseases, metabolic disorders, cancer, neurodegeneration, inflammatory diseases, and aging, we speculate that autophagy may contribute to exercise-mediated protection against diseases other than metabolic disorders (Choi et al., 2013; Handschin and Spiegelman, 2008; Levine and Kroemer, 2008; Mizushima and Komatsu, 2011; Physical Activity Guidelines Advisory Committee, 2008). Here, I will focus the literature review on the connection between exercise, autophagy, and their protective roles in cancer.

III.1.B. Exercise reduces cancer risk

Epidemiological evidence indicates a strong association between increased physical activity with reduced risk for cancer, especially for breast and colon cancers

(Thune and Furberg, 2001). Clinical trial evidence suggests that exercise is a safe and effective adjunct therapy to reduce common treatment-related side effects in cancer patients. Additional clinical trials are ongoing to evaluate whether exercise is associated with improved prognosis for cancer patients (Jones and Alfano, 2013). In laboratory settings, similar associations between exercise and reduced tumorigenesis have been demonstrated in animal models of breast, colon, and other cancers (Aoi et al., 2013; Gillette et al., 1997; Jones and Alfano, 2013; Michna et al., 2006; Na and Oliynyk, 2011; Pedersen et al., 2016). Recently, Lee Jones and colleagues demonstrated that voluntary wheel running, which is a mouse model for general physical activity in humans, decreases primary tumor growth and distant lung metastases in three independent models of murine breast cancer, including the E0771 injection model in C57BL/6 mice (Betof et al., 2015).

III.1.C. Proposed mechanisms mediating exercise protection against cancer

Despite the abundance of observations linking physical exercise to reduced cancer risk, the molecular mechanisms mediating this process remain to be clearly defined. Exercise modulation of metabolism, growth factors, sex hormones, inflammation, and immune surveillance are hypothesized to influence tumor initiation and progression. Of note, many of these factors are circulating in the blood, and are derived from one cell to affect other cells via paracrine or endocrine pathways (Fig. 3.1) (Rundle, 2011). Thus, these proposed mechanisms are mostly cell-extrinsic to the cancer or precancerous cells. Whether exercise exerts cell-intrinsic protection against cancer is yet unclear. Abundant evidence supports the concept that autophagy is a tumor suppressor pathway via both cell-intrinsic and cell-extrinsic mechanisms (detailed in the section “Autophagy and

Cancer”). Thus, it is possible that exercise-induced autophagy can regulate secretion of circulating factors, including cytokines, to mediate exercise benefits against cancer in a cell-extrinsic manner. Furthermore, exercise-induced autophagy may activate autophagy in the precancerous or cancerous cells to confer cell-intrinsic protection against cancer initiation or progression. In the current study, we focus on the hypothesis that exercise-induced autophagy provides cell-extrinsic protection to cancer progression by modulating tumor microenvironment.

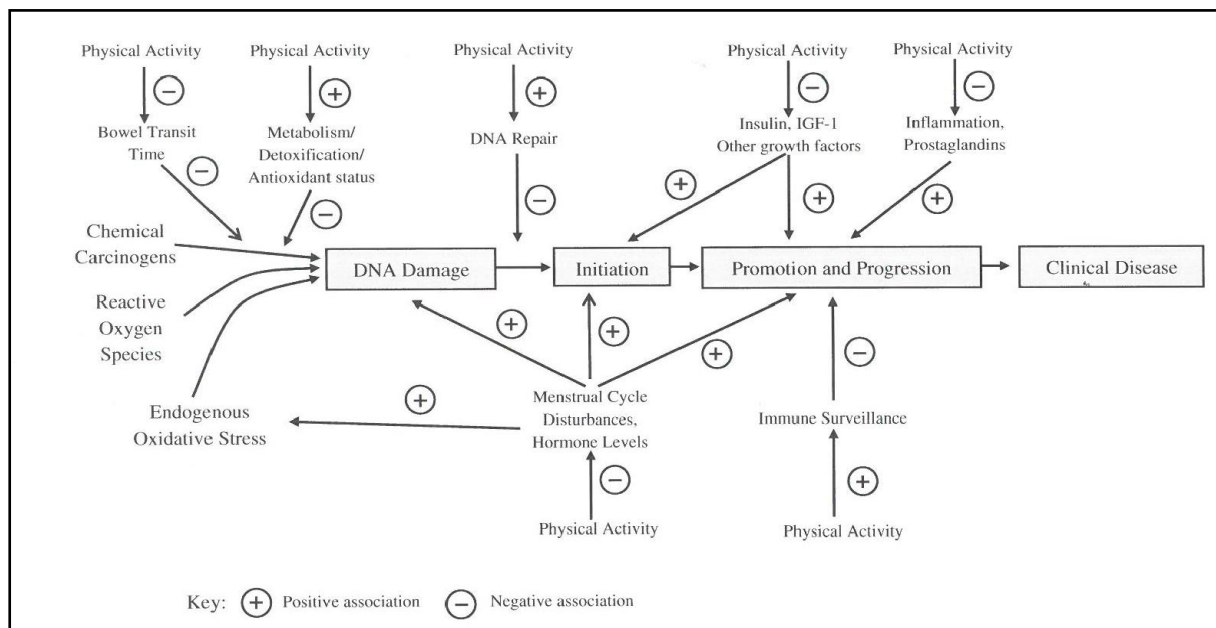


Figure 3.1. Summary of potential mechanisms underlying physical activity benefits to reduce cancer risk.

Hormones, growth factors, inflammation, and immune surveillance are leading pathways suggested to influence the progression of established cancers. (Figure adapted from Rundle, 2011).

Exercise has been known to regulate secretion from various cells, such as insulin secretion from pancreatic beta-cells and insulin-like growth factor 1 secretion from hepatocytes (McTiernan, 2008). Recently, skeletal muscle is increasingly recognized as an endocrine organ and a source for factors that mediate systemic responses to

exercise (Pedersen and Febbraio, 2012; Pedersen et al., 2016). Myokines are a collection of cytokines and metabolically active peptides released from contracting skeletal muscle. Some myokines have been shown to mediate some physiological benefits of exercise (Egan and Zierath, 2013; Pedersen and Febbraio, 2012). Specifically, secreted protein acidic and rich in cysteine (SPARC) and IL-6 have been implicated in exercise-mediated protection against cancer.

SPARC is a secreted glycoprotein involved in tissue remodeling, angiogenesis, and tumorigenesis (Watkins et al., 2005). It has been associated with both pro-cancer and anti-cancer functions (Nagaraju and Sharma, 2011; Watkins et al., 2005). Recently, a study found that circulating SPARC is elevated after acute exercise, and that chronic aerobic training reduces carcinogen-induced colon tumorigenesis in WT mice but not in SPARC-null mice (Aoi et al., 2013). Further in vitro experiments show that SPARC is secreted from myocytes after cyclic stretching and that SPARC attenuates cancer growth by increasing apoptosis in colon cancer cells (Aoi et al., 2013). Together, this suggests that SPARC is a myokine that mediates exercise protection against carcinogen-induced colon tumorigenesis (Aoi et al., 2013). How SPARC exerts protection against cancer and whether SPARC can protect against other types of cancers are yet unknown.

IL-6 is the most highly elevated myokine after acute exercise in human and in mice (Ellingsgaard et al., 2011; Ostrowski et al., 1998; Pedersen, 2000). Chronic endurance training, however, may decrease basal plasma IL-6 and attenuate IL-6 induction by acute exercise (Fischer, 2006). In vitro studies have reported both pro-tumor and anti-tumor functions of IL-6, suggesting that its actions may be context dependent on cancer

subtype, tumor microenvironment, and additional cofactors (Knupfer and Preiss, 2007). For Kaposi's sarcoma, renal cell carcinoma, cervical carcinoma, and certain T- and B-cell lymphomas, IL-6 functions as a growth factor (Eustace et al., 1993; Kawano et al., 1988; Miki et al., 1989; Miles et al., 1990; Shimizu et al., 1988; Yee et al., 1989). In the B16F10 melanoma mouse model, exercise-induced IL-6 promotes NK cell infiltration and delayed tumor progression (Pedersen et al., 2016). In human breast cancer patients, serum IL-6 levels inversely correlate with prognosis (Knupfer and Preiss, 2007). However, it remains to be tested whether IL-6 inhibits, promotes, or has no effect on breast cancer. Since IL-6 mediates pleiotropic downstream effects, more studies are required to evaluate the effects of exercise-induced IL-6 on various tumor types. In this study, we hypothesize that SPARC, IL-6, and other yet-to-be-identified circulating factors could be regulated by exercise-induced autophagy and confer protection against cancer.

III.1.D. Autophagy mutant mouse models with altered Bcl-2-Beclin 1 interaction

Beclin 1 is the mammalian homolog of the yeast core autophagy gene *ATG6*. It is the first mammalian gene shown to function in autophagy (Liang et al., 1999), and it serves a critical role in autophagy regulation through its function in the initiation complex (Kihara et al., 2001). Bcl-2 family members, including Bcl-2 and Bcl-X_L, bind to Beclin 1 and inhibit its function in autophagy (Pattingre et al., 2005). Mechanistic understanding of the Bcl-2/Beclin 1 interaction led to the development of several genetic mouse models for studying autophagy deficiency or excess.

First, since *beclin 1* is a required autophagy initiation, it was targeted for deletion to

generate a mouse model with deficient autophagy (Fig 3.2). Similar to other mouse models of *Atg* gene knockout, homozygous deletion of *beclin 1* is embryonic lethal. Mice with heterozygous deletion of *beclin 1* are viable, have reduced basal and stress-induced autophagy, and increased spontaneous tumorigenesis (He et al., 2012a; Qu et al., 2003; Yue et al., 2003). Additionally, *beclin 1* heterozygous knockout (KO) mice have increased susceptibility to other diseases, including infectious diseases and neurodegenerative disorders (Levine et al., 2015).

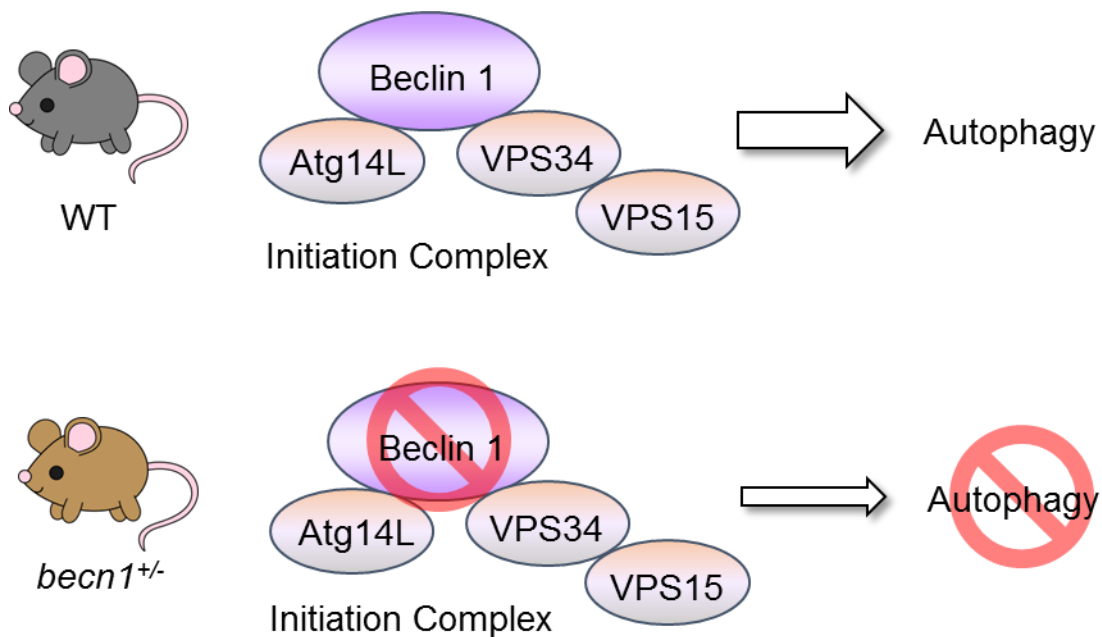


Figure 3.2. *Beclin 1* knockout mouse is deficient in autophagy.

Beclin 1 is a core autophagy protein functioning in the Class III PI3K initiation complex. Mice with heterozygous deletion of *beclin 1* (*becn1*^{+/-}) have reduced basal and stress-induced autophagy.

Next, a mouse model for decreased stress-induced autophagy, but normal baseline autophagy was generated. Under stress conditions, triple-site phosphorylation of Bcl-2 on the non-structured loop at the T69, S70, and S87 residues dissociate Bcl-2 from Beclin 1, thereby promoting autophagy (Fig. 3.3). A mutant form of Bcl-2 with three point mutations, T69A, T70A, and S87A (Bcl-2 AAA), cannot be phosphorylated at these

regulatory sites, and thus cannot dissociate from Beclin 1 under stress conditions. In cell culture, Bcl-2 AAA mutants have normal basal autophagy and defective starvation-induced autophagy (Wei et al., 2008). Bcl-2 AAA mice have normal basal autophagy but are deficient in both starvation- and exercise-induced autophagy in vivo (He et al., 2012a); thus, these mice provide a useful tool for studying the physiological functions of exercise-induced autophagy. Of note, the Bcl-2 AAA mice have no apparent phenotype associated with apoptosis (He et al., 2012a).

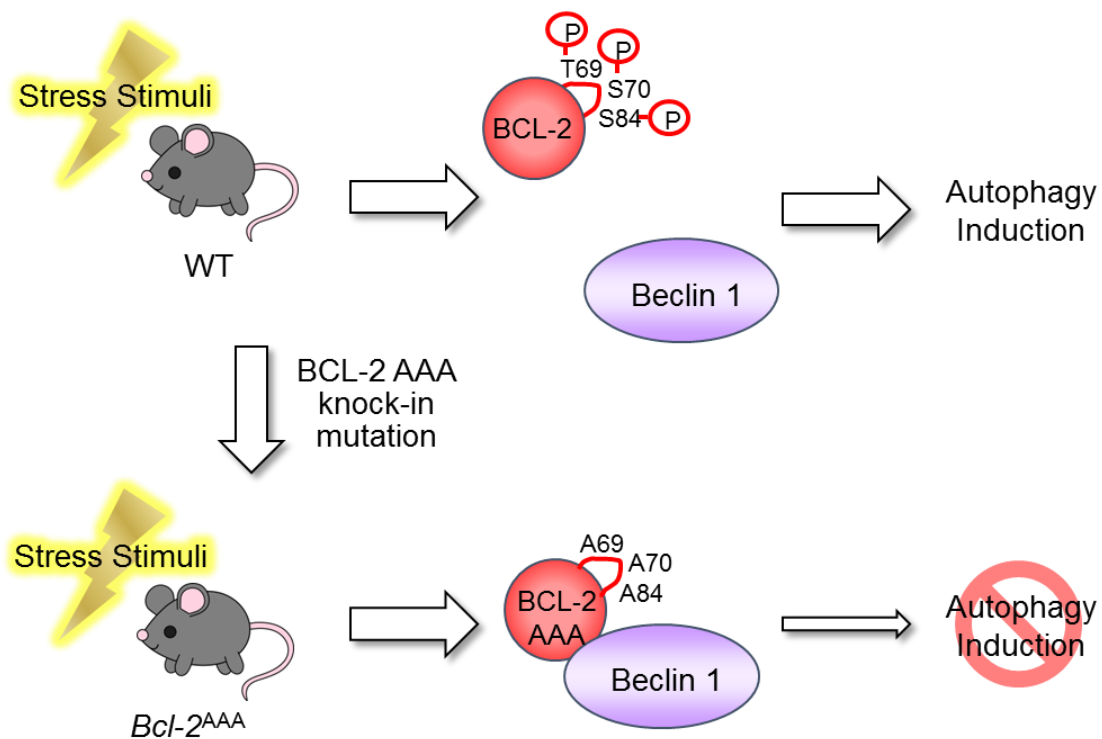


Figure 3.3. BCL2 AAA knock-in mouse is deficient in stress-induced autophagy.

Triple site phosphorylation at the T69, S70, and S87 residues on the non-structured loop of Bcl-2 allow BCL-2 to dissociate from Beclin 1 during autophagy-stimulating stresses such as nutrient starvation and physical exercise. Point mutations altering these three amino acid residues to alanine makes the loop non-phosphorylatable, and thus inhibits BCL-2 dissociation with Beclin 1. Mice containing the triple alanine (Bcl2 AAA) knock-in mutations (*Bcl2^{AAA}*) have defective stress-induced autophagy.

A third mouse model with altered Bcl-2/Beclin 1 interaction was generated to model excessive autophagy activation in vivo (Fig. 3.4). A point mutation F123A in the Bcl-2

binding domain of human Beclin 1 disrupts the interaction between Beclin 1 and Bcl-2 family members. This abolishes the negative regulation on autophagy induction in vitro (Pattingre et al., 2005). Mice with the F121A mutation (orthologous to F123A in human), are predicted to have increased basal and/or stress-induced autophagy, although this remains to be tested experimentally. In summary, these mouse models with mutations targeting Bcl-2-Beclin 1 interaction have altered autophagy initiation, thus are useful for studying the physiological role of basal and stress-induced autophagy in mammals. Other genetic models of autophagy mutants are mostly deficient in autophagy, and are reviewed recently ((Levine et al., 2015).

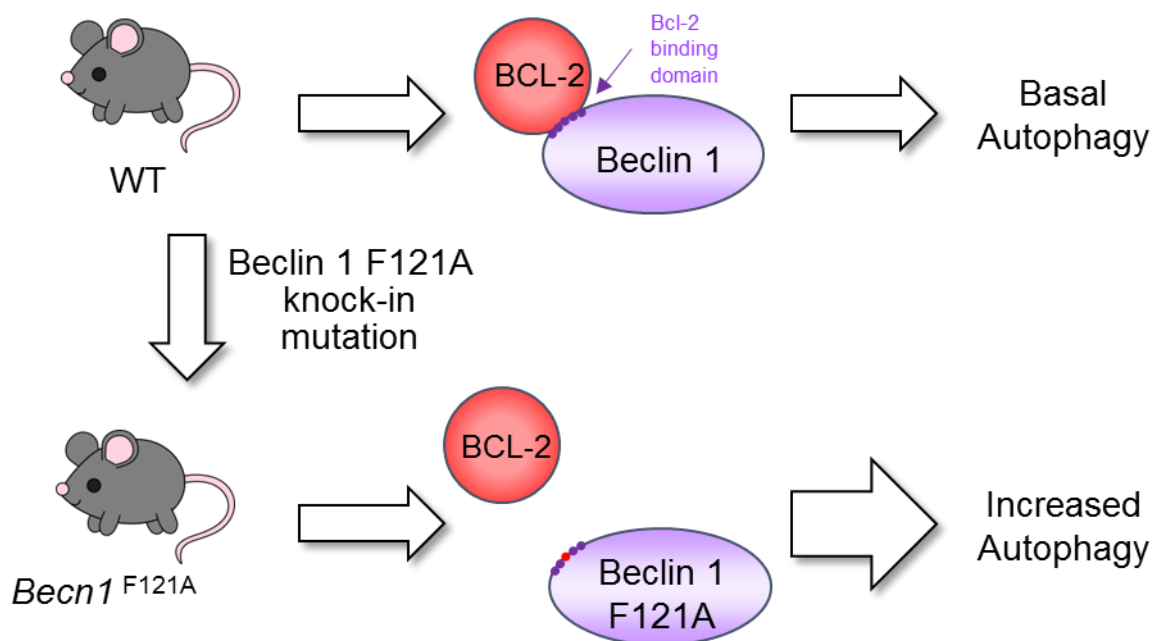


Figure 3.4. Beclin 1 F121A knock-in mouse has increased autophagy.

The F123A mutation on the Bcl-2 binding domain of human Beclin 1 inhibits Bcl-2 binding and has increased autophagy. Mice with the orthologous mutation F121A are proposed to have increased basal and stress-induced autophagy.

III.2. Introduction

Autophagy is a lysosomal degradation pathway that breaks down unwanted proteins and organelles from the cytoplasm to regenerate cellular building blocks. This process is constitutively active at low basal levels, and can be upregulated to promote cellular homeostasis and survival during stress conditions. Autophagy and exercise have both been independently associated with protection against many of the same human health conditions, including cancer, neurodegeneration, inflammatory diseases, aging, and metabolic disorders (Choi et al., 2013; Handschin and Spiegelman, 2008; Levine and Kroemer, 2008; Mizushima and Komatsu, 2011; Physical Activity Guidelines Advisory Committee, 2008). A previous study from the Levine laboratory demonstrated that exercise is a potent inducer of autophagy in multiple tissues and that autophagy contributes to exercise-mediated benefits to metabolism (He et al., 2012a). Therefore, we speculate that autophagy may contribute to exercise protection against other diseases. Although many epidemiological and laboratory studies have provided strong evidence that physical exercise decreases cancer risk and associated mortality, the underlying mechanisms are poorly understood (Na and Oliynyk, 2011; Physical Activity Guidelines Advisory Committee, 2008; Thune and Furberg, 2001). In this study, we investigated the role of autophagy as a potential mechanism contributing to exercise-mediated protection against cancer progression focusing on the potential role of exercise-induced autophagy in regulation of the tumor microenvironment. Using the E0771 injectable murine breast cancer model, our study examined the effect of aerobic training on cancer progression in wild-type (WT) mice and mutant mice that are deficient in exercise-induced autophagy (*Bcl-2^{AAA}* and *Becn1^{+/-}*). We examined the metabolome

and proteome in tissues from these mice for changes in tumor physiology and for factors that could influence the tumor microenvironment. Our preliminary results suggest that two forms of physical exercise, aerobic training and voluntary physical activity, delays E0771 tumor progression in WT mice but not in mice deficient in exercise-induced autophagy. Further experiments are required to validate our hypothesis that exercise-induced autophagy protects against tumor progression and elucidate the underlying mechanism.

III.3. Materials and methods

III.3.A. Cell culture

E0771 murine breast adenocarcinoma cells (Ewens et al., 2005) were cultured as described in RPMI media supplemented with 10% FBS, 10 mM HEPES buffer, 2 mM L-glutamine, and 1x penicillin/streptomycin at 37°C with 5% CO₂. E0771 cells stably transfected with GFP-LC3 (E0771/GFP-LC3 cells) were generated as previously described (Orvedahl et al., 2010) and maintained in media containing 10 µg/ml G418.

III.3.B. Mouse colonies

All animal procedures were performed in accordance with institutional guidelines and with approval from the Institutional Animal Care and Use Committee (IACUC). All mice were housed in barrier facilities in autoclave-sterilized ventilated microisolator cages, with 12 hour light/12 hour dark cycle and with ad libitum access to food and water. GFP-LC3 transgenic, *Becn1*^{+/-} (Liang et al., 1999), *Bcl-2*^{AAA} (He et al., 2012a), and *Becn1*^{F121A} (unpublished) mice have been previously generated. All strains were

backcrossed with WT C57BL/6J mice (Jackson Laboratories) for at least 10 generations. Age-matched 2- to 4-month-old nulliparous female mice were used in all experiments unless otherwise noted.

III.3.C. Genotyping PCR

To extract genomic DNA from mouse tails, ears, or toes, a small piece of tissue was cut from each mouse, and digested in tail PCR DNA digestion solution and proteinase K at 55°C for 4 hours to overnight and then heat-inactivated at 85°C for 1 hour. The samples were centrifuged for 1 minute at maximum speed to pellet the tissue debris. Supernatants containing genomic DNA were used for PCR genotyping. The following reaction mixes were used for PCR amplification of DNA: 0.5 µl genomic DNA, 0.25 µl primers with a concentration of 100 µM, 10 µl SapphireAmp Fast PCR Master Mix (Takara, RR350A), and dH₂O to make up final volume of 20 µl. PCR products were separated using 1.0% to 2.0% agarose gels in TAE buffer containing ethidium bromide and visualized using an imager (Alphalmager HP). Table 3.1 contains the PCR primer sequences.

Table 3.1. Genotyping PCR primer sequences

Genotype	Direction	Sequence	Amplicon size
<i>Bcl-2</i> WT	Forward	GGGACATGGCTGCCAGGACGT	430 bp
	Reverse	GACCCAGAATCCACTCACACCCC	
<i>Bcl-2</i> AAA	Forward	GGGACATGGCTGCCAGGGCGG	420 bp
	Reverse	GACCCAGAATCCACTCACACCCC	
<i>Beclin 1 F121A</i>	Forward	GGCAGTAGTATAATGTCTGCTCCAG	600 bp= F121A 300 bp= WT
	Reverse	TGGGTCTCTCATTGCATTTATTTAT	
<i>GFP-LC3</i>	Forward	ATAACTTGCTGGCCTTTCCACT	250 bp = GFP-LC3 350 bp= WT LC3
	Reverse #1	CGGGCCATTTACCGTAAGTTAT	
	Reverse #2	GCAGCTCATTGCTGTTCCCTCAA	

III.3.D. Aerobic training protocol #1

Mice were randomized to aerobic training or sedentary control groups at ages 2 to 4 months prior to the experiment. Mice were acclimated to and trained on a 10° uphill Exer 3/6 open treadmill (Columbus Instruments) for 2 days according to a previous protocol (He et al., 2012a). During day 1 of acclimation, mice ran for 5 minutes at 8 m/minute and during day 2 of acclimation mice ran for 5 minutes at 8 m/minute followed by another 5 minutes at 10 m/minute. On day 3, mice were injected with 2×10^5 E0771/GFP-LC3 cells in PBS in the 4th right mammary fat pad and then were allowed to rest. On day 5, mice in the aerobic training cohort started training at 17 m/minute for 50 minutes/day, 5 days/week. Aerobic training was conducted during the afternoon between 1 to 5 PM to minimize potential confounding experimental variables (such as circadian rhythm effects) as much as possible.

III.3.E. Aerobic training protocol #2

In this modified protocol, mice were trained on the treadmill with no incline level at increased intensity. Prior to the experiment, mice in the AT group were acclimated to the treadmill for 4 days. During day 1, mice ran at 10 m/minute for 10 minutes. During day 2, mice ran at 15 m/minute for 10 minutes. During day 3, mice ran at 15 m/minute for 10 minutes and then at 20 m/minute for 5 minutes. During day 4, mice ran at 15 m/minute for 10 minutes and then 20 m/minute for 10 minutes. On day 5, all mice were injected with 2×10^5 E0771/GFP-LC3 cells in PBS in the 4th right mammary fat pad. On days 6 to 8, mice recovered from the surgery without aerobic training. Starting on day 9, aerobic training group received training at 15 m/minute for 10 minutes and then at 20

m/minute for 50 minutes. Changes in speed were implemented at 1 m/minute/minute. Mice were trained 5 days/week. To promote treadmill running, mild electric shocks (≤ 0.3 mA) were delivered to mice that fell onto the shock grid at the end of the treadmill. To avoid excessive shocking, the shock grid was disengaged for mice that spend more than 10 seconds continuously on the shock grid without attempting to resume running. Completed running distance and qualitative assessment of running ability (based on the number of shocks the mouse received) were recorded for each mouse daily. Aerobic training was conducted during the afternoon between 1 to 5 PM. Sedentary control mice were placed in the treadmill at 2 m/minute for 60 minutes, 5 days/week.

III.3.F. Voluntary wheel running physical activity

Mice were housed individually in cages containing a Home Cage Running Wheel system (Columbus Instruments) for voluntary physical activity. Sedentary control mice were housed individually in cages without running wheels. The numbers of wheel rotations were recorded at 10-second intervals to track running patterns. Mice were acclimated to individual housing 7 days prior to experiment. On day 1 of experiment, mice were injected with 2×10^5 E0771/GFP-LC3 cells in 100 μ l PBS in the 4th right mammary fat pad.

III.3.G. Tumor progression analyses

To evaluate tumor volume progression over time, E0771 tumor dimensions were measured using a digital caliper 2 to 3 times weekly. The longest axis of the tumor (l) and the widest measurement perpendicular to the length (w) were used to calculate

tumor volume (volume= $\frac{1}{2} * l * w^2$). In accordance with IACUC guidelines, mice were sacrificed when the tumor size exceeded 2000 mm³ which was around 3 weeks after tumor injection. At the time of sacrifice, all tumors were dissected from the mice, and the tumor volumes and masses were recorded. Statistical analyses for tumor progression were conducted in collaboration with Drs. Guanghua Xiao, Yang Xie, and Rui Zhong at the University of Texas, Southwestern Medical Center. Mixed linear model for repeated measures was used to determine whether tumor volume progression over time was affected by exercise treatment for mice in each genotype group. ANOVA was used to analyze whether exercise treatment and genotype affected final tumor volume or tumor mass.

III.3.H. Tissue collection

Mice were sacrificed with isoflurane gas overdose as soon as possible after acute exercise. Plasma, quadriceps femoris, gastrocnemius, soleus, mammary fat pads, brain, and/or E0771/GFP-LC3 tumors were collected. Approximately 150 µl of plasma was collected per mouse, snap frozen in liquid nitrogen, and stored at - 80 °C in aliquots to avoid free-thaw degradation. Tissue for proteomics, metabolomics, and other biochemical assays were dissected from the mice immediately after sacrifice, snap frozen in liquid nitrogen, and stored at -80°C. Tissues for histological and immunostaining studies were collected from mice perfused with 4% paraformaldehyde (PFA) and then processed into frozen sections or paraffin-embedded sections.

III.3.I. Processing of tissue sections

Tissues collected from mice perfused with 4% PFA were incubated in PFA for an additional period of at least 4 hours. For frozen sections, tissues were incubated in 15% sucrose in PBS for ≥ 4 hours and then transferred to 30% sucrose for ≥ 4 hours at 4°C. For paraffin sections, tissues were incubated in PFA for ≥ 4 hours and then 70% ethanol for ≥ 4 hours at 4°C. The processed tissues were embedded in blocks and cut onto slides by the Experimental Molecular Pathology Core Facility at the Columbia University Medical Center.

III.3.J. Tissue homogenization

For each sample, ~ 50 mg snap frozen tissue was cut into smaller pieces on an ice-cold block using a razor blade. The tissue pieces were homogenized in ice-cold RIPA buffer (50 mM Tris-HCl pH 7.4, 150 mM NaCl, 1% triton X-100, 1% sodium deoxycholate, 0.1% SDS, 1 mM EDTA) with protease inhibitor, using the beads beater (BioSpec). Tissues were homogenized with five cycles of beating for 30 seconds alternating with 30 seconds on ice to avoid overheating the samples. The procedure was conducted in the 4°C cold room to minimize sample degradation. The resulting homogenate samples were transferred to new microtubes, centrifuged at maximum speed for 15 minutes at 4°C to remove tissue debris. The supernatants were transferred to new microtubes and stored at - 80°C.

III.3.K. Proteomics screen

A targeted proteomic screen was conducted in collaboration with the Keck Mass Spectrometry and Proteomics Resource laboratory at Yale University School of Medicine using 8-plex isobaric tag for relative and absolute quantification (iTRAQ). The general principle of isobaric tagging is shown in Fig. 3.5. Briefly, biological samples were processed in parallel and tagged with the isobaric reporter tags. The tagging reagent includes three components: the reactive component covalently binds with a peptide; the reporter component in each sample generates a distinct mass to charge ratio (m/z) for quantification; and the balance component ensures that the overall mass of each tag is identical. After tagging, the samples are pooled and analyzed on LC-MS/MS simultaneously. The ability to run all samples simultaneously overcomes the variability between runs allowing for improved accuracy in quantification of protein abundance (Gingras et al., 2007).

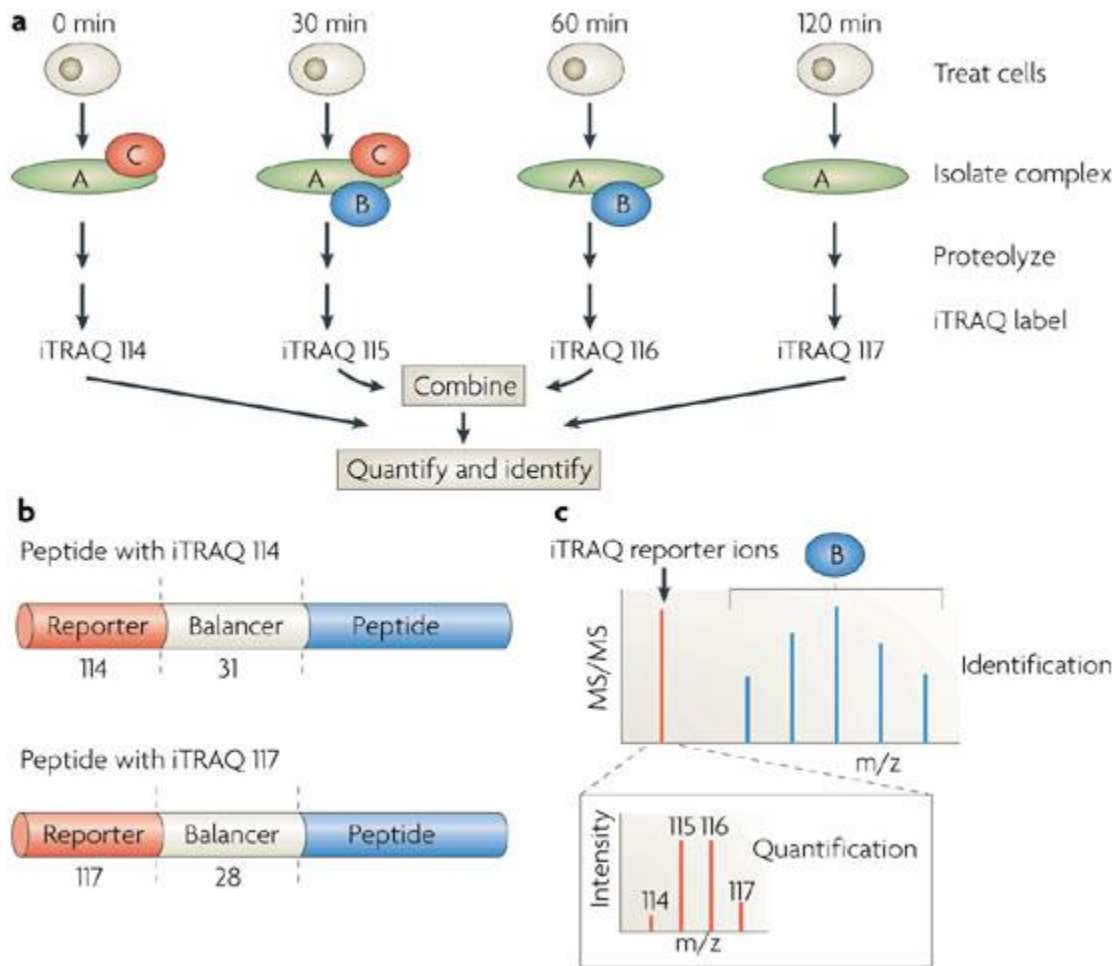


Figure 3.5. Schematic for iTRAQ.

(a) Biological samples such as cells or tissues are processed in parallel. iTRAQ isobaric tags are added chemically to each sample and then the samples are combined and analyzed using LC-MS/MS simultaneously. (b) Peptides from different biological samples are labeled with the different isobaric tags with different reporter and balancer masses. Each tag combining the reporter and balancer is the same mass. (c) MS/MS analysis generates a spectrum for the peptide (shown in blue) that allows for identification of the protein. The analysis also generates relative quantification data using the spectrum of the reporter fragments (shown in red). (adapted from Gingras et al, 2007)

Tissue samples were processed as similarly as possible with the same number of freeze/thaw cycles and same time of exposure to room temperature. We compared skeletal muscle samples from WT and *Bcl-2^{AAA}* mice collected during the sedentary state, after acute exercise, or after chronic aerobic training (n=4 per group). This screen was designed to identify candidate myokines (i.e. muscle secreted proteins) that may potentially regulate physiological benefits of exercise-induced autophagy. Top

candidates from the screen were validated using immunoassays such as western blotting or enzyme-linked immunosorbent assay (ELISA).

III.3.L. Metabolomic screen #1

The first metabolomic screen was conducted in collaboration with Dr. Clary Clish at the Broad Institute. Plasma, mammary fat, and skeletal muscle (quadriceps femoris) samples were collected from a cohort of WT and *Bcl-2^{AAA}* female mice after undergoing acute exercise, chronic aerobic training, or sedentary control treatment. For the acute exercise group, tissues were collected after the mice ran for 50 minutes at 17 m/minute. For the chronic aerobic training group, mice were subjected to treadmill running for 4 weeks daily according to aerobic training protocol #1, and tissues were collected 24 hours after the preceding exercise bout to represent baseline alterations after aerobic training. The sedentary group mice were placed in the treadmill without exercise to control for handling stress. Pairwise samples were analyzed using the Wilcoxon rank sum tests and pathway enrichment analyses to identify metabolic differences in the following sample pairs: *Bcl-2^{AAA}* aerobic training versus *Bcl-2^{AAA}* sedentary, WT aerobic training versus WT sedentary, and *Bcl-2^{AAA}* aerobic training versus WT aerobic training. Pathway enrichment analysis was conducted to analyze the aggregate metabolomics data.

III.3.M. Metabolomic screen #2

The second metabolomic screen was conducted in collaboration with Drs. Ralph DeBerardinis, Zeping Hu, and Ling Cai at the University of Texas Southwestern Medical

Center using plasma collected from a cohort of WT, *Bcl-2^{AAA}*, and *Becn1^{+/-}* mice with E0771/GFP-LC3 tumors and subjected to chronic aerobic training or sedentary control treatment. At 14 days and 21 days post-injection with E0771/GFP-LC3 cells, tumors were collected for analysis. Day 14 was chosen because tumor sizes were similar between all treatment and genotype groups at this early time point. Day 21 was chosen as the late time point when tumors were expected to reach terminal size. Metabolites were extracted from tissue homogenates using methanol precipitation, and a targeted panel of approximately 200 metabolites covering major metabolic pathways was detected using liquid chromatography-mass spectroscopy (LC-MS). MS data were normalized using total ion current (TIC) as internal control to derive relative quantitation of each metabolite in each sample.

III.3.N.qRT-PCR with mouse tissues

RNA from skeletal muscles homogenates was extracted using RNeasy Fibrous Tissue Mini Kit (Qiagen). RNA from all other tissue homogenates was extracted using RNeasy Plus Mini Kit (Qiagen) according to the manufacturer's instructions. Each RNA sample was eluted in 50 µl dH₂O twice to maximize RNA concentration. Protocols for assessing RNA quality and quantity and for qRT-PCR are described in the Chapter 2 Materials and Methods section. Primers for evaluating expression of specific genes related to exercise adaptation are listed in Table 3.2.

Table 3.2. qRT-PCR primer sequences for evaluating expression of genes related to exercise training

Gene	Direction	Sequence	Amplicon size
β -Actin	Forward	CGTGAAAAGATGACCCAGATCA	66 bp
	Reverse	CTGGATGGCTACGTACATGGCT	
SPARC	Forward	CTGCTCAGTTTGACCCTCAGT	130 bp
	Reverse	CGTGAGGTCGCCTGATTCT	
Idh2	Forward	AGTGTGGCTGTCAAGTGTGC	95 bp
	Reverse	ATCGTTCCGTTAGGGCTCTT	
Ndufa13	Forward	ACGGCCCCATCGACTACAA	120 bp
	Reverse	CCTGGTTCCACCTCATCATTCT	

III.4. Results

III.4.A. Evaluating the role of autophagy in chronic aerobic training protection against E0771 tumor progression

To evaluate whether exercise-induced autophagy confers protection against progression, we evaluated wild-type (WT) and *Bcl-2*^{AAA} mice injected with E0771/GFP-LC3 cells. E0771 is an estrogen-positive breast medullary adenocarcinoma cell line previously established from a spontaneous mammary tumor in C57BL/6 mice (Ewens et al., 2005). We chose this cancer model because E0771 cells could be easily maintained in cultured and injected orthotopically into the mammary fat pad of C57BL/6 female mice to form a subcutaneous solid tumor allograft. Additionally, our collaborator Dr. Lee Jones at Memorial Sloan Kettering Cancer Center showed that voluntary wheel running exercise reduces E0771 tumor progression in C57BL/6 mice (Betof et al., 2015). In the current study, we used E0771 cells stably expressing GFP-LC3 (E0771/GFP-LC3) for monitoring tumor autophagy levels.

Previously, the Levine laboratory showed that 8 weeks of daily aerobic training by treadmill running protected WT mice from high-fat-diet induced glucose intolerance, while *Bcl-2*^{AAA} mice with deficient exercise-induced autophagy did not experience exercise protection (He et al., 2012a). Using this exercise protocol (aerobic training

protocol #1), we observed no exercise effect on E0771/GFP-LC3 tumor progression in WT mice (data not shown). We suspect that a higher aerobic exercise dose may be required to achieve a protective effect on E0771/GFP-LC3 allograft growth over the relatively short time frame of 3-4 weeks before tumors reach terminal size. Thus, we increased running speed and total running distance in a modified aerobic training protocol (aerobic training protocol #2, Fig 3.6a). We also subjected the sedentary control mice to slow moving treadmill for 1 hour daily to mimic the handling stress and circadian rhythm disruption experienced by mice in the aerobic training group. Using aerobic training protocol #2, we observed significant exercise benefits to delay tumor progression in WT mice ($p < 0.05$, mixed linear model for repeated measure) but not in *Bcl-2^{AAA}* mice ($p > 0.05$, mixed linear model for repeated measure) (Fig. 3.6b). At 30 days after tumor initiation, WT mice with aerobic training had 39% reduced tumor burden compared with sedentary WT mice ($p < 0.05$, ANOVA). In contrast, aerobic training did not reduce tumor burden in *Bcl-2^{AAA}* mice ($p > 0.05$, ANOVA). Since *Bcl-2^{AAA}* mice are deficient in exercise-induced autophagy, our data suggest that exercise-induced autophagy may be required for exercise-mediated protection against the progression of established breast tumors.

To confirm our findings, we further examined aerobic training effects on E0771/GFP-LC3 tumor progression in an independent cohort of WT and *Bcl-2^{AAA}* mice using aerobic training protocol #2. In this cohort, we confirmed that exercise delayed tumor progression in WT mice ($p = 5.4 \times 10^{-6}$, mixed linear model for repeated measure) but not in *Bcl-2^{AAA}* mice ($p = 0.4$, mixed linear model for repeated measure) (Fig. 3.6c). At 23 days after tumor initiation, WT mice with aerobic training had 37% reduction in tumor

volume ($p < 0.05$, ANOVA) and 43% reduction in tumor mass ($p = 0.065$, ANOVA) compared to the sedentary control WT mice (Fig. 3.6d). In contrast, at 23 days after tumor initiation, *Bcl-2^{AAA}* mice with aerobic training had no reduction in tumor volume ($p = 0.2$, ANOVA) and no reduction in tumor mass ($p = 0.86$, ANOVA) compared to the sedentary control *Bcl-2^{AAA}* mice. We observed no difference in tumor progression between sedentary WT and *Bcl-2^{AAA}* mice.

To examine whether E0771 cells are autophagy competent, we evaluated starvation-induced autophagy in vitro by western blot analysis of p62 degradation and LC3 conversion. Nutrient starvation induced p62 degradation, LC3-I to LC3-II conversion, and total LC3 degradation in E0771 cells (Fig. 3.6e), indicating that they have an intact autophagy pathway. Since we injected autophagy-competent tumor cells into host animals that are either competent for stress-induced autophagy (WT) or not (*Bcl-2^{AAA}*), our experimental design allowed us to rule out cell-intrinsic effects of autophagy on tumor growth. Thus, our results suggest that exercise-induced autophagy likely suppresses tumor progression via a cell-extrinsic pathway in our experimental setting. That is, exercise induction of autophagy in host tissues other than the tumor is important for tumor suppression. However, our study was not designed to address the potential contribution of exercise-induced protection against tumor progression in a cell-intrinsic mechanism. Future experiments comparing tumor grafts using cancer cells with or without competent autophagy would address that question.

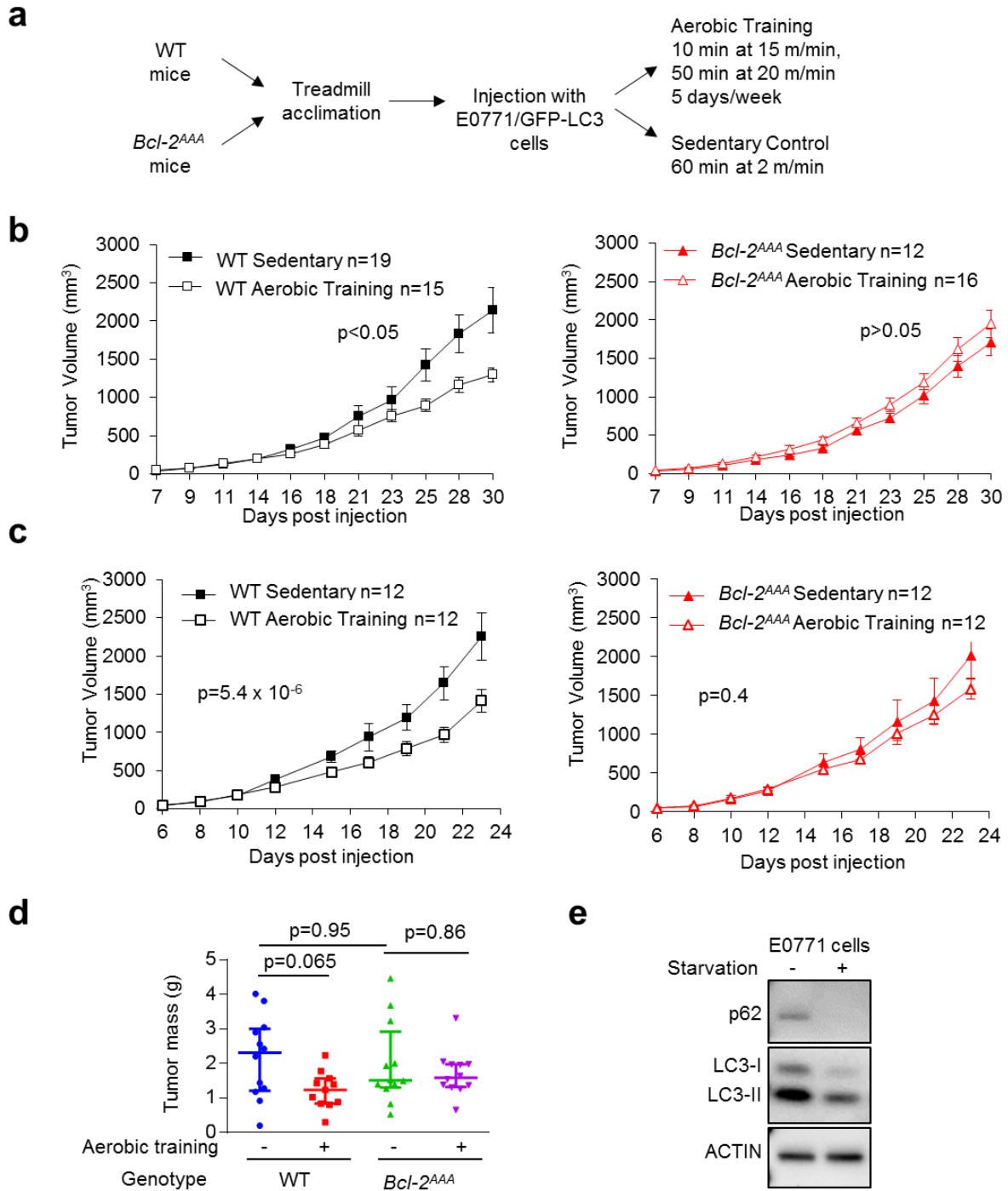


Figure 3.6. Chronic aerobic training delays breast cancer progression in WT and not *Bcl-2^{AAA}* mice. (a) Schematic of aerobic training in mice injected with E0771/GFP-LC3 tumor allograft. (b-c) E0771 tumor volume progression mice from two independent cohorts. Mixed linear model for repeated measures. (d) Final tumor mass in mice shown in c. ANOVA. (e) Western blot detection of p62 and LC3 in E0771 cells cultured in normal medium (starvation "-") or EBSS (starvation "+") for 4 hours.

Next, we wanted to assess whether mice with increased level of exercise-induced autophagy may be protected against cancer progression. *Becn1*^{F121A} mice were hypothesized to have increased autophagy in vivo, although this had not been confirmed experimentally. We examined whether the *Becn1*^{F121A}/GFP-LC3 mice have increased numbers of GFP-LC3 puncta in skeletal muscle during the basal state or after single bout of acute treadmill exercise. We found that *Becn1*^{F121A} mice had similar number of GFP-LC3 puncta as WT mice during basal state and elevated exercise-induced GFP-LC3 puncta compared to WT mice (Fig 3.7). The observed increase in GFP-LC3 puncta number is likely due to increased induction after stress instead of decreased clearance, as in vitro evaluation of human cells expressing *Becn1*^{F121A} have normal autophagic flux (Pattingre et al., 2005). Thus, we conclude that the *Becn1*^{F121A} mice have increased exercise-induced autophagy and may be a suitable model for studying whether elevated exercise-induced autophagy may provide additional protection against cancer and other diseases.

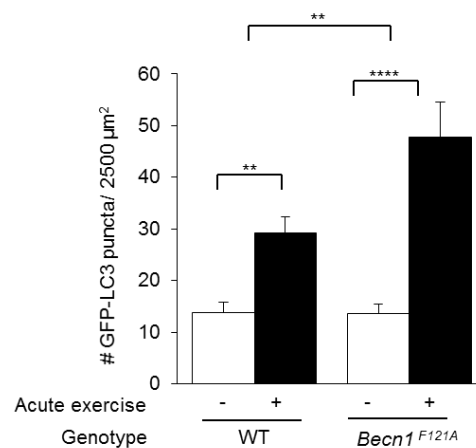


Figure 3.7. *Becn1*^{F121A} mice have excess exercise-induced autophagy.

GFP-LC3 puncta in skeletal muscle from 2-4 month-old female mice of the indicated genotype and treatment group. The acute exercise group ran at 17 m/min for 80 minutes; the sedentary group was placed on a stationary treadmill, n=3 per group. GFP-LC3 puncta number is significantly affected by both genotype (p<0.01) and treatment (p<0.0001), ** p<0.01, ****p<0.0001; two way ANOVA with adjustment for multiple comparisons.

Multiple attempts to consistently reproduce our phenotypic finding that chronic aerobic training inhibits of tumor progression in WT mice were unsuccessful. In more than 10 trials, aerobic training did not protect WT mice from tumor progression; thus, we were unable to interpret the results for *Bcl-2*^{AAA} mice in these cohorts. Of note, we did not observe exercise protection against tumor progression in *Bcl-2*^{AAA} mice, nor did we observe effects of exercise on tumor progression in WT mice in any of these experiments. Thus, the negative data likely suggest that while exercise-mediated autophagy may be required for inhibition of tumorigenesis, the animal housing conditions (and their effects on basal and exercise-induced autophagy), cancer model, and/or exercise regimen in this study design may be suboptimal. Further optimization is required to generate a protocol that consistently reproduces the phenotype.

III.4.B. Evaluating the role of autophagy in voluntary physical activity protection against E0771 tumor progression

We had two main criteria for optimizing the exercise protocol for mice injected with E0771/GFP-LC3 tumors; we wanted to deliver the maximum dose of aerobic exercise while minimizing stress on the animals. We were unable to increase exercise dose by increasing the treadmill running speed beyond 20 m/minute or the duration beyond 60 minutes/day because the mice cannot tolerate it. A previous study showed that C57BL/6 mice were the worst treadmill runners compared to 5 other laboratory mouse strains (Lerman et al., 2002). In our experiments, young adult C57BL/6 female can run ~ 1 km daily on the treadmill. However, C57BL/6 mice typically perform well on voluntary running wheels, running > 5 km daily (Lerman et al., 2002). Furthermore, our

collaborator Dr. Lee Jones and colleagues showed that voluntary wheel running reduced E0771 tumor progression in C57BL/6 mice (Betof et al., 2015). Thus, we used the running wheel as a high dose, low stress mode of exercise for mice. Using this protocol, we aimed to reduce stresses from physical handling, treadmill noise, electric shocks, and disruption of the natural circadian rhythm in mice.

Previously, *Bcl-2^{AAA}* mice and *Becn1^{+/-}* mice were observed to have reduced aerobic exercise tolerance on treadmill compared with WT control mice, possibly due to their inability to properly upregulate blood glucose uptake into skeletal muscles during exercise (He et al., 2012a). We observed similar voluntary wheel running patterns in WT, *Bcl-2^{AAA}*, and *Becn1^{+/-}* mice (Fig. 3.8). WT, *Bcl-2^{AAA}*, and *Becn1^{+/-}* mice ran similar total distance per day (~ 5 km per day), with similar average running speeds. Thus, we concluded that voluntary wheel running is a suitable method for assessing exercise protection against tumor progression in these mice.

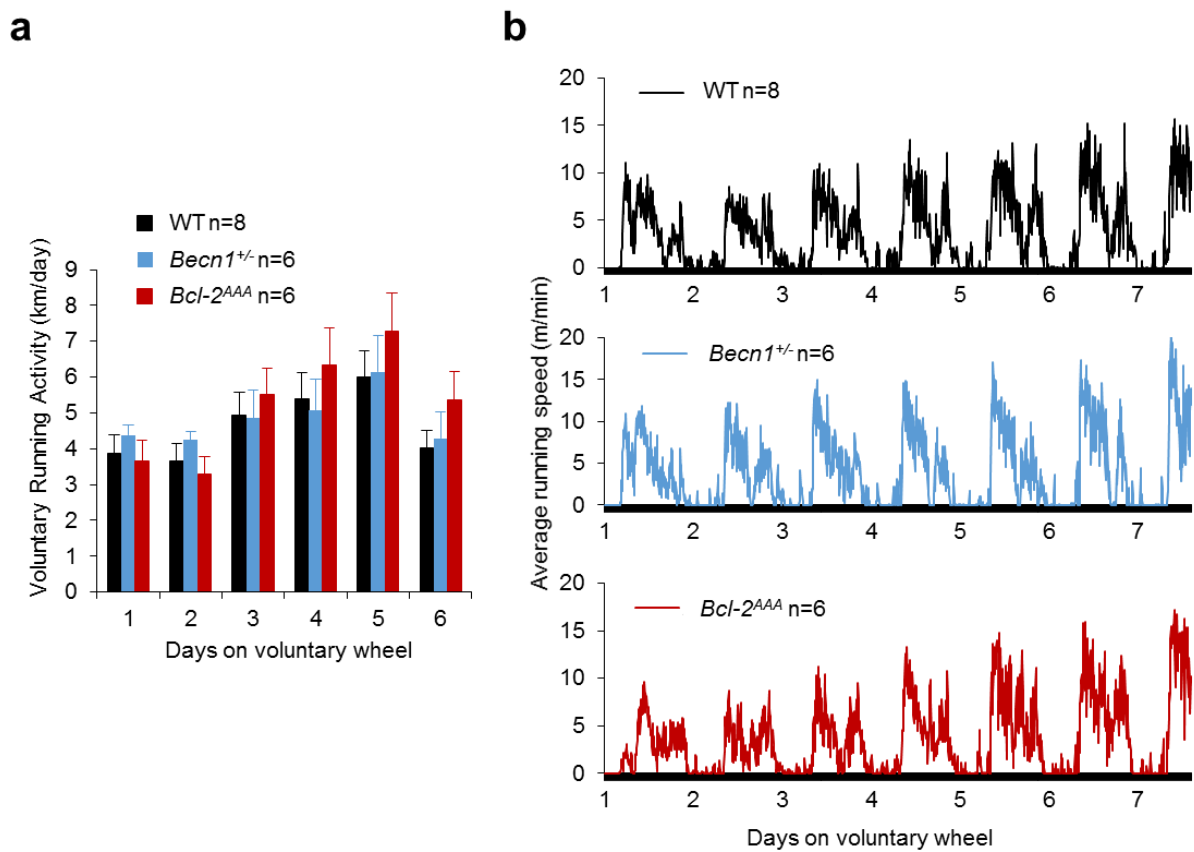


Figure 3.8. Voluntary wheel running pattern is similar between WT, *Bcl-2*^{AAA} and *Becn1*^{+/-} mice. (a) Average daily running distance and (b) representative voluntary wheel running pattern from WT, *Bcl-2*^{AAA} and *Becn1*^{+/-} mice. Shown are data collected from 2 month-old male mice. Similar results were observed for female mice.

We housed each mouse individually in cages with wheels for 7 days for acclimation and to observe their running patterns prior to injection with E0771/GFP-LC3 cells (Fig. 3.9a). Using the voluntary physical activity model, we observed marginal exercise benefits for delaying tumor progression in WT mice ($p=0.14$, mixed linear model for repeated measure) but not in *Bcl-2*^{AAA} mice ($p=0.69$) or in *Becn1*^{+/-} mice ($p=0.86$) (Fig 3.9b). The tumor burden at 23 days after injection was not affected by voluntary physical activity in any of the genotypes. At 23 days after injection, WT mice with voluntary physical activity showed a trend for reduced tumor mass compared with

sedentary WT mice ($p=0.07$, ANOVA). In contrast, we did not observe a trend for reduction in tumor mass in *Bcl-2^{AAA}* mice ($p=0.37$, ANOVA) nor in *Becn1^{+/-}* mice ($p=0.26$, ANOVA) (Fig. 3.9c). In this cohort, we observed no difference in wheel running pattern between genotype groups over the course of the experiment (Fig. 3.9d). In summary, our data showed no significant impact of voluntary wheel running on E0771 tumor progression in WT, *Bcl-2^{AAA}* or *Becn1^{+/-}* mice. The lack of statistical significance for voluntary wheel running effect on tumor progression is likely due to the large degree of variability within each experimental group. Thus, repeating the experiment with a larger sample size may benefit future experiments.

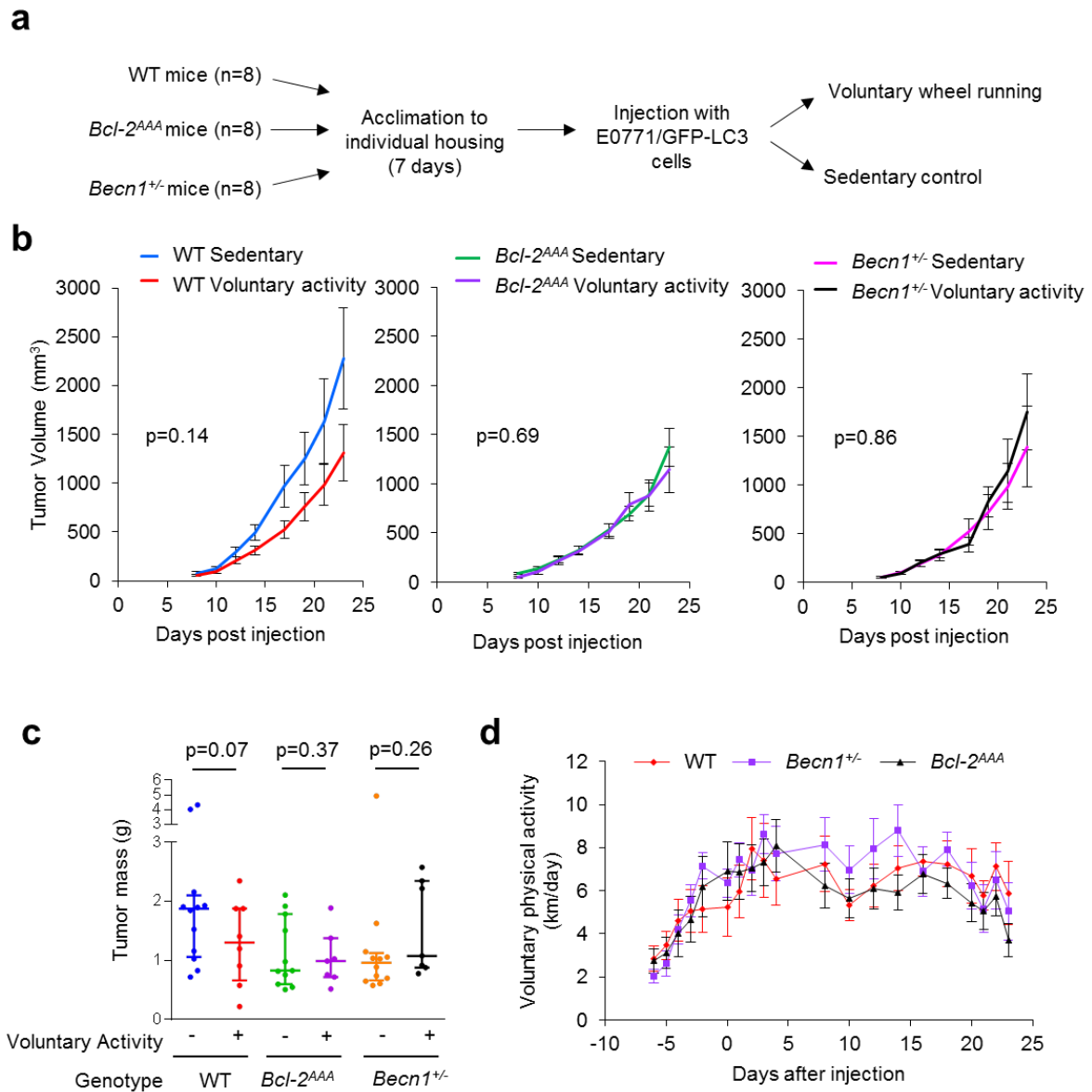


Figure 3.9. Voluntary physical activity delays breast cancer progression in WT mice but not in *Bcl-2^{AAA}* or *Becn1^{+/-}* mice.

(a) Schematic of voluntary physical activity on running wheels in mice injected with E0771/GFP-LC3 tumor allograft. (b) E0771/GFP-LC3 tumor volume progression in WT, *Bcl-2^{AAA}*, and *Becn1^{+/-}* mice with or without physical activity. P-values represent statistical analysis for interactions. (c) Tumor mass at 23 days after E0771 injection in mice of the indicated genotype and treatment groups. P-values represent t-test results. No significant difference was detected between genotypes by one-way ANOVA with adjustment for multiple comparisons. (d) Voluntary wheel running physical activity for the mice in this cohort.

III.4.C. Metabolomic screening for factors and pathways regulated by exercise-induced autophagy

We hypothesized that autophagy induction during exercise may be important for modulating metabolic adaptation during acute or chronic exercise in various tissues. To investigate the downstream metabolic pathways regulated by exercise-induced autophagy, we took an unbiased screening approach for characterizing the metabolome via LC-MS. We collected tissues from mice after chronic aerobic training, acute aerobic exercise, or no exercise. We analyzed the metabolome in skeletal muscle, as it is the main tissue activated during exercise. We also analyzed the mammary fat and blood, which are important components of the tumor microenvironment that may undergo exercise-induced changes to prevent tumor development.

First, we analyzed tissues collected from mice that underwent aerobic training protocol #1 without any tumor injection (Fig. 3.10a). MS detection yielded identification and relative quantification of ~ 350 metabolites. The *Bcl-2^{AAA}* mice had altered plasma pyrimidine and branched chain amino acid levels. Specifically, aerobic training increased baseline plasma thymine and thymidine levels in WT mice but not in *Bcl-2^{AAA}* mice (Fig. 3.10b,c). Also, aerobic training reduced baseline plasma valine and isoleucine levels in WT mice but not in *Bcl-2^{AAA}* mice (Fig. 3.10d,e). These changes in plasma metabolites may reflect exercise adaptation mediated by autophagy, and may potentially regulate exercise health benefits.

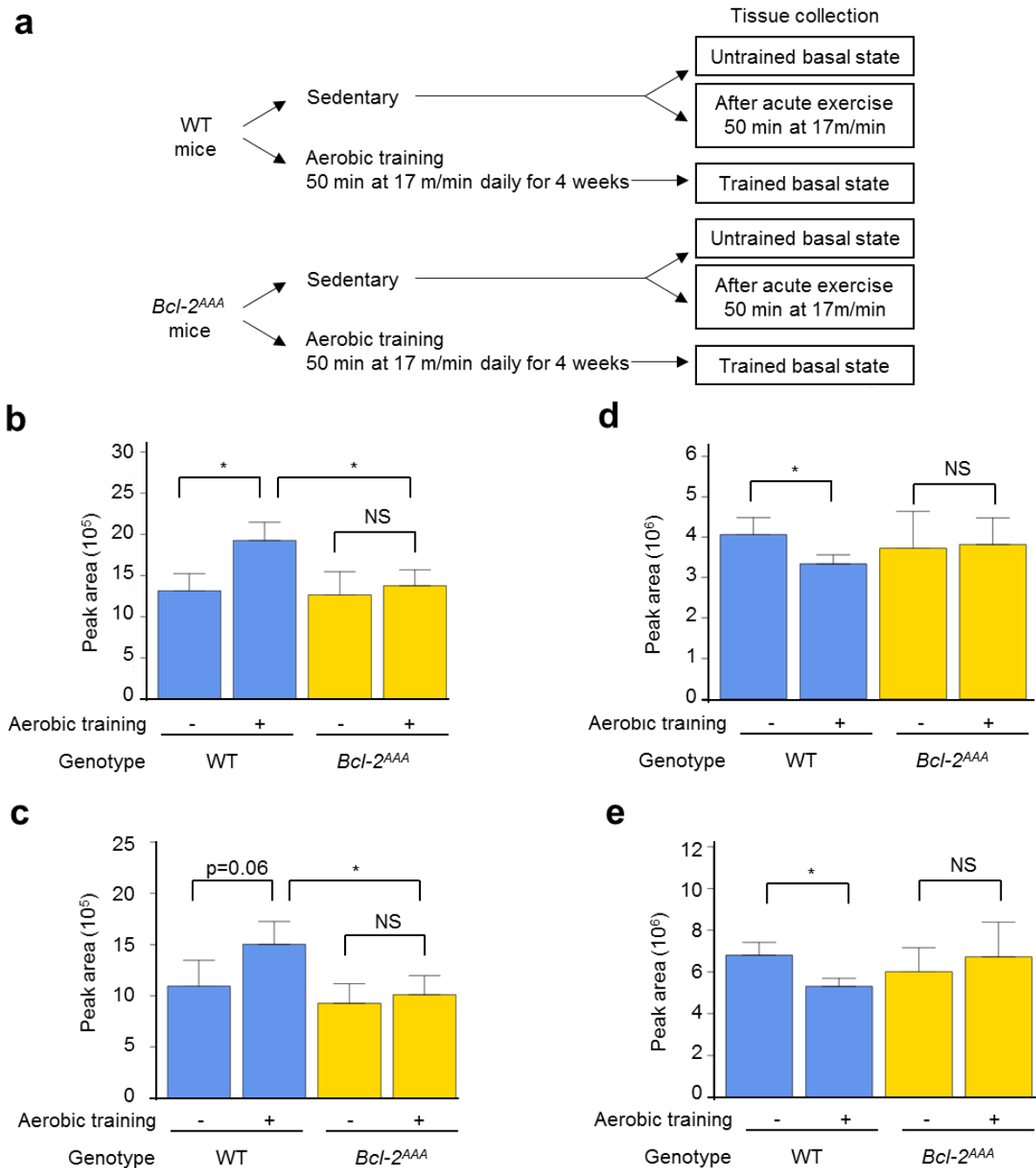


Figure 3.10. Plasma metabolomic screen for pathways regulated by exercise-induced autophagy.

(a) Schematic for exercise and tissue collection protocol in age-matched 2 to 4 month-old female WT and *Bcl-2^{AAA}* mice, n=4 per group. (b-c) Plasma pyrimidine levels in mice with or without aerobic training during basal state. Shown are mass spectrometry peak areas for plasma thymine (b) or thymidine (c). (d-e) Plasma branched chain amino acids in mice with or without aerobic training during basal state. Shown are mass spectrometry peak areas for plasma valine (d) and isoleucine (e). * p<0.05; Wilcoxon rank sum test.

Next, we collected tissues from a cohort of mice with E0771/GFP-LC3 tumors (aerobic training protocol #2) for another metabolomic screen (Fig. 3.11a). Tissues were collected at the terminal time point (21 d after tumor injection), as well as an early time point (14 d after tumor injection) to control for differences in the metabolome that may arise from different tumor sizes at the terminal stage. MS detection yielded identification and relative quantification of ~200 metabolites. Metabolomic profiling of plasma identified some treatment-dependent effects on metabolite levels; however, these effects were not genotype-dependent. For example, plasma levels of 5-aminoimidazole-4-carboxamide ribonucleotide (AICAR) and 3-hydroxybutyrate increased with aerobic training in all genotypes (Fig. 3.11b,c). The lack of significant genotype-dependent and treatment-dependent metabolomics differences may be due to the large variation within each experimental group. Furthermore, our inability to reproduce consistently the anti-tumor effects with our exercise protocol complicated the interpretation of the metabolomics data. It is likely that the lack of differences between the aerobic trained WT and sedentary WT mice, and between the aerobic trained WT and aerobic trained *Bcl-2^{AAA}* mice may be false negatives. Repeat of the metabolomics analysis using tissues from a cohort of mice with demonstrated efficacious exercise inhibition of cancer progression in WT mice is necessary to draw definitive conclusions.

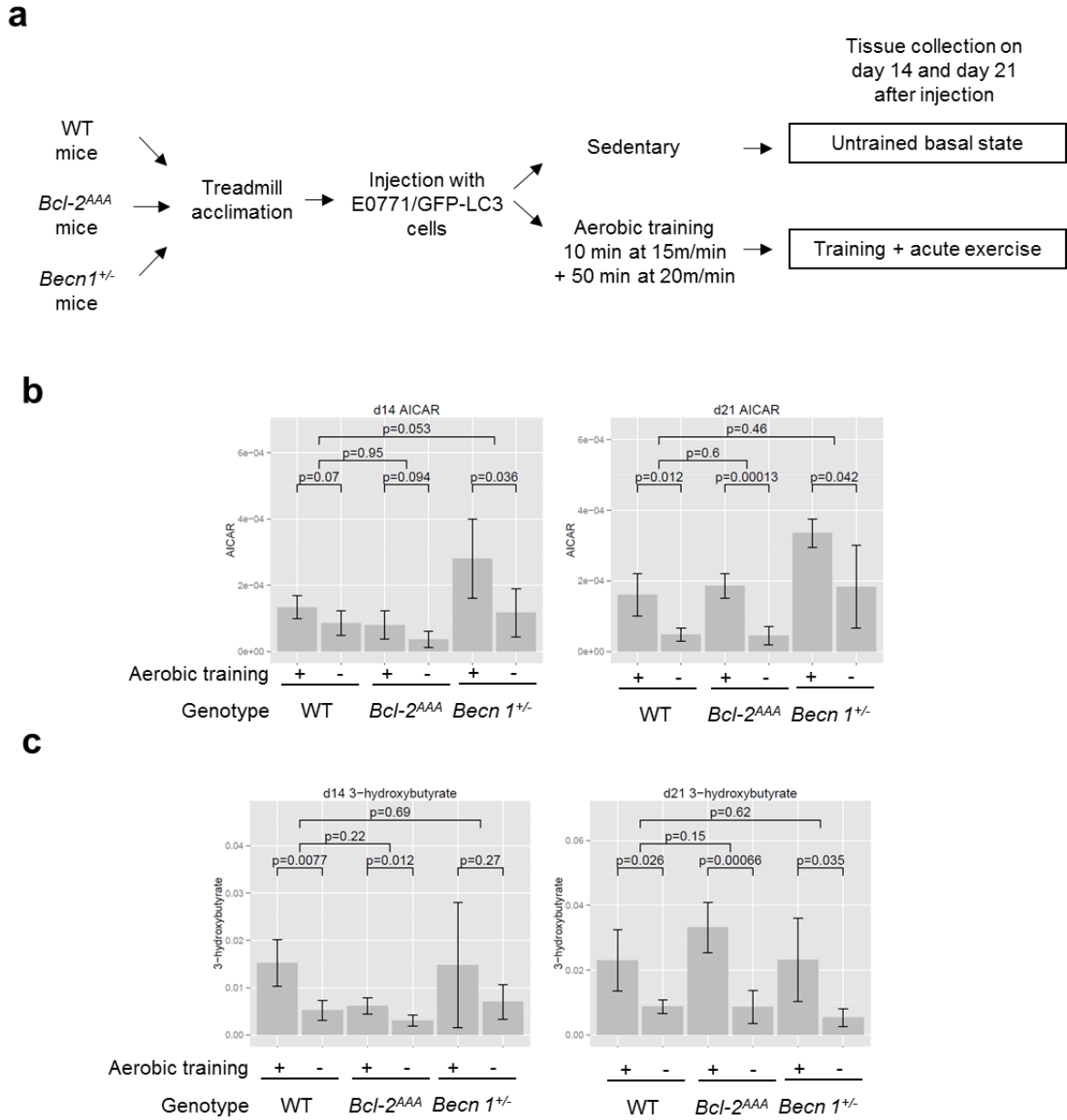


Figure 3.11. Plasma metabolomic screen for pathways regulated by exercise-induced autophagy in mice with E0771 tumors.

(a) Schematic for exercise and tissue collection protocol in age-matched 2 to 4 month-old female WT, *Bcl-2^{AAA}*, and *Becn1^{+/-}* mice, n=10 per group. Tissues were collected from five mice per group at day 14 after tumor injection, and collected from the remaining five mice per group at day 21 after tumor injection. (b-c) Plasma levels of AICAR (b) and 3-hydroxybutyrate (c) in mice of the indicated genotypes with or without aerobic training, from plasma collected on the indicated day after E0771 injection.

III.4.D. Proteomic screening for factors and pathways regulated by exercise-induced autophagy

In addition to metabolomic analysis, we conducted a large-scale proteomic screen to identify candidate factors and pathways regulating physiological benefits of exercise-induced autophagy. We analyzed skeletal muscle from WT and *Bcl-2^{AAA}* mice that underwent aerobic training protocol #1 without tumor injection (Fig. 3.10a). From this screen, we identified NADH dehydrogenase (ubiquinone) 1 alpha subcomplex, 13 (NDUFA13, also known as GRIM19) and isocitrate dehydrogenase [NADP], mitochondria (IDH2) as candidate circulating factors that are regulated by exercise-induced autophagy (Fig 3.12a,b). Aerobic training increased skeletal muscle expression of NDUFA13 and IDH2 in WT mice but not in *Bcl-2^{AAA}* mice. qRT-PCR analysis showed no significant genotype or exercise effect in *Ndufa13* and *Idh2* transcript expression, although the general trend is similar to that of the proteomic screen result (Fig. 3.12c,d).

Ndufa13 has a well-known role as a tumor suppressor (Moreira et al., 2011). Monoallelic loss of this gene in mice leads to constitutive STAT3 activity and promotes tumorigenesis (Kalakonda et al., 2013), and overexpression of this gene in cancer cells reduce cancer growth (Okamoto et al., 2010). Previously, mutant forms of IDH1/2 have been implicated in the pathogenesis of acute myeloid leukemia through neomorphic enzyme activity leading to production of an alternate metabolite (Figueroa et al., 2010) (Ward et al., 2010). Whether altered expression of wild-type IDH2 has an impact on tumorigenesis is unknown. Interestingly, both of these candidate exercise-induced anti-cancer factors are mitochondrial proteins. This suggests the possibility that exercise-induced general autophagy or mitophagy may have an important role in regulation of

mitochondrial homeostasis and adaptation to exercise. Further experiments with a larger sample size are needed to evaluate the regulation of these factors by exercise and autophagy, and to evaluate their potential tumor-suppressive functions in breast cancer.

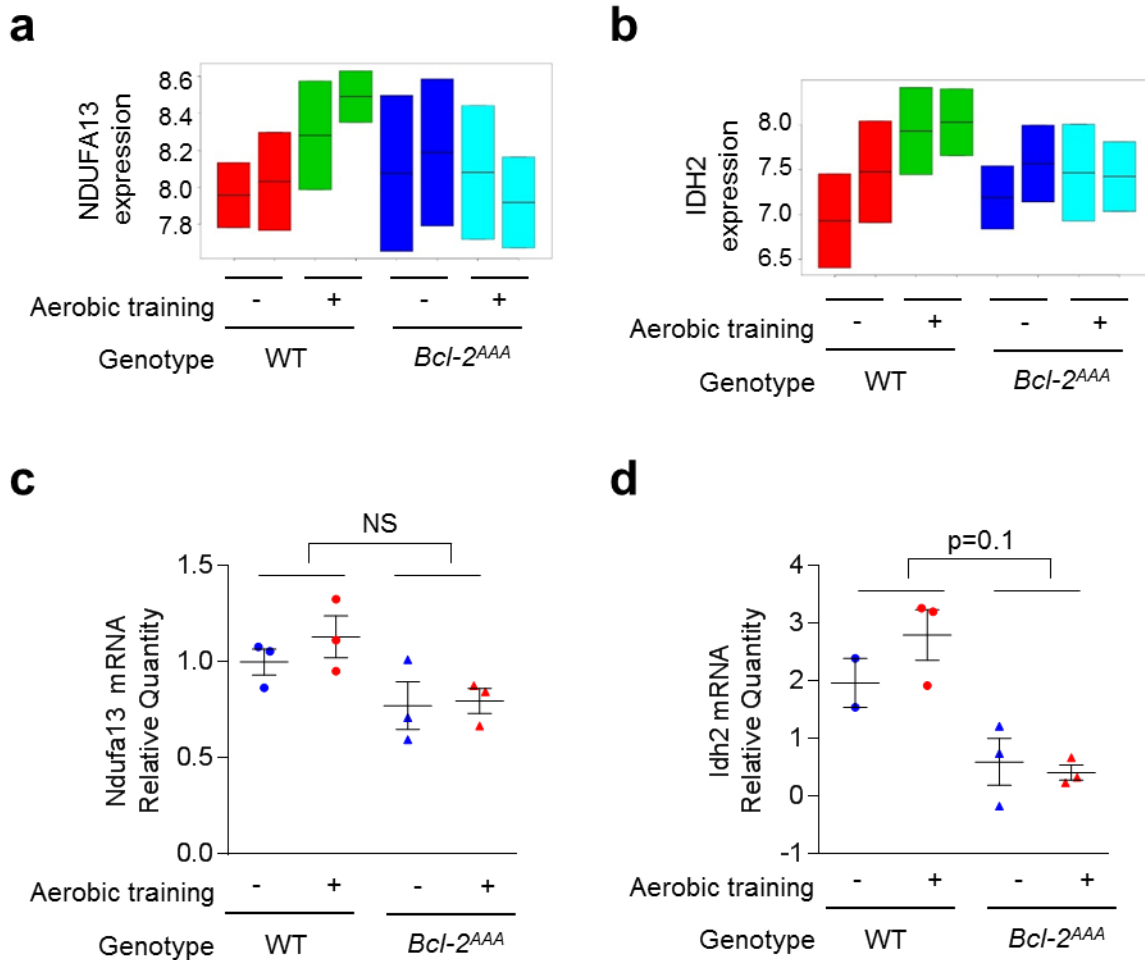


Figure 3.12. Skeletal muscle proteomic screen for pathways regulated by exercise-induced autophagy.

(a-b) Relative expression of Ndufa13 (a) and Idh2 (b) from iTRAQ proteomic analysis. (c-d) qRT-PCR confirmation of Grim19 (c) and Idh2 (d) transcript level in skeletal muscle. NS = not significant; two-way ANOVA.

III.4.E. Targeted cytokine and chemokine panel analysis for factors regulated by exercise-induced autophagy

In addition to large-scaled proteomic screening, we also focused on a targeted panel of cytokines, chemokines, and other bioactive proteins that have been implicated in exercise and/or cancer suppression. A previous study reported an increase in plasma SPARC after a single bout of exercise (Aoi et al., 2013). Chronic aerobic training is also associated with increased skeletal muscle secretion of the myokine SPARC and decreased colon tumorigenesis (Aoi et al., 2013). To investigate whether SPARC could be a candidate anti-tumor myokine regulated by exercise and autophagy, we first examined its transcript level in skeletal muscle by qRT-PCR. We found that aerobic training did not significantly alter SPARC expression in either genotype (Fig. 3.13a). However, SPARC level showed an increasing trend in WT but a decreasing trend in *Bcl-2^{AAA}* mice after aerobic training. This differential exercise response in SPARC expression was marginally different in between genotype ($p=0.07$). Upon further confirmation using ELISA, however, we detected no significant difference in the aerobic training effects on plasma SPARC levels between the genotypes (Fig. 3.13b).

Another candidate factor regulating exercise- and autophagy-induced anti-cancer benefits is decorin, a secreted matrix proteoglycan implicated in controlling breast tumor microenvironment (Buraschi et al., 2012; Neill et al., 2012). Decorin expression is induced by nutrient starvation (Gubbiotti et al., 2015); however, it is unknown whether decorin expression is also regulated by other metabolic stresses such as exercise. To investigate the hypothesis that exercise and autophagy regulate decorin expression, we collaborated with Dr. Renato Iozzo's laboratory to detect plasma decorin levels by

ELISA (Fig 3.13c). We did not observe any effects of genotype or exercise (50 minutes treadmill) on plasma decorin levels in this cohort. Future experiments may investigate whether a more intense exercise regimen may be required to induce decorin.

Chemokines and cytokines are well known for controlling the tumor microenvironment; inflammation generally promotes cancer development and progression while immunosurveillance and killing by T cells and NK cells are generally considered anti-cancer (Grivennikov et al., 2010). Autophagy has an emerging role in regulation of inflammation and immunity (Deretic et al., 2013). Thus, we hypothesize that modulation of chemokines and cytokines in the tumor microenvironment may be a mechanism by which exercise-induced autophagy regulates cancer progression. To investigate this hypothesis, we conducted a targeted screen for a panel of plasma chemokines and cytokines, including IL-1 α , IL-1 β , IL-6, IL-15, leukemia inhibitory factor (LIF), macrophage inflammatory protein-1 β (MIP-1 β), and tumor necrosis factor alpha (TNF- α). We observed no difference in the levels of plasma IL-1 α , IL-1 β , IL-6, MIP-1 β , and TNF- α (Fig. 3.13d-j). We found that plasma IL-15 and LIF were elevated after exercise in WT mice, but decreased after exercise in *Bcl-2*^{AAA} mice (Fig 3.13g,h). Further studies are required to confirm whether these factors are indeed regulated by exercise-induced autophagy, and elucidate the mechanism by which they may regulate cancer progression.

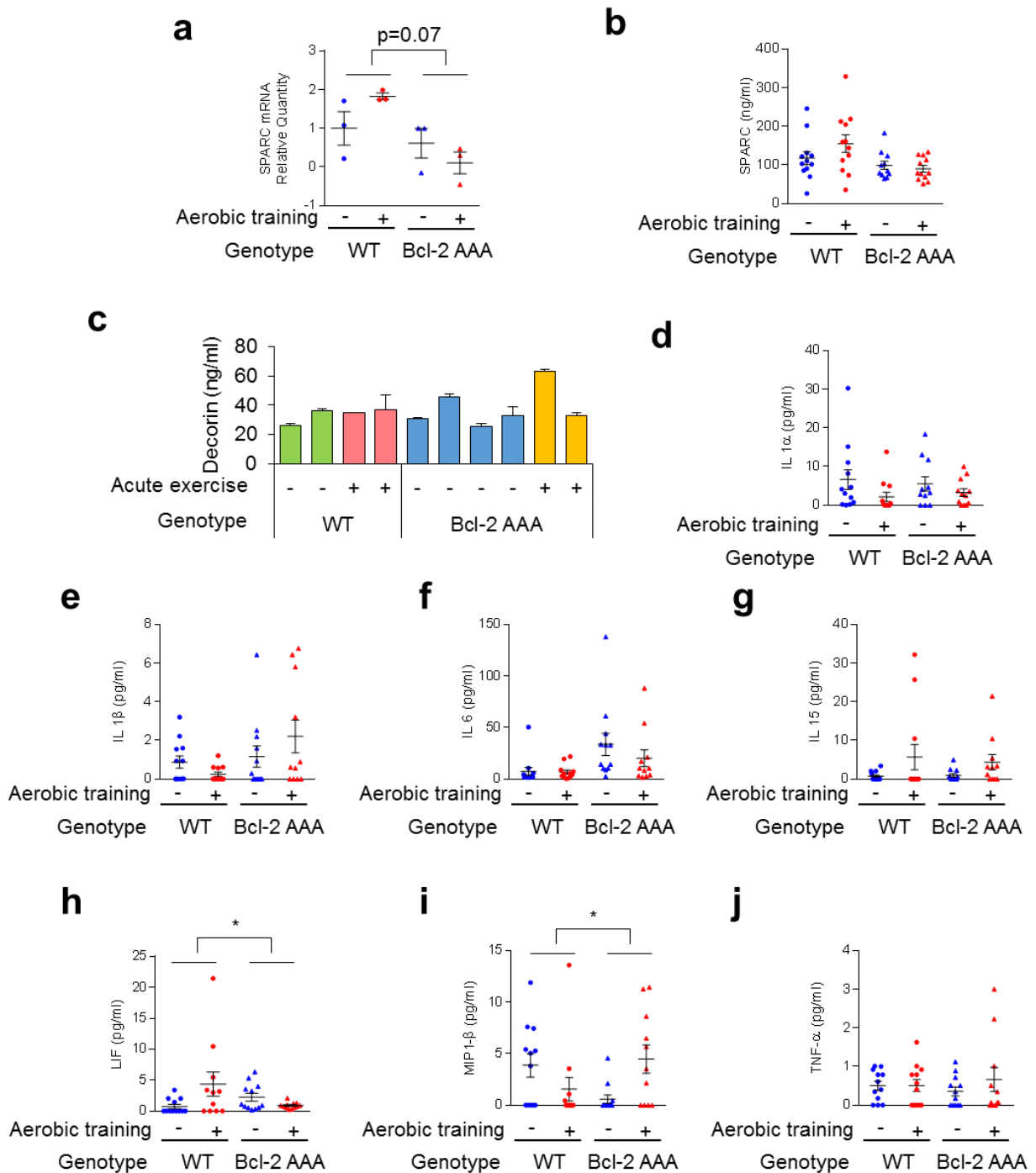


Figure 3.13. Targeted panel of candidate plasma proteins regulated by exercise-induced autophagy.

(a) qRT-PCR detection of SPARC expression in skeletal muscle. (b) ELISA detection of SPARC protein expression in plasma. (c) ELISA detection of decorin protein expression in plasma. (d-j) Milliplex detection of the indicated cytokines and chemokines from plasma. *p < 0.05; two-way ANOVA.

III.5. Discussion and future directions

In this study, we found forced aerobic training on a treadmill protected against E0771 breast cancer progression in mice while voluntary physical exercise on the running wheel may have marginal protection against E0771 cancer progression. This protective effect likely depends on autophagy, as the exercise benefit was abolished in *Bcl-2^{AAA}* mice and in *Becn1^{+/-}* mice lacking exercise-induction of autophagy. This exercise protection against cancer progression is likely cell-extrinsic. As E0771 cells have an intact autophagy pathway, it is likely that autophagy can be activated during acute exercise in *Bcl-2^{AAA}* mice and in *Becn1^{+/-}* mice similar to in WT mice. The defective exercise induction of autophagy in other host tissues (e.g. skeletal muscle, adipose tissue, lymphocytes) are likely the main source for the protective effects of exercise in this experimental model. Cell-intrinsic anti-cancer effects of exercise-induced autophagy were not addressed in this study. We identified several candidate factors regulated by exercise-induced autophagy. Further experiments are needed to evaluate the mechanism underlying exercise-mediated protection against cancer progression through autophagy.

During this study, we attempted to repeat the exercise inhibition of tumor progression experiment multiple times with variable success. Currently, it is unclear why certain cohorts of C57BL/6 mice demonstrate exercise-mediated protection against tumor progression while others do not. A possible explanation could be that the microbiota in our mouse colonies changed throughout the course of this study. Emerging evidence are showing the importance of gut microbiota on cancer susceptibility (Garrett, 2015; Schwabe and Jobin, 2013). While chronic infection with

specific pathogens such as *Helicobacter pylori* (Wang et al., 2014) and human papillomaviruses (zur Hausen, 2002) are well known for causing malignancies, recent evidence suggest that a global change in the microbiome may also contribute to disease pathogenesis (Schwabe and Jobin, 2013). We suspected altered microbiota in our mouse colonies because while our mice generally appeared healthy, some young adult WT mice displayed several abnormal phenotypes that may be explained by a subclinical infection or altered microbiota. These abnormal mice had elevated basal autophagy, hyperplastic lymph nodes, and some mice in our colony had abnormal microvesicular structures in the liver. Autophagy is an important pathway for regulating infections through its role the development and homeostasis of the immune system (Levine et al., 2011). Under selective pressure, certain microbes have evolved strategies to modulate autophagy. Thus, altered microbiome may increase or decrease autophagic flux. Since the abnormal mice have elevated autophagy even during sedentary states, our exercise regimens may did not significantly induce autophagy further, leading to the lack of reproducibility in our animal experiments.

To address the potential contribution of microbiota alteration to autophagy and cancer phenotypes, we re-derived all the mouse strains for this study into a clean facility using in vitro fertilization. However, we were still unable to reproduce the phenotype of exercise protection against cancer in the re-derived colony. This suggests that the presence as well as the absence of certain microbes can be important factors impacting autophagy and cancer regulation. The identity of specific microbes involved in this process is yet undetermined, but could be an interesting topic of future investigation.

Since mice are nocturnal animals, day-time treadmill running in our study protocol disrupts their natural circadian rhythm. Interestingly, the intimate relationship between autophagy and circadian rhythm was described as early as the 1970s (Pfeifer, 1973; Pfeifer and Bertling, 1977). Autophagy normally undergoes rhythmic variation in adult mammals in accordance with circadian patterns of activity and feeding. In nocturnal animals, autophagy peaks during the end of the resting period (light phase) and decreases early in the active and feeding period (dark phase) (Pfeifer, 1973; Pfeifer and Strauss, 1981). Although it is yet unclear whether circadian clock directly regulates autophagy, or whether autophagy directly regulates cycling of cellular clocks, these two processes seem to share a functional connection, as dysregulation in autophagy and circadian rhythm are associated with similar set of diseases. Specifically, autophagy and circadian rhythm dysregulation are implicated in tumorigenesis, aging, and neurodegeneration (Sachdeva and Thompson, 2008). The potential impact of circadian rhythm on autophagy and cancer may be considered for optimizing the exercise protocol in future experiments. For example, a night-time exercise regimen may be more beneficial compared with day-time exercise, as it may induce a high level of autophagy during a time when baseline autophagy is normally low in mice. Exercise regimens that minimize sleep disruption may also reduce the confounding contribution of circadian dysregulation to cancer development.

REFERENCES

- Agrawal, G., Fassas, S.N., Xia, Z.J., and Subramani, S. (2016). Distinct requirements for intra-ER sorting and budding of peroxisomal membrane proteins from the ER. *J Cell Biol* 212, 335-348.
- Akizu, N., Cantagrel, V., Zaki, M.S., Al-Gazali, L., Wang, X., Rosti, R.O., Dikoglu, E., Gelot, A.B., Rosti, B., Vaux, K.K., *et al.* (2015). Biallelic mutations in SNX14 cause a syndromic form of cerebellar atrophy and lysosome-autophagosome dysfunction. *Nat Genet* 47, 528-534.
- Amaravadi, R.K., Yu, D., Lum, J.J., Bui, T., Christophorou, M.A., Evan, G.I., Thomas-Tikhonenko, A., and Thompson, C.B. (2007). Autophagy inhibition enhances therapy-induced apoptosis in a Myc-induced model of lymphoma. *J Clin Invest* 117, 326-336.
- Aoi, W., Naito, Y., Takagi, T., Tanimura, Y., Takanami, Y., Kawai, Y., Sakuma, K., Hang, L.P., Mizushima, K., Hirai, Y., *et al.* (2013). A novel myokine, secreted protein acidic and rich in cysteine (SPARC), suppresses colon tumorigenesis via regular exercise. *Gut* 62, 882-889.
- Baumgart, E., Vanhorebeek, I., Grabenbauer, M., Borgers, M., Declercq, P.E., Fahimi, H.D., and Baes, M. (2001). Mitochondrial alterations caused by defective peroxisomal biogenesis in a mouse model for Zellweger syndrome (PEX5 knockout mouse). *Am J Pathol* 159, 1477-1494.
- Betof, A.S., Lascola, C.D., Weitzel, D., Landon, C., Scarbrough, P.M., Devi, G.R., Palmer, G., Jones, L.W., and Dewhirst, M.W. (2015). Modulation of murine breast tumor vascularity, hypoxia and chemotherapeutic response by exercise. *J Natl Cancer Inst* 107.

Bjorkoy, G., Lamark, T., Brech, A., Outzen, H., Perander, M., Overvatn, A., Stenmark, H., and Johansen, T. (2005). p62/SQSTM1 forms protein aggregates degraded by autophagy and has a protective effect on huntingtin-induced cell death. *J Cell Biol* 171, 603-614.

Bonekamp, N.A., and Schrader, M. (2012). Transient complex peroxisomal interactions: A new facet of peroxisome dynamics in mammalian cells. *Commun Integr Biol* 5, 534-537.

Braschi, E., Goyon, V., Zunino, R., Mohanty, A., Xu, L., and McBride, H.M. (2010). Vps35 mediates vesicle transport between the mitochondria and peroxisomes. *Curr Biol* 20, 1310-1315.

Buraschi, S., Neill, T., Owens, R.T., Iniguez, L.A., Purkins, G., Vadigepalli, R., Evans, B., Schaefer, L., Peiper, S.C., Wang, Z.X., *et al.* (2012). Decorin protein core affects the global gene expression profile of the tumor microenvironment in a triple-negative orthotopic breast carcinoma xenograft model. *PLoS One* 7, e45559.

Burnett, S.F., Farre, J.C., Nazarko, T.Y., and Subramani, S. (2015). Peroxisomal Pex3 activates selective autophagy of peroxisomes via interaction with the pexophagy receptor Atg30. *J Biol Chem* 290, 8623-8631.

Choi, A.M., Ryter, S.W., and Levine, B. (2013). Autophagy in human health and disease. *N Engl J Med* 368, 1845-1846.

Costes, S.V., Daelemans, D., Cho, E.H., Dobbin, Z., Pavlakis, G., and Lockett, S. (2004). Automatic and quantitative measurement of protein-protein colocalization in live cells. *Biophys J* 86, 3993-4003.

Crichton, D., Wilkinson, S., O'Prey, J., Syed, N., Smith, P., Harrison, P.R., Gasco, M., Garrone, O., Crook, T., and Ryan, K.M. (2006). DRAM, a p53-induced modulator of autophagy, is critical for apoptosis. *Cell* 126, 121-134.

Cullup, T., Kho, A.L., Dionisi-Vici, C., Brandmeier, B., Smith, F., Urry, Z., Simpson, M.A., Yau, S., Bertini, E., McClelland, V., *et al.* (2013). Recessive mutations in EPG5 cause Vici syndrome, a multisystem disorder with defective autophagy. *Nat Genet* 45, 83-87.

De Duve, C., and Baudhuin, P. (1966). Peroxisomes (microbodies and related particles). *Physiol Rev* 46, 323-357.

De Duve, C., and Wattiaux, R. (1966). Functions of lysosomes. *Annu Rev Physiol* 28, 435-492.

Degenhardt, K., Mathew, R., Beaudoin, B., Bray, K., Anderson, D., Chen, G., Mukherjee, C., Shi, Y., Gelinis, C., Fan, Y., *et al.* (2006). Autophagy promotes tumor cell survival and restricts necrosis, inflammation, and tumorigenesis. *Cancer Cell* 10, 51-64.

del Campo, M., Hall, B.D., Aeby, A., Nassogne, M.C., Verloes, A., Roche, C., Gonzalez, C., Sanchez, H., Garcia-Alix, A., Cabanas, F., *et al.* (1999). Albinism and agenesis of the corpus callosum with profound developmental delay: Vici syndrome, evidence for autosomal recessive inheritance. *Am J Med Genet* 85, 479-485.

Delille, H.K., and Schrader, M. (2008). Targeting of hFis1 to peroxisomes is mediated by Pex19p. *J Biol Chem* 283, 31107-31115.

Deosaran, E., Larsen, K.B., Hua, R., Sargent, G., Wang, Y., Kim, S., Lamark, T., Jauregui, M., Law, K., Lippincott-Schwartz, J., *et al.* (2013). NBR1 acts as an autophagy receptor for peroxisomes. *J Cell Sci* 126, 939-952.

Deretic, V., Jiang, S., and Dupont, N. (2012). Autophagy intersections with conventional and unconventional secretion in tissue development, remodeling and inflammation.

Trends Cell Biol 22, 397-406.

Deretic, V., and Levine, B. (2009). Autophagy, immunity, and microbial adaptations. *Cell Host Microbe* 5, 527-549.

Deretic, V., Saitoh, T., and Akira, S. (2013). Autophagy in infection, inflammation and immunity. *Nat Rev Immunol* 13, 722-737.

Ding, W.X., and Yin, X.M. (2012). Mitophagy: mechanisms, pathophysiological roles, and analysis. *Biol Chem* 393, 547-564.

Dixit, E., Boulant, S., Zhang, Y., Lee, A.S., Odendall, C., Shum, B., Hacohen, N., Chen, Z.J., Whelan, S.P., Fransen, M., *et al.* (2010). Peroxisomes are signaling platforms for antiviral innate immunity. *Cell* 141, 668-681.

Dupont, N., Jiang, S., Pilli, M., Ornatowski, W., Bhattacharya, D., and Deretic, V. (2011). Autophagy-based unconventional secretory pathway for extracellular delivery of IL-1beta. *EMBO J* 30, 4701-4711.

Ebrahimi-Fakhari, D., Saffari, A., Wahlster, L., Lu, J., Byrne, S., Hoffmann, G.F., Jungbluth, H., and Sahin, M. (2016). Congenital disorders of autophagy: an emerging novel class of inborn errors of neuro-metabolism. *Brain* 139, 317-337.

Egan, B., and Zierath, J.R. (2013). Exercise metabolism and the molecular regulation of skeletal muscle adaptation. *Cell Metab* 17, 162-184.

Ellingsgaard, H., Hauselmann, I., Schuler, B., Habib, A.M., Baggio, L.L., Meier, D.T., Eppler, E., Bouzakri, K., Wueest, S., Muller, Y.D., *et al.* (2011). Interleukin-6 enhances

insulin secretion by increasing glucagon-like peptide-1 secretion from L cells and alpha cells. *Nat Med* 17, 1481-1489.

Eustace, D., Han, X., Gooding, R., Rowbottom, A., Riches, P., and Heyderman, E. (1993). Interleukin-6 (IL-6) functions as an autocrine growth factor in cervical carcinomas in vitro. *Gynecol Oncol* 50, 15-19.

Ewens, A., Mihich, E., and Ehrke, M.J. (2005). Distant metastasis from subcutaneously grown E0771 medullary breast adenocarcinoma. *Anticancer Res* 25, 3905-3915.

Ezaki, J., Komatsu, M., Yokota, S., Ueno, T., and Kominami, E. (2009). Method for monitoring pexophagy in mammalian cells. *Methods Enzymol* 452, 215-226.

Farre, J.C., Manjithaya, R., Mathewson, R.D., and Subramani, S. (2008). PpAtg30 tags peroxisomes for turnover by selective autophagy. *Dev Cell* 14, 365-376.

Feng, Y., He, D., Yao, Z., and Klionsky, D.J. (2014). The machinery of macroautophagy. *Cell Res* 24, 24-41.

Feng, Z., Zhang, H., Levine, A.J., and Jin, S. (2005). The coordinate regulation of the p53 and mTOR pathways in cells. *Proc Natl Acad Sci U S A* 102, 8204-8209.

Fernandez-Suarez, M., and Ting, A.Y. (2008). Fluorescent probes for super-resolution imaging in living cells. *Nat Rev Mol Cell Biol* 9, 929-943.

Figueroa, M.E., Abdel-Wahab, O., Lu, C., Ward, P.S., Patel, J., Shih, A., Li, Y., Bhagwat, N., Vasanthakumar, A., Fernandez, H.F., *et al.* (2010). Leukemic IDH1 and IDH2 mutations result in a hypermethylation phenotype, disrupt TET2 function, and impair hematopoietic differentiation. *Cancer Cell* 18, 553-567.

Fischer, C.P. (2006). Interleukin-6 in acute exercise and training: what is the biological relevance? *Exerc Immunol Rev* 12, 6-33.

Fujiki, Y., Okumoto, K., Mukai, S., Honsho, M., and Tamura, S. (2014). Peroxisome biogenesis in mammalian cells. *Front Physiol* 5, 307.

Galluzzi, L., Bravo-San Pedro, J.M., and Kroemer, G. (2016). Autophagy Mediates Tumor Suppression via Cellular Senescence. *Trends Cell Biol* 26, 1-3.

Galluzzi, L., Pietrocola, F., Levine, B., and Kroemer, G. (2014). Metabolic control of autophagy. *Cell* 159, 1263-1276.

Gandre-Babbe, S., and van der Bliek, A.M. (2008). The novel tail-anchored membrane protein Mff controls mitochondrial and peroxisomal fission in mammalian cells. *Mol Biol Cell* 19, 2402-2412.

Garrett, W.S. (2015). Cancer and the microbiota. *Science* 348, 80-86.

Ghaedi, K., Honsho, M., Shimozawa, N., Suzuki, Y., Kondo, N., and Fujiki, Y. (2000). PEX3 is the causal gene responsible for peroxisome membrane assembly-defective Zellweger syndrome of complementation group G. *Am J Hum Genet* 67, 976-981.

Gillette, C.A., Zhu, Z., Westerlind, K.C., Melby, C.L., Wolfe, P., and Thompson, H.J. (1997). Energy availability and mammary carcinogenesis: effects of calorie restriction and exercise. *Carcinogenesis* 18, 1183-1188.

Gingras, A.C., Gstaiger, M., Raught, B., and Aebersold, R. (2007). Analysis of protein complexes using mass spectrometry. *Nat Rev Mol Cell Biol* 8, 645-654.

Gould, S.J., Kalish, J.E., Morrell, J.C., Bjorkman, J., Urquhart, A.J., and Crane, D.I. (1996). Pex13p is an SH3 protein of the peroxisome membrane and a docking factor for the predominantly cytoplasmic PTs1 receptor. *J Cell Biol* 135, 85-95.

Green, D.R., and Levine, B. (2014). To be or not to be? How selective autophagy and cell death govern cell fate. *Cell* 157, 65-75.

Grivennikov, S.I., Greten, F.R., and Karin, M. (2010). Immunity, inflammation, and cancer. *Cell* 140, 883-899.

Gubbiotti, M.A., Neill, T., Frey, H., Schaefer, L., and Iozzo, R.V. (2015). Decorin is an autophagy-inducible proteoglycan and is required for proper in vivo autophagy. *Matrix Biol* 48, 14-25.

Guo, J.Y., Chen, H.Y., Mathew, R., Fan, J., Strohecker, A.M., Karsli-Uzunbas, G., Kamphorst, J.J., Chen, G., Lemons, J.M., Karantza, V., *et al.* (2011). Activated Ras requires autophagy to maintain oxidative metabolism and tumorigenesis. *Genes Dev* 25, 460-470.

Guo, J.Y., Xia, B., and White, E. (2013). Autophagy-mediated tumor promotion. *Cell* 155, 1216-1219.

Handschin, C., and Spiegelman, B.M. (2008). The role of exercise and PGC1alpha in inflammation and chronic disease. *Nature* 454, 463-469.

Hanna, R.A., Quinsay, M.N., Orogo, A.M., Giang, K., Rikka, S., and Gustafsson, A.B. (2012). Microtubule-associated protein 1 light chain 3 (LC3) interacts with Bnip3 protein to selectively remove endoplasmic reticulum and mitochondria via autophagy. *J Biol Chem* 287, 19094-19104.

Hardwick, J.M., and Levine, B. (2000). Sindbis virus vector system for functional analysis of apoptosis regulators. *Methods Enzymol* 322, 492-508.

He, C., Bassik, M.C., Moresi, V., Sun, K., Wei, Y., Zou, Z., An, Z., Loh, J., Fisher, J., Sun, Q., *et al.* (2012a). Exercise-induced BCL2-regulated autophagy is required for muscle glucose homeostasis. *Nature* 481, 511-515.

He, C., and Klionsky, D.J. (2009). Regulation mechanisms and signaling pathways of autophagy. *Annu Rev Genet* 43, 67-93.

He, C., Sumpter, R., Jr., and Levine, B. (2012b). Exercise induces autophagy in peripheral tissues and in the brain. *Autophagy* 8, 1548-1551.

Huang, R., Xu, Y., Wan, W., Shou, X., Qian, J., You, Z., Liu, B., Chang, C., Zhou, T., Lippincott-Schwartz, J., *et al.* (2015). Deacetylation of nuclear LC3 drives autophagy initiation under starvation. *Mol Cell* 57, 456-466.

Ichimura, Y., Kumanomidou, T., Sou, Y.S., Mizushima, T., Ezaki, J., Ueno, T., Kominami, E., Yamane, T., Tanaka, K., and Komatsu, M. (2008). Structural basis for sorting mechanism of p62 in selective autophagy. *J Biol Chem* 283, 22847-22857.

Inami, Y., Waguri, S., Sakamoto, A., Kouno, T., Nakada, K., Hino, O., Watanabe, S., Ando, J., Iwadate, M., Yamamoto, M., *et al.* (2011). Persistent activation of Nrf2 through p62 in hepatocellular carcinoma cells. *J Cell Biol* 193, 275-284.

Jiang, P., and Mizushima, N. (2014). Autophagy and human diseases. *Cell Res* 24, 69-79.

Jiang, X., Overholtzer, M., and Thompson, C.B. (2015). Autophagy in cellular metabolism and cancer. *J Clin Invest* 125, 47-54.

Jones, J.M., Morrell, J.C., and Gould, S.J. (2001). Multiple distinct targeting signals in integral peroxisomal membrane proteins. *J Cell Biol* 153, 1141-1150.

Jones, L.W., and Alfano, C.M. (2013). Exercise-oncology research: past, present, and future. *Acta Oncol* 52, 195-215.

Kabeya, Y., Mizushima, N., Ueno, T., Yamamoto, A., Kirisako, T., Noda, T., Kominami, E., Ohsumi, Y., and Yoshimori, T. (2000). LC3, a mammalian homologue of yeast

Apg8p, is localized in autophagosome membranes after processing. *EMBO J* 19, 5720-5728.

Kalakonda, S., Nallar, S.C., Jaber, S., Keay, S.K., Rorke, E., Munivenkatappa, R., Lindner, D.J., Fiskum, G.M., and Kalvakolanu, D.V. (2013). Monoallelic loss of tumor suppressor GRIM-19 promotes tumorigenesis in mice. *Proc Natl Acad Sci U S A* 110, E4213-4222.

Karsli-Uzunbas, G., Guo, J.Y., Price, S., Teng, X., Laddha, S.V., Khor, S., Kalaany, N.Y., Jacks, T., Chan, C.S., Rabinowitz, J.D., *et al.* (2014). Autophagy is required for glucose homeostasis and lung tumor maintenance. *Cancer Discov* 4, 914-927.

Kaur, J., and Debnath, J. (2015). Autophagy at the crossroads of catabolism and anabolism. *Nat Rev Mol Cell Biol* 16, 461-472.

Kawano, M., Hirano, T., Matsuda, T., Taga, T., Horii, Y., Iwato, K., Asaoku, H., Tang, B., Tanabe, O., Tanaka, H., *et al.* (1988). Autocrine generation and requirement of BSF-2/IL-6 for human multiple myelomas. *Nature* 332, 83-85.

Khaminets, A., Behl, C., and Dikic, I. (2016). Ubiquitin-Dependent And Independent Signals In Selective Autophagy. *Trends Cell Biol* 26, 6-16.

Kihara, A., Kabeya, Y., Ohsumi, Y., and Yoshimori, T. (2001). Beclin-phosphatidylinositol 3-kinase complex functions at the trans-Golgi network. *EMBO Rep* 2, 330-335.

Kim, P.K., and Hettema, E.H. (2015). Multiple pathways for protein transport to peroxisomes. *J Mol Biol* 427, 1176-1190.

Kirkin, V., McEwan, D.G., Novak, I., and Dikic, I. (2009). A role for ubiquitin in selective autophagy. *Mol Cell* 34, 259-269.

Klionsky, D.J., Abdalla, F.C., Abeliovich, H., Abraham, R.T., Acevedo-Arozena, A., Adeli, K., Agholme, L., Agnello, M., Agostinis, P., Aguirre-Ghiso, J.A., *et al.* (2012). Guidelines for the use and interpretation of assays for monitoring autophagy. *Autophagy* 8, 445-544.

Klionsky, D.J., Abdelmohsen, K., Abe, A., Abedin, M.J., Abeliovich, H., Acevedo Arozena, A., Adachi, H., Adams, C.M., Adams, P.D., Adeli, K., *et al.* (2016). Guidelines for the use and interpretation of assays for monitoring autophagy (3rd edition). *Autophagy* 12, 1-222.

Klouwer, F.C., Berendse, K., Ferdinandusse, S., Wanders, R.J., Engelen, M., and Poll-The, B.T. (2015). Zellweger spectrum disorders: clinical overview and management approach. *Orphanet J Rare Dis* 10, 151.

Knupfer, H., and Preiss, R. (2007). Significance of interleukin-6 (IL-6) in breast cancer (review). *Breast Cancer Res Treat* 102, 129-135.

Kobayashi, S., Tanaka, A., and Fujiki, Y. (2007). Fis1, DLP1, and Pex11p coordinately regulate peroxisome morphogenesis. *Exp Cell Res* 313, 1675-1686.

Koch, A., Yoon, Y., Bonekamp, N.A., McNiven, M.A., and Schrader, M. (2005). A role for Fis1 in both mitochondrial and peroxisomal fission in mammalian cells. *Mol Biol Cell* 16, 5077-5086.

Koneri, K., Goi, T., Hirono, Y., Katayama, K., and Yamaguchi, A. (2007). Beclin 1 gene inhibits tumor growth in colon cancer cell lines. *Anticancer Res* 27, 1453-1457.

Korac, J., Schaeffer, V., Kovacevic, I., Clement, A.M., Jungblut, B., Behl, C., Terzic, J., and Dikic, I. (2013). Ubiquitin-independent function of optineurin in autophagic clearance of protein aggregates. *J Cell Sci* 126, 580-592.

Krause, C., Rosewich, H., Woehler, A., and Gartner, J. (2013). Functional analysis of PEX13 mutation in a Zellweger syndrome spectrum patient reveals novel homooligomerization of PEX13 and its role in human peroxisome biogenesis. *Hum Mol Genet* 22, 3844-3857.

Kroemer, G. (1997). The proto-oncogene Bcl-2 and its role in regulating apoptosis. *Nat Med* 3, 614-620.

Kroemer, G. (2015). Autophagy: a druggable process that is deregulated in aging and human disease. *J Clin Invest* 125, 1-4.

Lazarou, M., Sliter, D.A., Kane, L.A., Sarraf, S.A., Wang, C., Burman, J.L., Sideris, D.P., Fogel, A.I., and Youle, R.J. (2015). The ubiquitin kinase PINK1 recruits autophagy receptors to induce mitophagy. *Nature* 524, 309-314.

Lee, K.M., Hwang, S.K., and Lee, J.A. (2013). Neuronal autophagy and neurodevelopmental disorders. *Exp Neurobiol* 22, 133-142.

Lerman, I., Harrison, B.C., Freeman, K., Hewett, T.E., Allen, D.L., Robbins, J., and Leinwand, L.A. (2002). Genetic variability in forced and voluntary endurance exercise performance in seven inbred mouse strains. *J Appl Physiol* (1985) 92, 2245-2255.

Levine, B., and Kroemer, G. (2008). Autophagy in the pathogenesis of disease. *Cell* 132, 27-42.

Levine, B., Mizushima, N., and Virgin, H.W. (2011). Autophagy in immunity and inflammation. *Nature* 469, 323-335.

Levine, B., Packer, M., and Codogno, P. (2015). Development of autophagy inducers in clinical medicine. *J Clin Invest* 125, 14-24.

Li, M.L., Wang, H.L., and Stollar, V. (1997). Complementation of and interference with Sindbis virus replication by full-length and deleted forms of the nonstructural protein, nsP1, expressed in stable transfectants of HeLa cells. *Virology* 227, 361-369.

Liang, X.H., Jackson, S., Seaman, M., Brown, K., Kempkes, B., Hibshoosh, H., and Levine, B. (1999). Induction of autophagy and inhibition of tumorigenesis by beclin 1. *Nature* 402, 672-676.

Liang, X.H., Kleeman, L.K., Jiang, H.H., Gordon, G., Goldman, J.E., Berry, G., Herman, B., and Levine, B. (1998). Protection against fatal Sindbis virus encephalitis by beclin, a novel Bcl-2-interacting protein. *J Virol* 72, 8586-8596.

Lim, C.Y., Bi, X., Wu, D., Kim, J.B., Gunning, P.W., Hong, W., and Han, W. (2015). Tropomodulin3 is a novel Akt2 effector regulating insulin-stimulated GLUT4 exocytosis through cortical actin remodeling. *Nat Commun* 6, 5951.

Liu, H., He, Z., von Rutte, T., Yousefi, S., Hunger, R.E., and Simon, H.U. (2013). Down-regulation of autophagy-related protein 5 (ATG5) contributes to the pathogenesis of early-stage cutaneous melanoma. *Sci Transl Med* 5, 202ra123.

Liu, L., Feng, D., Chen, G., Chen, M., Zheng, Q., Song, P., Ma, Q., Zhu, C., Wang, R., Qi, W., *et al.* (2012). Mitochondrial outer-membrane protein FUNDC1 mediates hypoxia-induced mitophagy in mammalian cells. *Nat Cell Biol* 14, 177-185.

Liu, Y., Bjorkman, J., Urquhart, A., Wanders, R.J., Crane, D.I., and Gould, S.J. (1999). PEX13 is mutated in complementation group 13 of the peroxisome-biogenesis disorders. *Am J Hum Genet* 65, 621-634.

Liu, Z., Chen, P., Gao, H., Gu, Y., Yang, J., Peng, H., Xu, X., Wang, H., Yang, M., Liu, X., *et al.* (2014). Ubiquitylation of autophagy receptor Optineurin by HACE1 activates selective autophagy for tumor suppression. *Cancer Cell* 26, 106-120.

Ma, C., Agrawal, G., and Subramani, S. (2011). Peroxisome assembly: matrix and membrane protein biogenesis. *J Cell Biol* 193, 7-16.

Maiuri, M.C., Zalckvar, E., Kimchi, A., and Kroemer, G. (2007). Self-eating and self-killing: crosstalk between autophagy and apoptosis. *Nat Rev Mol Cell Biol* 8, 741-752.

Mandell, M.A., Jain, A., Arko-Mensah, J., Chauhan, S., Kimura, T., Dinkins, C., Silvestri, G., Munch, J., Kirchhoff, F., Simonsen, A., *et al.* (2014). TRIM proteins regulate autophagy and can target autophagic substrates by direct recognition. *Dev Cell* 30, 394-409.

Manjithaya, R., Anjard, C., Loomis, W.F., and Subramani, S. (2010). Unconventional secretion of *Pichia pastoris* Acb1 is dependent on GRASP protein, peroxisomal functions, and autophagosome formation. *J Cell Biol* 188, 537-546.

Manjithaya, R., and Subramani, S. (2011). Autophagy: a broad role in unconventional protein secretion? *Trends Cell Biol* 21, 67-73.

Mathew, R., Karantza-Wadsworth, V., and White, E. (2007a). Role of autophagy in cancer. *Nat Rev Cancer* 7, 961-967.

Mathew, R., Kongara, S., Beaudoin, B., Karp, C.M., Bray, K., Degenhardt, K., Chen, G., Jin, S., and White, E. (2007b). Autophagy suppresses tumor progression by limiting chromosomal instability. *Genes Dev* 21, 1367-1381.

Matsumoto, G., Wada, K., Okuno, M., Kurosawa, M., and Nukina, N. (2011). Serine 403 phosphorylation of p62/SQSTM1 regulates selective autophagic clearance of ubiquitinated proteins. *Mol Cell* 44, 279-289.

Mattiazzi Usaj, M., Brloznic, M., Kaferle, P., Zitnik, M., Wolinski, H., Leitner, F., Kohlwein, S.D., Zupan, B., and Petrovic, U. (2015). Genome-Wide Localization Study of Yeast Pex11 Identifies Peroxisome-Mitochondria Interactions through the ERMES Complex. *J Mol Biol* 427, 2072-2087.

Maxwell, M., Bjorkman, J., Nguyen, T., Sharp, P., Finnie, J., Paterson, C., Tonks, I., Paton, B.C., Kay, G.F., and Crane, D.I. (2003). Pex13 inactivation in the mouse disrupts peroxisome biogenesis and leads to a Zellweger syndrome phenotype. *Mol Cell Biol* 23, 5947-5957.

McTiernan, A. (2008). Mechanisms linking physical activity with cancer. *Nat Rev Cancer* 8, 205-211.

Michaud, M., Martins, I., Sukkurwala, A.Q., Adjemian, S., Ma, Y., Pellegatti, P., Shen, S., Kepp, O., Scoazec, M., Mignot, G., *et al.* (2011). Autophagy-dependent anticancer immune responses induced by chemotherapeutic agents in mice. *Science* 334, 1573-1577.

Michna, L., Wagner, G.C., Lou, Y.R., Xie, J.G., Peng, Q.Y., Lin, Y., Carlson, K., Shih, W.J., Conney, A.H., and Lu, Y.P. (2006). Inhibitory effects of voluntary running wheel exercise on UVB-induced skin carcinogenesis in SKH-1 mice. *Carcinogenesis* 27, 2108-2115.

Miki, S., Iwano, M., Miki, Y., Yamamoto, M., Tang, B., Yokokawa, K., Sonoda, T., Hirano, T., and Kishimoto, T. (1989). Interleukin-6 (IL-6) functions as an in vitro autocrine growth factor in renal cell carcinomas. *FEBS Lett* 250, 607-610.

Miles, S.A., Rezai, A.R., Salazar-Gonzalez, J.F., Vander Meyden, M., Stevens, R.H., Logan, D.M., Mitsuyasu, R.T., Taga, T., Hirano, T., Kishimoto, T., *et al.* (1990). AIDS Kaposi sarcoma-derived cells produce and respond to interleukin 6. *Proc Natl Acad Sci U S A* 87, 4068-4072.

Miracco, C., Cosci, E., Oliveri, G., Luzi, P., Pacenti, L., Monciatti, I., Mannucci, S., De Nisi, M.C., Toscano, M., Malagnino, V., *et al.* (2007). Protein and mRNA expression of autophagy gene Beclin 1 in human brain tumours. *Int J Oncol* 30, 429-436.

Mizushima, N. (2007). Autophagy: process and function. *Genes Dev* 21, 2861-2873.

Mizushima, N., and Komatsu, M. (2011). Autophagy: Renovation of Cells and Tissues. *Cell* 147, 728-741.

Mizushima, N., and Levine, B. (2010). Autophagy in mammalian development and differentiation. *Nat Cell Biol* 12, 823-830.

Mizushima, N., Yamamoto, A., Matsui, M., Yoshimori, T., and Ohsumi, Y. (2004). In vivo analysis of autophagy in response to nutrient starvation using transgenic mice expressing a fluorescent autophagosome marker. *Mol Biol Cell* 15, 1101-1111.

Mizushima, N., Yoshimori, T., and Levine, B. (2010). Methods in mammalian autophagy research. *Cell* 140, 313-326.

Moreira, S., Correia, M., Soares, P., and Maximo, V. (2011). GRIM-19 function in cancer development. *Mitochondrion* 11, 693-699.

Motley, A.M., Nuttall, J.M., and Hettema, E.H. (2012). Pex3-anchored Atg36 tags peroxisomes for degradation in *Saccharomyces cerevisiae*. *EMBO J* 31, 2852-2868.

Na, H.-K., and Oliynyk, S. (2011). Effects of physical activity on cancer prevention. *Annals of the New York Academy of Sciences* 1229, 176-183.

Nagaraju, G.P., and Sharma, D. (2011). Anti-cancer role of SPARC, an inhibitor of adipogenesis. *Cancer Treat Rev* 37, 559-566.

Naldini, L., Blomer, U., Gallay, P., Ory, D., Mulligan, R., Gage, F.H., Verma, I.M., and Trono, D. (1996). In vivo gene delivery and stable transduction of nondividing cells by a lentiviral vector. *Science* 272, 263-267.

Narendra, D., Kane, L.A., Hauser, D.N., Fearnley, I.M., and Youle, R.J. (2010). p62/SQSTM1 is required for Parkin-induced mitochondrial clustering but not mitophagy; VDAC1 is dispensable for both. *Autophagy* 6, 1090-1106.

Neill, T., Painter, H., Buraschi, S., Owens, R.T., Lisanti, M.P., Schaefer, L., and Iozzo, R.V. (2012). Decorin antagonizes the angiogenic network: concurrent inhibition of Met, hypoxia inducible factor 1alpha, vascular endothelial growth factor A, and induction of thrombospondin-1 and TIMP3. *J Biol Chem* 287, 5492-5506.

Neuspiel, M., Schauss, A.C., Braschi, E., Zunino, R., Rippstein, P., Rachubinski, R.A., Andrade-Navarro, M.A., and McBride, H.M. (2008). Cargo-selected transport from the mitochondria to peroxisomes is mediated by vesicular carriers. *Curr Biol* 18, 102-108.

Noda, N.N., Kumeta, H., Nakatogawa, H., Satoo, K., Adachi, W., Ishii, J., Fujioka, Y., Ohsumi, Y., and Inagaki, F. (2008). Structural basis of target recognition by Atg8/LC3 during selective autophagy. *Genes Cells* 13, 1211-1218.

Novak, I., Kirkin, V., McEwan, D.G., Zhang, J., Wild, P., Rozenknop, A., Rogov, V., Lohr, F., Popovic, D., Occhipinti, A., *et al.* (2010). Nix is a selective autophagy receptor for mitochondrial clearance. *EMBO Rep* 11, 45-51.

Ohsumi, Y. (2001). Molecular dissection of autophagy: two ubiquitin-like systems. *Nat Rev Mol Cell Biol* 2, 211-216.

Okamoto, T., Inozume, T., Mitsui, H., Kanzaki, M., Harada, K., Shibagaki, N., and Shimada, S. (2010). Overexpression of GRIM-19 in cancer cells suppresses STAT3-mediated signal transduction and cancer growth. *Mol Cancer Ther* 9, 2333-2343.

Orvedahl, A., MacPherson, S., Sumpter, R., Jr., Talloczy, Z., Zou, Z., and Levine, B. (2010). Autophagy protects against Sindbis virus infection of the central nervous system. *Cell Host Microbe* 7, 115-127.

Orvedahl, A., Sumpter, R., Jr., Xiao, G., Ng, A., Zou, Z., Tang, Y., Narimatsu, M., Gilpin, C., Sun, Q., Roth, M., *et al.* (2011). Image-based genome-wide siRNA screen identifies selective autophagy factors. *Nature* 480, 113-117.

Ostrowski, K., Rohde, T., Zacho, M., Asp, S., and Pedersen, B.K. (1998). Evidence that interleukin-6 is produced in human skeletal muscle during prolonged running. *J Physiol* 508 (Pt 3), 949-953.

Oz-Levi, D., Ben-Zeev, B., Ruzzo, E.K., Hitomi, Y., Gelman, A., Pelak, K., Anikster, Y., Reznik-Wolf, H., Bar-Joseph, I., Olender, T., *et al.* (2012). Mutation in TECPR2 reveals a role for autophagy in hereditary spastic paraparesis. *Am J Hum Genet* 91, 1065-1072.

Padman, B.S., Bach, M., Lucarelli, G., Prescott, M., and Ramm, G. (2013). The protonophore CCCP interferes with lysosomal degradation of autophagic cargo in yeast and mammalian cells. *Autophagy* 9, 1862-1875.

Pankiv, S., Clausen, T.H., Lamark, T., Brech, A., Bruun, J.A., Outzen, H., Overvatn, A., Bjorkoy, G., and Johansen, T. (2007). p62/SQSTM1 binds directly to Atg8/LC3 to facilitate degradation of ubiquitinated protein aggregates by autophagy. *J Biol Chem* 282, 24131-24145.

Pattingre, S., Petiot, A., and Codogno, P. (2004). Analyses of Galpha-interacting protein and activator of G-protein-signaling-3 functions in macroautophagy. *Methods Enzymol* 390, 17-31.

Pattingre, S., Tassa, A., Qu, X., Garuti, R., Liang, X.H., Mizushima, N., Packer, M., Schneider, M.D., and Levine, B. (2005). Bcl-2 antiapoptotic proteins inhibit Beclin 1-dependent autophagy. *Cell* 122, 927-939.

Pedersen, B.K. (2000). Special feature for the Olympics: effects of exercise on the immune system: exercise and cytokines. *Immunol Cell Biol* 78, 532-535.

Pedersen, B.K., and Febbraio, M.A. (2012). Muscles, exercise and obesity: skeletal muscle as a secretory organ. *Nat Rev Endocrinol* 8, 457-465.

Pedersen, L., Idorn, M., Olofsson, G.H., Lauenborg, B., Nookaew, I., Hansen, R.H., Johannesen, H.H., Becker, J.C., Pedersen, K.S., Dethlefsen, C., *et al.* (2016). Voluntary Running Suppresses Tumor Growth through Epinephrine- and IL-6-Dependent NK Cell Mobilization and Redistribution. *Cell Metab* 23, 554-562.

Pfeifer, U. (1973). Cellular autophagy and cell atrophy in the rat liver during long-term starvation. A quantitative morphological study with regard to diurnal variations. *Virchows Arch B Cell Pathol* 12, 195-211.

Pfeifer, U., and Bertling, J. (1977). A morphometric study of the inhibition of autophagic degradation during restorative growth of liver cells in rats re-fed after starvation.

Virchows Arch B Cell Pathol 24, 109-120.

Pfeifer, U., and Strauss, P. (1981). Autophagic vacuoles in heart muscle and liver. A comparative morphometric study including circadian variations in meal-fed rats. J Mol Cell Cardiol 13, 37-49.

Physical Activity Guidelines Advisory Committee (2008). 2008 Physical Activity Guidelines for Americans, US Department of Health and Human Services, ed. (Washington, DC).

Polson, H.E., de Lartigue, J., Rigden, D.J., Reedijk, M., Urbe, S., Clague, M.J., and Tooze, S.A. (2010). Mammalian Atg18 (WIPI2) localizes to omegasome-anchored phagophores and positively regulates LC3 lipidation. Autophagy 6, 506-522.

Qu, X., Yu, J., Bhagat, G., Furuya, N., Hibshoosh, H., Troxel, A., Rosen, J., Eskelinen, E.L., Mizushima, N., Ohsumi, Y., *et al.* (2003). Promotion of tumorigenesis by heterozygous disruption of the beclin 1 autophagy gene. J Clin Invest 112, 1809-1820.

Rogov, V., Dotsch, V., Johansen, T., and Kirkin, V. (2014). Interactions between autophagy receptors and ubiquitin-like proteins form the molecular basis for selective autophagy. Mol Cell 53, 167-178.

Rosewich, H., Waterham, H.R., Wanders, R.J., Ferdinandusse, S., Henneke, M., Hunneman, D., and Gartner, J. (2006). Pitfall in metabolic screening in a patient with fatal peroxisomal beta-oxidation defect. Neuropediatrics 37, 95-98.

Rundle, A. (2011). Mechanisms Underlying the Effects of Physical Activity on Cancer. In *Physical Activity, Dietary Calorie Restriction, and Cancer*, A. McTiernan, ed. (New York: Springer Science + Business Media).

Sachdeva, U.M., and Thompson, C.B. (2008). Diurnal rhythms of autophagy: implications for cell biology and human disease. *Autophagy* 4, 581-589.

Saitou, H., Nishimura, T., Muramatsu, K., Kodera, H., Kumada, S., Sugai, K., Kasai-Yoshida, E., Sawaura, N., Nishida, H., Hoshino, A., *et al.* (2013). De novo mutations in the autophagy gene WDR45 cause static encephalopathy of childhood with neurodegeneration in adulthood. *Nat Genet* 45, 445-449, 449e441.

Salpietro, V., Phadke, R., Saggari, A., Hargreaves, I.P., Yates, R., Fokoloros, C., Mankad, K., Hertecant, J., Ruggieri, M., McCormick, D., *et al.* (2015). Zellweger syndrome and secondary mitochondrial myopathy. *Eur J Pediatr* 174, 557-563.

Schrader, M., Godinho, L.F., Costello, J.L., and Islinger, M. (2015). The different facets of organelle interplay-an overview of organelle interactions. *Front Cell Dev Biol* 3, 56.

Schumann, U., and Subramani, S. (2008). Special delivery from mitochondria to peroxisomes. *Trends Cell Biol* 18, 253-256.

Schwabe, R.F., and Jobin, C. (2013). The microbiome and cancer. *Nat Rev Cancer* 13, 800-812.

Shimi, T., Butin-Israeli, V., Adam, S.A., Hamanaka, R.B., Goldman, A.E., Lucas, C.A., Shumaker, D.K., Kosak, S.T., Chandel, N.S., and Goldman, R.D. (2011). The role of nuclear lamin B1 in cell proliferation and senescence. *Genes Dev* 25, 2579-2593.

Shimizu, S., Hirano, T., Yoshioka, R., Sugai, S., Matsuda, T., Taga, T., Kishimoto, T., and Konda, S. (1988). Interleukin-6 (B-cell stimulatory factor 2)-dependent growth of a Lennert's lymphoma-derived T-cell line (KT-3). *Blood* 72, 1826-1828.

Shimozawa, N., Suzuki, Y., Zhang, Z., Imamura, A., Ghaedi, K., Fujiki, Y., and Kondo, N. (2000). Identification of PEX3 as the gene mutated in a Zellweger syndrome patient lacking peroxisomal remnant structures. *Hum Mol Genet* 9, 1995-1999.

Shimozawa, N., Suzuki, Y., Zhang, Z., Imamura, A., Toyama, R., Mukai, S., Fujiki, Y., Tsukamoto, T., Osumi, T., Orii, T., *et al.* (1999). Nonsense and temperature-sensitive mutations in PEX13 are the cause of complementation group H of peroxisome biogenesis disorders. *Hum Mol Genet* 8, 1077-1083.

Shoji-Kawata, S., Sumpter, R., Leveno, M., Campbell, G.R., Zou, Z., Kinch, L., Wilkins, A.D., Sun, Q., Pallauf, K., MacDuff, D., *et al.* (2013). Identification of a candidate therapeutic autophagy-inducing peptide. *Nature* 494, 201-206.

Stewart, S.A., Dykxhoorn, D.M., Palliser, D., Mizuno, H., Yu, E.Y., An, D.S., Sabatini, D.M., Chen, I.S., Hahn, W.C., Sharp, P.A., *et al.* (2003). Lentivirus-delivered stable gene silencing by RNAi in primary cells. *RNA* 9, 493-501.

Stolz, A., Ernst, A., and Dikic, I. (2014). Cargo recognition and trafficking in selective autophagy. *Nat Cell Biol* 16, 495-501.

Strohecker, A.M., Guo, J.Y., Karsli-Uzunbas, G., Price, S.M., Chen, G.J., Mathew, R., McMahon, M., and White, E. (2013). Autophagy sustains mitochondrial glutamine metabolism and growth of BrafV600E-driven lung tumors. *Cancer Discov* 3, 1272-1285.

Su, T., Suzui, M., Wang, L., Lin, C.S., Xing, W.Q., and Weinstein, I.B. (2003). Deletion of histidine triad nucleotide-binding protein 1/PKC-interacting protein in mice enhances cell growth and carcinogenesis. *Proc Natl Acad Sci U S A* 100, 7824-7829.

Sumpter, R., Jr., and Levine, B. (2010). Autophagy and innate immunity: triggering, targeting and tuning. *Semin Cell Dev Biol* 21, 699-711.

Takamura, A., Komatsu, M., Hara, T., Sakamoto, A., Kishi, C., Waguri, S., Eishi, Y., Hino, O., Tanaka, K., and Mizushima, N. (2011). Autophagy-deficient mice develop multiple liver tumors. *Genes Dev* 25, 795-800.

Tang, G., Gudsnuk, K., Kuo, S.H., Cotrina, M.L., Rosoklija, G., Sosunov, A., Sonders, M.S., Kanter, E., Castagna, C., Yamamoto, A., *et al.* (2014). Loss of mTOR-dependent macroautophagy causes autistic-like synaptic pruning deficits. *Neuron* 83, 1131-1143.

Tang, H., Sebti, S., Titone, R., Zhou, Y., Isidoro, C., Ross, T.S., Hibshoosh, H., Xiao, G., Packer, M., Xie, Y., *et al.* (2015). Decreased mRNA Expression in Human Breast Cancer is Associated with Estrogen Receptor-Negative Subtypes and Poor Prognosis. *EBioMedicine* 2, 255-263.

Thomas, A.C., Williams, H., Seto-Salvia, N., Bacchelli, C., Jenkins, D., O'Sullivan, M., Mengrelis, K., Ishida, M., Ocaka, L., Chanudet, E., *et al.* (2014). Mutations in SNX14 cause a distinctive autosomal-recessive cerebellar ataxia and intellectual disability syndrome. *Am J Hum Genet* 95, 611-621.

Thune, I., and Furberg, A.-S. (2001). Physical activity and cancer risk: dose-response and cancer, all sites and site-specific. *Medicine & Science in Sports & Exercise* 33, S530.

Tian, Y., Li, Z., Hu, W., Ren, H., Tian, E., Zhao, Y., Lu, Q., Huang, X., Yang, P., Li, X., *et al.* (2010). *C. elegans* screen identifies autophagy genes specific to multicellular organisms. *Cell* 141, 1042-1055.

Van Ael, E., and Fransen, M. (2006). Targeting signals in peroxisomal membrane proteins. *Biochim Biophys Acta* 1763, 1629-1638.

Vantaggiato, C., Crimella, C., Airoidi, G., Polishchuk, R., Bonato, S., Brighina, E., Scarlato, M., Musumeci, O., Toscano, A., Martinuzzi, A., *et al.* (2013). Defective autophagy in spastizin mutated patients with hereditary spastic paraparesis type 15. *Brain* 136, 3119-3139.

Wanders, R.J. (2004). Metabolic and molecular basis of peroxisomal disorders: a review. *Am J Med Genet A* 126A, 355-375.

Wanders, R.J., and Waterham, H.R. (2005). Peroxisomal disorders I: biochemistry and genetics of peroxisome biogenesis disorders. *Clin Genet* 67, 107-133.

Wanders, R.J., and Waterham, H.R. (2006). Biochemistry of mammalian peroxisomes revisited. *Annu Rev Biochem* 75, 295-332.

Wang, F., Meng, W., Wang, B., and Qiao, L. (2014). Helicobacter pylori-induced gastric inflammation and gastric cancer. *Cancer Lett* 345, 196-202.

Wang, R.C., Wei, Y., An, Z., Zou, Z., Xiao, G., Bhagat, G., White, M., Reichelt, J., and Levine, B. (2012). Akt-mediated regulation of autophagy and tumorigenesis through Beclin 1 phosphorylation. *Science* 338, 956-959.

Ward, P.S., Patel, J., Wise, D.R., Abdel-Wahab, O., Bennett, B.D., Collier, H.A., Cross, J.R., Fantin, V.R., Hedvat, C.V., Perl, A.E., *et al.* (2010). The common feature of

leukemia-associated IDH1 and IDH2 mutations is a neomorphic enzyme activity converting alpha-ketoglutarate to 2-hydroxyglutarate. *Cancer Cell* 17, 225-234.

Watkins, G., Douglas-Jones, A., Bryce, R., Mansel, R.E., and Jiang, W.G. (2005). Increased levels of SPARC (osteonectin) in human breast cancer tissues and its association with clinical outcomes. *Prostaglandins Leukot Essent Fatty Acids* 72, 267-272.

Weber, K.L., Fischer, R.S., and Fowler, V.M. (2007). Tmod3 regulates polarized epithelial cell morphology. *J Cell Sci* 120, 3625-3632.

Wei, Y., Pattingre, S., Sinha, S., Bassik, M., and Levine, B. (2008). JNK1-mediated phosphorylation of Bcl-2 regulates starvation-induced autophagy. *Mol Cell* 30, 678-688.

Wei, Y., Zou, Z., Becker, N., Anderson, M., Sumpter, R., Xiao, G., Kinch, L., Koduru, P., Christudass, Christhunesa S., Veltri, Robert W., *et al.* (2013). EGFR-Mediated Beclin 1 Phosphorylation in Autophagy Suppression, Tumor Progression, and Tumor Chemoresistance. *Cell* 154, 1269-1284.

White, E. (2015). The role for autophagy in cancer. *J Clin Invest* 125, 42-46.

Wild, P., Farhan, H., McEwan, D.G., Wagner, S., Rogov, V.V., Brady, N.R., Richter, B., Korac, J., Waidmann, O., Choudhary, C., *et al.* (2011). Phosphorylation of the autophagy receptor optineurin restricts Salmonella growth. *Science* 333, 228-233.

Yamashita, S., Abe, K., Tatemichi, Y., and Fujiki, Y. (2014). The membrane peroxin PEX3 induces peroxisome-ubiquitination-linked pexophagy. *Autophagy* 10, 1549-1564.

Yang, S., Wang, X., Contino, G., Liesa, M., Sahin, E., Ying, H., Bause, A., Li, Y., Stommel, J.M., Dell'antonio, G., *et al.* (2011a). Pancreatic cancers require autophagy for tumor growth. *Genes Dev* 25, 717-729.

Yang, Z.J., Chee, C.E., Huang, S., and Sinicrope, F.A. (2011b). The role of autophagy in cancer: therapeutic implications. *Mol Cancer Ther* 10, 1533-1541.

Yee, C., Biondi, A., Wang, X.H., Iscove, N.N., de Sousa, J., Aarden, L.A., Wong, G.G., Clark, S.C., Messner, H.A., and Minden, M.D. (1989). A possible autocrine role for interleukin-6 in two lymphoma cell lines. *Blood* 74, 798-804.

Yoshii, S.R., Kishi, C., Ishihara, N., and Mizushima, N. (2011). Parkin mediates proteasome-dependent protein degradation and rupture of the outer mitochondrial membrane. *J Biol Chem* 286, 19630-19640.

Yoshikawa, Y., Ogawa, M., Hain, T., Yoshida, M., Fukumatsu, M., Kim, M., Mimuro, H., Nakagawa, I., Yanagawa, T., Ishii, T., *et al.* (2009). *Listeria monocytogenes* ActA-mediated escape from autophagic recognition. *Nat Cell Biol* 11, 1233-1240.

Young, A.R., Narita, M., Ferreira, M., Kirschner, K., Sadaie, M., Darot, J.F., Tavaré, S., Arakawa, S., Shimizu, S., Watt, F.M., *et al.* (2009). Autophagy mediates the mitotic senescence transition. *Genes Dev* 23, 798-803.

Yue, Z., Jin, S., Yang, C., Levine, A.J., and Heintz, N. (2003). Beclin 1, an autophagy gene essential for early embryonic development, is a haploinsufficient tumor suppressor. *Proc Natl Acad Sci U S A* 100, 15077-15082.

Zeharia, A., Ebberink, M.S., Wanders, R.J., Waterham, H.R., Gutman, A., Nissenkorn, A., and Korman, S.H. (2007). A novel PEX12 mutation identified as the cause of a peroxisomal biogenesis disorder with mild clinical phenotype, mild biochemical abnormalities in fibroblasts and a mosaic catalase immunofluorescence pattern, even at 40 degrees C. *J Hum Genet* 52, 599-606.

Zhang, J., Kim, J., Alexander, A., Cai, S., Tripathi, D.N., Dere, R., Tee, A.R., Tait-Mulder, J., Di Nardo, A., Han, J.M., *et al.* (2013). A tuberous sclerosis complex signalling node at the peroxisome regulates mTORC1 and autophagy in response to ROS. *Nat Cell Biol* 15, 1186-1196.

Zhao, H., Zhao, Y.G., Wang, X., Xu, L., Miao, L., Feng, D., Chen, Q., Kovacs, A.L., Fan, D., and Zhang, H. (2013). Mice deficient in Epg5 exhibit selective neuronal vulnerability to degeneration. *J Cell Biol* 200, 731-741.

Zinchuk, V., Zinchuk, O., and Okada, T. (2007). Quantitative colocalization analysis of multicolor confocal immunofluorescence microscopy images: pushing pixels to explore biological phenomena. *Acta Histochem Cytochem* 40, 101-111.

Zufferey, R., Nagy, D., Mandel, R.J., Naldini, L., and Trono, D. (1997). Multiply attenuated lentiviral vector achieves efficient gene delivery in vivo. *Nat Biotechnol* 15, 871-875.

zur Hausen, H. (2002). Papillomaviruses and cancer: from basic studies to clinical application. *Nat Rev Cancer* 2, 342-350.